
Optimization of the reaction conditions of two enzymes for use in a carbon sequestration process, and investigation into immobilization via encapsulation within polymersomes

by

Gordon L. Nish

A thesis submitted in partial fulfillment of the requirements for the degree of

Master of Science

in

Chemical Engineering

Department of Chemical and Materials Engineering
University of Alberta

© Gordon L. Nish, 2016

Abstract

Carbon dioxide emissions from human activities contribute to an increase of greenhouse gases in the atmosphere. In nature, this gas is sequestered through the use of enzymes found in the Calvin-Benson-Bassham cycle, with useful molecules such as sugars being synthesized as products. A biomimetic approach to capturing carbon dioxide and using it to synthesize useful chemicals, by way of these enzymes in a bioprocess, has been proposed. To achieve this, active enzymes must be harvested and their kinetic properties need to be characterized. Optimal process conditions must be established, with an appropriate enzyme immobilization technique being applied to ameliorate the overall bioprocess.

In this work, the phosphoribulokinase enzyme was produced in the bacterial cell platform *Escherichia coli* using molecular cloning techniques. The kinetic conditions affecting the rates of the enzymes ribose 5-phosphate isomerase A from *E. coli*, and phosphoribulokinase from *Synechococcus elongatus*, were locally optimized through surface response methodology and mathematical modeling. These models predicted the optimal pH levels, temperature, substrate concentration and other factors used in the assays. The rate of ribose 5-phosphate isomerase product formation under optimized conditions showed an increase of about 37 % over the measured rate under initial conditions, while that of phosphoribulokinase activity increased around 21 %. Enzyme characterization revealed K_m constants for the sugar substrates to be 0.12 mM for phosphoribulokinase and 9.4 mM for ribose 5-phosphate isomerase, with half-lives of 177 minutes and 89 hours, respectively, at room temperature. Furthermore, immobilization via encapsulation within polymersomes was investigated by using a

digestive assay and fluorescence correlation spectroscopy. The encapsulation efficiency of the enzyme Rpi was found to be about 23 %. This represents a final enzyme concentration of 1.2 μM having been encapsulated.

The enzyme phosphoribulokinase was successfully purified from a bacterial platform. This enzyme and ribose 5-phosphate isomerase were characterized using reaction kinetics, resulting in calculated half-lives and Michaelis constants. Locally optimized reaction conditions were found through experimental modeling, resulting in apparent increases in the reaction rate of both of the enzymes. The enzyme ribose 5-phosphate isomerase was successfully encapsulated within polymersomes.

Acknowledgments

I would like to thank these individuals and organizations for their support in this project:

Dr. Carlo Montemagno for his guidance, inspiration and tutelage

Dr. Paolo Mussone for his sage advice and help in editing this thesis

Dr. Hyo-Jick Choi and Dr. Arno de Klerk for help in revising this thesis

Dr. Sinoj Abraham, Sumalee Salahub and Dr. Surjith Kumaran for preparing polymer, and for the help in getting the system to work

Hui Qiu (Julie) for the transmission electron microscopy work in section 2.14.3

The Climate Change and Emissions Management Corporation for their generous funding of the project

My children Isaac and Mia, for behaving while their father was away at the lab

My loving wife Morgan, for supporting me wholeheartedly in my endeavors

Table of Contents

Chapter 1. Introduction	1
1.1 Carbon Emissions	1
1.2 Calvin-Benson-Bassham cycle	5
1.3 Biomimicry	8
1.4 Project overview and objectives	9
Chapter 2. Literature review	11
2.1 Enzymes and kinetic characterization.....	11
2.2 Optimization methods.....	25
2.3 Improving enzymatic stability	29
2.4 Immobilization.....	30
2.5 Encapsulation.....	31
Materials and Methods.....	35
2.6 Ribose 5-phosphate isomerase from <i>E. coli</i>	36
2.7 Phosphoribulokinase from <i>Spinacia oleracea</i>	41
2.8 Phosphoribulokinase from <i>Synechococcus elongates</i>	50
2.9 Kinetic characterization of Rpi	52
2.10 Kinetic characterization of PRK.....	58
2.11 Optimization of enzymatic reaction conditions	62
2.12 Polymer preparation.....	64
2.13 Polymersome formation and purification	67
2.14 Characterization of polymersomes	69
2.15 Post-encapsulation experiments.....	72
Chapter 3. Experimental results.....	76
3.1 Expression and purification of PRK.....	76

3.2 Kinetic characterization of Rpi and PRK.....	86
3.3 Stability of enzymes.....	92
3.4 Local optimization of kinetic activity.....	95
3.5 Polymer results.....	108
3.6 Polymersome purification and characterization.....	109
3.7 Post encapsulation experimental results.....	111
Chapter 4. Discussion of results and conclusion.....	119
4.1 PRK expression and purification.....	119
4.2 Kinetic characterization.....	123
4.3 Optimization results.....	127
4.4 Characterization of polymersomes.....	134
4.5 Conclusion and future work.....	140
References.....	143
Appendix.....	159

List of figures

Figure 1.1 Simplified overview of enzymes involved in the regeneration of ribulose 1,5-bisphosphate in the Calvin cycle.....	7
Figure 2.1 Reaction mechanism for RpiA catalysis.....	19
Figure 2.2 Reaction mechanism of PRK.....	22
Figure 2.3 Geometry of a Box-Behnken design.....	27
Figure 2.4 Geometry of a circumscribed central composite design.....	28
Figure 2.5 Schematic of enzyme encapsulation within polymersome.....	33
Figure 0.1 Gel images of the expression and purification of Rpi.....	37
Figure 0.2 Example of raw data from Rpi kinetic assay, n=3.....	55
Figure 0.3 Example of absorbance data from a PRK kinetic assay, n=3.....	59
Figure 3.1 Agarose gel of PRK gene and pET-15b vector.....	76
Figure 3.2 SDS-PAGE of PRK expression in BL-21 cells.....	79
Figure 3.3 SDS-PAGE of PRK expression in C-43 cells.....	80
Figure 3.4 SDS-PAGE of PRK expression in T7 cells.....	81

Figure 3.5 SDS-polyacrylamide gel of ion exchange elution fractions.	82
Figure 3.6 Partially purified <i>S. oleracea</i> PRK	84
Figure 3.7 Chromatogram showing the elution profile of proteins	85
Figure 3.8 SDS-PAGE of 6His-PRK	86
Figure 3.9 Graph of Ru5P product formed over time.....	87
Figure 3.10 Michaelis-menten saturation curve for Rpi	88
Figure 3.11 Standard curve of NADH stock used in the PRK kinetic assays	89
Figure 3.12	90
Figure 3.13 Michaelis-Menten saturation curve of PRK activity for the substrate Ru5P	91
Figure 3.14 Michaelis-menten saturation curve of PRK activity for the substrate ATP ..	91
Figure 3.15 Activity of Rpi over time.....	92
Figure 3.16 Activity of PRK over time when stored at room temperature.....	93
Figure 3.17 Graph of Ru5P formed over time by Rpi exposed to UV light.	94
Figure 3.18 Graph of RuBP formed over time by PRK exposed to UV light.	95
Figure 3.19 Main effects plots of the levels of buffer concentration and R5P	99
Figure 3.20 The main effects of four factors on the mean activity rate of PRK.....	105
Figure 3.21 Gel permeation chromatogram of the triblock copolymer dissolved in chloroform.....	108
Figure 3.22 Elution profile of polymersomes	109
Figure 3.23 Size distribution curve by intensity of polymersomes	110
Figure 3.24 SEM images of polymersomes laden with Rpi.	110
Figure 3.25 Cryo-TEM images of polymersomes.	111
Figure 3.26 Kinetic activity of digested free Rpi and encapsulated Rpi prior to PMSF and lysis treatments.....	111
Figure 3.27 Comparison of activities of solutions	113
Figure 3.28 Elution profile of Rpi/FitC conjugates	114
Figure 3.29 Measured count rate averages of fluorescent samples.	115
Figure 3.30 Normalized autocorrelation curve of fluorescent conjugate samples.....	116
Figure 3.31 Standard curve of Rpi/fluorescein conjugate.	117

List of tables

Table 2.1 Selected kinetic parameters of Rpi from different species	18
---	----

Table 2.2 Selected kinetic parameters of PRK from different species	22
Table 2.3 Comparison of immobilization techniques.....	30
Table 0.1 Summary of experiments used in this study.....	35
Table 0.2 Genetic sequence of Rpi	36
Table 0.3 Materials used in the expression and purification of Rpi	38
Table 0.4 Equipment used in the expression and purification of Rpi.....	39
Table 0.5 Materials used in the Bradford assay.....	40
Table 0.6 Equipment used in the Bradford assay procedure	40
Table 0.7: Genetic sequence of PRK	42
Table 0.8 The factorial design to maximize PRK expression.....	45
Table 0.9 Materials used in experiments to purify PRK from <i>S. oleracea</i>	48
Table 0.10 Equipment used in the expression and purification of PRK from <i>S. oleracea</i>	50
Table 0.11 Materials used in the purification of PRK from <i>S. elongates</i>	52
Table 0.12 Equipment used in the purification of PRK from <i>S. elongates</i>	52
Table 0.13 Materials used in the kinetic characterization of Rpi	57
Table 0.14 Equipment used in the kinetic characterization of Rpi.....	57
Table 0.15 Batches of PRK prepared for experimental procedures.....	60
Table 0.16 Materials used in the kinetic characterization of PRK	62
Table 0.17 The experimental domain for the local optimization of Rpi.....	62
Table 0.18 The experimental domain for the second Rpi response surface experiment ..	63
Table 0.19 Experimental domain for the local optimization of PRK.	63
Table 0.20 Experimental domain for the second surface response optimization of PRK. activity.....	64
Table 0.21 Materials used in the preparation of polymer	66
Table 0.22 Equipment used in the preparation of polymer.....	67
Table 0.23 Materials used in the formation and purification of polymersomes	69
Table 0.24 Equipment used in the formation and purification of polymersomes.....	69
Table 0.25 Materials used in the characterization of polymersomes.....	71
Table 0.26 Equipment used in the characterization of polymersomes	71
Table 0.27 Materials used in post-encapsulation experiments	75
Table 0.28 Equipment used in post-encapsulation experiments.....	75
Table 3.1 Alignment of forward and reverse sequencing results produced by Clustal Omega.	78

Table 3.2 Conditions which produced the most apparent PRK.....	81
Table 3.3 Results of MALDI-TOF protein identification submission.....	83
Table 3.4 Michaelis constants of Rpi found in literature.....	88
Table 3.5 Michaelis constants of PRK found in literature.....	92
Table 3.6 Activity of the enzymes following UV exposure	95
Table 3.7 Coded results of regression analysis of Rpi local activity optimization.	96
Table 3.8 Factors and levels of the first central composite surface design for RpiA activity.....	98
Table 3.9 Analysis of variance for the quadratic model of RpiA activity.	98
Table 3.10 Coded results of the second experimental regression analysis of Rpi.....	99
Table 3.11 Factors and levels of the second central composite surface design for RpiA activity.....	100
Table 3.12 Analysis of variance for the second quadratic model of RpiA activity.	101
Table 3.13 Coded regression analysis results of PRK activity.	102
Table 3.14 Factors and levels of the central composite surface design for PRK activity	104
Table 3.15 Results of the analysis of variance between predicted and measured PRK activity.....	104
Table 3.16 Coded results of the second experimental regression analysis of the activity of PRK.....	105
Table 3.17 Factors and levels of the second composite surface design for PRK activity	106
Table 3.18 Results of the second analysis of variance of predicted and observed kinetic rates of PRK.....	106
Table 3.19 Comparison of the original factor levels investigated to the optimal levels.	107
Table 3.20 ANOVA results.....	112
Table 3.21 ANOVA results comparing pre-treatments to free Rpi and lysed polymersomes	112
Table 3.22 Effects of the blank polymer concentration on encapsulation efficiency calculations	117

List of abbreviations

3PG-3-phosphoglycerate

AChE-Acetylcholinesterase

ADP-Adenosine diphosphate

AMP-Adenosine monophosphate

ATP-Adenosine triphosphate

BSA-Bovine serum albumin

CBB-Calvin-Benson-Bassham cycle

CCL-Chemical-looping combustion

DEAE-Diethylaminoethanol

DLS-Dynamic light scattering

DTT-Dithiothreitol

EE-Encapsulation efficiency

FCS- Fluorescence correlation spectroscopy

FitC-Fluorescein 5(6)-isocyanate

G3P-Glyceraldehyde 3-phosphate

K_{cat} -Rate constant/turnover number

K_i -Inhibitor constant

K_m -Michaelis constant

kDa-Kilodalton

LD/PK-Lactic dehydrogenase/pyruvate kinase

mM-Millimolar

MOF-Metal-organic frameworks

MWCO-Molecular weight cut-off

NADH-Nicotinamide adenine dinucleotide

nm-Nanometre

nM-Nanomolar

OD-Optical density

PDI-Polydispersity index

PEP-Phosphoenolpyruvate

PMOXA-PDMS-PMOXA- Poly(2-methyloxazoline)-block-poly(dimethylsiloxane)-
block-poly(2-methyloxazoline)

PPE-Phosphopentose epimerase

PRK-Phosphoribulokinase

PS-PIAT-polystyrene-b-poly(L-isocyanoalanine-(2-thiophene-3-yl-ethyl)amide

R5P-Ribose 5-phosphate

R15P-Ribose 1,5-bisphosphate

Rpi-Ribose-5-phosphate isomerase

RSM-Response surface methodology

RuBP-Ribulose-1,5-bisphosphate

RuBisCO-Ribulose 1,5-bisphosphate carboxylase/oxygenase

SDS-PAGE-Sodium Dodecyl Sulfate Polyacrylamide gel electrophoresis

μ M-Micromolar

V_{\max} -Maximal reaction rate

v/v-Volume to volume percent

w/v-Weight to volume percent

X5P- Xylulose 5-phosphate

Chapter 1. Introduction

1.1 Carbon Emissions

Carbon dioxide (CO₂) is a well-documented greenhouse gas, which is an unfortunate byproduct of many industrial processes, as well as the common day-to-day activities of many humans around the world. The majority of the global community has signed benchmarks, targeting lowered emissions¹. One method to achieve these targets would have emitters be taxed by way of emission standards, to disincentive the use of fossil fuel. This could directly reduce economic activity, and in turn negatively affect the jurisdiction that enforces this policy².

An alternative to this proposal is mitigation through technological advances. Engineered improvements in production efficiency with the goal of reduced emissions have been proposed and demonstrated in various industries, from cement manufacturers to power plants^{3,4}. In addition to process output reductions, the emissions proper may be captured and sequestered (stored) following production.

1.1.1 Current capture technologies

Carbon capture technologies can be used to remove CO₂ before combustion, during combustion, or after combustion. The electricity sector was the third largest CO₂ emitter in Canada in 2012, producing 86 megatonnes collectively⁵. In the United States, 82 % of generated electricity originates from fossil fuels, which released 2,022 megatonnes of CO₂ in 2013, making it the largest emitting sector⁶. A large body of research has focused on this industry. A fossil fuel based thermal power plant will emit CO₂ following combustion, and generate flue gas. This gas is at atmospheric pressure, will have a CO₂ concentration of approximately 7-15 %, and contain other gaseous impurities⁷. At this pressure, the partial pressure of CO₂ will be less than 0.15 atm⁸.

This low thermodynamic driving force of CO₂ is a problem with many proposed capture processes, and may be overcome by preventing the CO₂ from mixing with air and other gases during its production. Pre-combustion and oxy-fuel techniques prevent this mixing. Pre-combustion capture involves a reaction of the fuel source with oxygen or air, often in the presence of steam, to produce syngas, which is largely composed of carbon monoxide and hydrogen. This syngas is then reacted with steam in a shift converter to form CO₂ and hydrogen⁹. The average cost of capture using this technology was estimated at 43 USD/tonne in 2011¹⁰. Chemical-looping combustion (CCL) is an example of oxy-fuel separation, and it prevents the mixing of CO₂ with flue gases. A metal oxide is employed as an oxygen carrier in place of atmospheric air. This produces both pure CO₂ and water vapour¹¹. The average cost of capture using oxy-fuel combustion was estimated at 52 USD/tonne¹⁰. Pre-combustion and oxy-fuel methods allow purified CO₂ to be removed immediately, removing the need for post-combustion capture technologies; however, they do have drawbacks. Pre-combustion has limited applications, requires more development to increase efficiencies and suffers from high costs⁹. Oxy-fuel also has requires high capital costs, and was found to reduce the efficiency of a plant by 9 % in driving oxygen separation and gas compression¹².

Post-combustion methods have been designed to separate CO₂ from the flue gas. This is the most widely applicable technology for industrial sectors other than energy producers, and is more accessible using retrofitting strategies than pre-combustion and oxy-fuel methods¹³. Several reviews highlight post-combustion CO₂ capture technologies that are currently in use^{7,14}. A few of these technologies include: absorption, adsorption, membrane technology and enzyme based systems. The process of absorption involves molecules being taken up by a volume, and may be considered both physical and chemical in nature. The reaction is a physical one due to the dissolution of gaseous CO₂ to the liquid form. The chemical portion is due to the reaction between the CO₂ and chemical solvent. The solvents which are used most often are amine based, and the technology is considered the most mature and commercialized method of post-combustion capture^{15,16}. The amines act as a base, and bicarbonate is the predominate product of this reaction. These amines may be destroyed by oxidative degradation via

dissolved oxygen from the flue gases. To counteract this, additives must be considered¹⁷. The solvent must be regenerated, as it is consumed during the process. This is energy intensive, offsetting the effectiveness of net CO₂ removed due to the capture system. The cost of using amine based capture was estimated to be 58 USD/tonne¹⁰. Research is being conducted at finding suitable solvents that can process more CO₂ and require less energy to be regenerated¹⁸.

Adsorption is the adhesion of molecules from a mixture onto a solid surface. It typically involves packed columns filled with adsorbent, to which CO₂ will adhere. An ideal adsorbent should be low in cost, have high CO₂ adsorption capacity, fast kinetics and be highly selective for CO₂. Materials such as activated carbon, amine-based chemical supports and metal-organic frameworks (MOF) have been investigated in past studies¹⁵. Carbon and MOF based materials are most suitable to CO₂ capture at low temperatures and high pressures, and suffer from reduced capacity in the presence of moisture. Chemical supports are gaining interest due to their more favourable operating conditions; however, loading of amines and scale up of material synthesis remain problematic¹⁹. Following equilibrium, desorption must occur to release purified CO₂ and to regenerate the adsorbent material. This can be achieved through changes in pressure, temperature and application of voltage to the adsorbent, which further reduce the efficiency of the overall reduction of CO₂ emitted.

Membrane technology involves semi-permeable barriers, which separate CO₂ from other gases. They are composed of materials such as polymers, carbon, ceramics or metals. Membranes are a low cost method of separation, reliable, respond rapidly to variations in the CO₂ stream and allow modularity in replacement and expansion⁷. They do not require regeneration following operation. Separation is highly dependent on the partial pressure difference to drive the diffusion of molecules through the membrane, in addition, the concentration of CO₂ in the stream should surpass the threshold of 20 % or the feasibility of the technology decreases¹³. Selectivity and permeability are at odds within membrane technology, as higher selectivity reduces permeability performance²⁰.

In high-temperature applications, the gases must be cooled prior to exposure to the membrane.

Enzyme biotechnology has attracted attention due to its environmentally friendly approach, the rapid turnover rates and small amount of enzyme needed²¹. They are based on the natural reactions involving CO₂ found within living organisms, with the protein based enzymes catalyzing the reaction. The enzyme carbonic anhydrase (CA) has seen much attention in this field²². CA is able to catalyze reversible reaction:

$\text{CO}_2 + \text{H}_2\text{O} \xrightleftharpoons{\text{CA}} \text{H}_2\text{CO}_3$, where water and CO₂ form carbonic acid, which largely deprotonates into bicarbonate (HCO₃⁻). This may be removed, or precipitated with calcium to form solid calcium carbonate (CaCO₃)²³. The forward reaction of CA will approach 10⁶ s⁻¹ in the presence of an appropriate buffer. The reverse reaction is proton dependent, which is limited by buffer diffusion, allowing this high turnover rate²⁴. This rapid forward reaction is limited by CO₂ dissolution into the buffer. CO₂ carrying capacity is limited by the buffering capacity⁷. Various bed reactors spray columns and combinations with membrane technologies²² have been patented and experimented on to increase the gas/liquid dissolution and CO₂ conversion amounts. Highly temperature stable variants have been created, and tests at the pilot scale showed captured 68 kg of CO₂/day²⁵. Immobilization of CA at the gas/liquid interface could increase the mass transfer in theory, although this could lead to other technical challenges such as surface fouling, loss of enzyme activity and scale up issues.

Pre-combustion, oxy-fuel and post-combustion methods of capture each offer a solution to CO₂ emissions. In addition to the highlighted drawbacks, one common issue among capture technologies, with the exception of enzyme systems, is that post-capture sequestration of the carbon is a separate affair. They are rarely composed of a single capture/storage technology. CO₂ must be either utilized on site, or transported and stored to mitigate the emission footprint. CO₂ is currently stored in geological formations such as unmineable coal beds and saline aquifers. These storage solutions have been estimated

to cost between 0.2-30.2 USD/tonne CO₂²⁶. Deep ocean storage has also been proposed²⁷, but has not been undertaken due to global treaties and cost of transport.

CO₂ utilization currently accounts for an estimated 2 % of emissions worldwide, through conversion into chemicals such as polymers and urea, and use in oil recovery through injection methods^{28,29}. These projects partially offset the cost of capture and incentivize industries to reduce emissions; however, using captured CO₂ to recover oil, which is likely destined to be combusted, and then releasing said captured CO₂ into the atmosphere would result in net CO₂ production²⁸. Chemical synthesis can result in a reduction of use in energy, as a feedstock is provided, removing a portion of production or acquisition energy requirements. At present, CO₂ is also used in the production of pigments, inorganic carbonates, salicylic acid and as technological fluids²⁸. These specialty chemicals are not high enough in demand to significantly reduce CO₂ emissions, assuming a 100 % conversion rate, their use would account for 4 % of worldwide carbon emissions³⁰. More general chemicals, fuels or feedstocks for other processes would provide diversification for captured carbon use, and could incentivize carbon utilization methods. In the early 2000's, the research group of Dr. Sanjoy Bhattacharya was largely focused on CA system improvements. This work eventually led into research of alternative enzymes that could sequester CO₂. They hypothesized that the enzyme Ribulose-1,5-bisphosphate carboxylase/oxygenase (RuBisCO) could be a potential candidate for use in a fixation bioprocess³¹. This enzyme would open the possibility for production of very useful chemicals from CO₂³².

1.2 Calvin-Benson-Bassham cycle

RuBisCO catalyzes the binding of either aqueous CO₂ or O₂ to the five carbon sugar ribulose 1,5-bisphosphate (RuBP). This is a key reaction in the Calvin-Benson-Bassham (CBB) cycle, which is also referred to as the Calvin cycle, and constitutes the initial reaction in the light-independent reactions used by photosynthetic organisms in carbon fixation. The binding of O₂ is called photorespiration, and involves oxidation of RuBP. This is largely an undesirable reaction, as it reduces the efficiency of photosynthesis, removing RuBP for use in the CBB cycle and requiring energy to

regenerate the RuBP³³. It has been proposed that the enzymes specificity for CO₂ may not be enhanced without loss in catalytic turnover, and that the enzyme has reached perfection³⁴ in optimization over the past 3.5 billion years of evolution, despite undesirable oxidation reactions³⁵.

Activation of the enzyme involves binding of CO₂ with a conserved active site on the enzyme, forming a carbamate³⁶. This is stabilized by the binding of a magnesium ion, followed closely with RuBP binding with the now active enzyme. Water and the substrate CO₂ molecule are then added to the RuBP molecule in a four step reaction process³⁵. The product is an unstable 6 carbon structure, 3-keto-2-carboxyarabinitol 1,5-bisphosphate. This structure decays to form two molecules of 3-phosphoglycerate (3PG). These molecules are further reduced through two enzymatic steps to form glyceraldehyde-3-phosphate (G3P). For every three molecules of CO₂ fixated, six molecules of G3P will be formed. One of those G3P molecules is then transported from the chloroplast to the cytosol to be used for cellular functions. To form a complete cycle, the initial substrate RuBP must be regenerated from the remaining five G3P molecules. There are 11 essential enzymes in total that are required for the carboxylation, reduction and regeneration of the acceptor molecule RuBP.

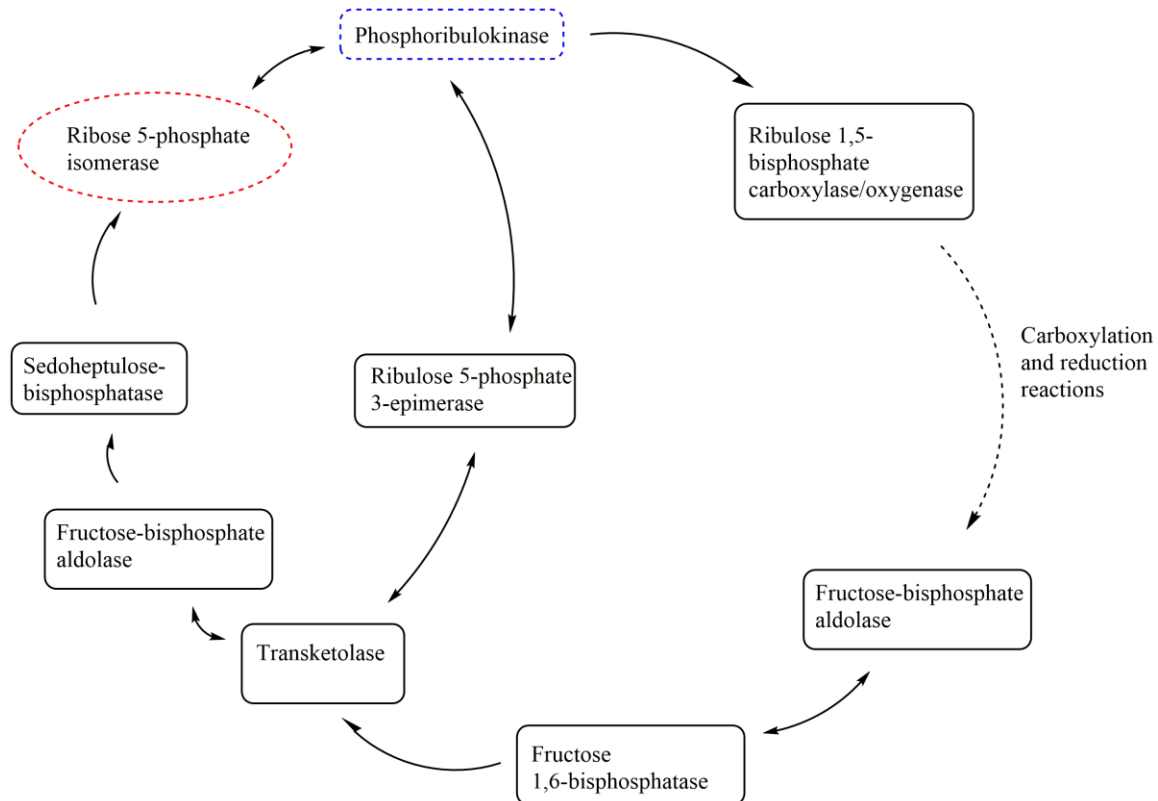


Figure 1.1 Simplified overview of enzymes involved in the regeneration of ribulose 1,5-bisphosphate in the Calvin cycle. The circular and square dashed boxes (Ribose 5-phosphate isomerase and Phosphoribulokinase) are enzymes that were focused on in this project.

RuBisCo can perform between 2 and 12 carboxylation reactions per catalytic site sec^{-1} , making it the rate limiting enzyme of the CBB cycle³⁷. This fact is compounded by undesired oxidation side reactions and strong inhibition by generated products, making RuBisCO the natural target of engineered improvements³⁵. As mentioned, manipulation to this enzyme is a challenging mission, as the enzyme structure and mechanism are both quite complex, with only a few papers reporting limited success in this area^{38,39}. A more immediate solution to the shortcomings of RuBisCO may be found by focusing on the extrinsic factors that affect CO_2 fixation in the cell.

RuBisCO functions in the stroma of the chloroplast *in vivo*, which is typically at a pH of 8. At this slightly basic pH level, CO_2 within the cell reacts with water and approximately 80 % will be found in the bicarbonate form⁴⁰. This must be converted to

CO₂ and then diffuse to the active site. CA must be present to aid in this conversion. Inhibitors may also be present, either in the form of products, or regulatory factors to control the cycle due to environmental fluctuations⁴¹. Much greater control over RuBisCO activity can be had by removing it from *in vivo* conditions and utilizing it under *ex vivo* conditions. Stabilizing factors and pH levels can be monitored and readily changed. Substrate concentration and product removal may be provided, while O₂ may be reduced or removed to mitigate unwanted oxidation reactions³¹.

The removal of RuBisCO for use in carbon sequestration is only a partial enzymatic solution. Substrate and cofactors must be regenerated to allow a continual process. Regeneration of the energy molecule ATP, which is a needed cofactor by several CBB enzymes, has been previously demonstrated in conjunction with carbon fixation⁴². RuBP may be purchased at \$206 CAD for 10mg. Assuming 100 % carboxylation of RuBP, the cost to sequester 1 tonne of CO₂ would exceed \$145 billion CAD. Regeneration or creation from 3PG, of this substrate would be absolutely necessary, and would require the 10 remaining CBB cycle enzymes to ensure generation or regeneration. At this point, the proposed CBB cycle will be completely *ex vivo*, imitating the original cycle within a controlled bioprocess, representing a biomimetic system.

1.3 Biomimicry

Biomimicry can be defined as mimicking natural products to improve man made materials, processes or structures. Nature has produced various chemicals, adhesion methods, antibacterials and other useful materials over the course of history. These products provide inspiration in a number of fields from pharmaceuticals and polymer chemistry to fashion and architecture⁴³. It is a multidisciplinary discipline that has gained momentum in the past two decades within the field of nanotechnology. Fabrication techniques used in forming complex silica nanostructures encountered limitations due to reaction process conditions⁴⁴. Spicules are able to be formed in nature by the sea sponge *Tethya aurantia* by way of a protein using biosilicification. The sponge uses the spicules for support, growth and to provide defense against predation. Following harvest and characterization of the protein responsible for this reaction, oligopeptides were later

synthesized, which mimicked their function in a reaction with silica^{45,46}. This allowed for synthesis of ordered matrices of silica under ambient conditions.

Enzyme bioprocesses have also been influenced by biomimicry. Mukai *et al.* (2013) were inspired by tethered enzymes found in mammalian spermatozoa⁴⁷. Enzymes involved in producing ATP to power flagellar motility are bound to fibrous sheath, which enables local ATP production, as sufficient ATP transport from head or mid-piece to the tail is not possible⁴⁸. These tethered enzymes are bound by specific domains, and not randomly attached to the sheath. The group immobilized two sequential enzymes used in glycolysis, by both biomimetic tethering via specific domains, and by a chemically specific but non-oriented method. They found that site specific immobilization resulted in higher specific activity (explained in detail in section 2.4) and coupled enzyme activity was 3.2-4.4 times higher in the forward and reverse direction respectively.

1.4 Project overview and objectives

Biomimicry offers inspiration for creation, or may influence improvements to existing systems. The effectiveness of a novel biomimetic technology can remain hindered by the intrinsic properties of the materials used. Biological catalysts are prone to degradation, susceptible to changes in pH and temperature, and subsequently lose activity over time⁴⁹. When Dr. Bhattacharya's group began looking into RuBisCO as a potential enzyme in a carbon fixation process, the group commenced with research into stabilization of the enzyme. Their goals were to increase the retention in activity over the soluble enzyme, enhance shelf-lives and prevent leaching³¹. Overcoming these challenges is important in marketing the technology to the industrial sector. They also foresaw the necessity in regenerating RuBP, and created a cascade of bioreactors to convert 3PG into RuBP. They achieved a yield of 56 %, compared to the 90 % predicted⁵⁰. They partly attributed this low yield to their approximation of kinetic modeling. It was also proposed that residual cofactors such as ADP (adenosine diphosphate) and NADH (nicotinamide adenine dinucleotide) used in previous conversions inhibited downstream reactions. Knowing the effects of cofactor concentration on kinetic parameters would allow insight into optimal operating conditions. Other conditions could be further optimized, such as

pH and temperature conditions, to increase the rate of RuBP production. In summary, an effective biomimetic carbon capture process is proposed, based on the CBB cycle, and should require the following:

1. Purification of the 11 enzymes found in the cycle required to bind CO₂ and regenerate RuBP.
2. Regeneration of cofactors required in the cycle, such as Nicotinamide adenine dinucleotide (NADH) and Adenosine triphosphate (ATP) to reduce the need for costly feedstocks to continue sequestration.
3. An appropriate bioreactor to facilitate CO₂ mixing with RuBisCO, and regeneration reactors will also be necessary for ATP generation and RuBP regeneration.
4. To produce useful downstream commodities such as glucose from the generated G3P molecules, several more enzymes and bioprocesses would also be needed³².
5. Investigation into the kinetic parameters of the enzymes is needed, which would allow for basic modeling and optimization of the system.
6. Investigation into how the variances in substrate, temperature, pH and cofactors affect the enzyme. These variances can be optimized and controlled to allow increased product turnover rates.
7. Research into immobilization of the enzymes is also a relevant endeavor. It was hypothesized that immobilization could both aid in stabilization of the enzymes over time and facilitate in recycling or removal of enzyme.

Out of these many requirements for a fully functional enzyme based carbon sequestration project, this thesis of research was conducted with focus on points 1,5,6 and 7, and included the following research goals:

- Discover a reliable source of purified phosphoribulokinase (PRK), as this enzyme was not available commercially.

- Characterization of soluble PRK and Ribose 5-phosphate isomerase (Rpi), in regards to their deactivation rates (half-life) and K_m values.
- Optimization of the process conditions of the soluble enzymes, it was hypothesized that the kinetic reaction rates for enzymes may be increased from initial assay levels.
- Investigatory research into the method of encapsulation, to immobilize the enzymes. The research interests included a demonstration of enzyme encapsulation and characterization of the immobilized structures. In addition, investigation into the protection afforded to enzymes, enhancement of stability, facile separation of products and enzymes and the effects of encapsulation on the half-lives, K_m values and kinetic rates of the enzymes in relation to their soluble forms was also to be pursued.

Chapter 2. Literature review

2.1 Enzymes and kinetic characterization

2.1.1 Expression and purification

Enzymes are sophisticated biological catalysts, which are largely composed of proteins. They may require metal ions, carbohydrates or nucleotides to achieve activity. Some can be highly specific in discerning between two stereochemical forms of a potential substrate, and are able to perform certain complex actions which inorganic catalysts are not capable of. There is a large aspect of evolutionary conservation in similar enzymes between species. Conserved genetic sequences are common, and parallels are often drawn between homologs⁵¹. Between these many homologs, kinetic parameters show as much variance, with some being much more rapid or efficient than

others. As these enzymes are essential in cellular processes, they may be utilized using *in vivo* whole cell techniques, or purified and utilized *in vitro*⁵².

Purification of enzymes allows for direct investigation of the reaction of choice, largely removes the potential inhibitory effects within the cell on enzymatic activity, and allows utilization of the formed products. Purification inevitably results in physical loss of enzyme at each purifying step, and the final protein solution will likely contain damaged and deactivated enzyme, resulting in a small percentage of final active protein when compared with the initial amount found in the cell. This necessitates a degree of control of the expression, to maximize the possible yield, as well as a planned purification scheme that preserves activity.

Several systems exist for protein production, the most common are typically bacterial or eukaryotic cell based. Cell-free protein synthesis has gained popularity over the past decade, but remains limited in use due to expensive reagent cost and low protein production rates⁵³. Of the cell-based systems, *E. coli* has proven to be the most popular. It has a very short doubling growth time of approximately 20 minutes, can achieve high cell densities, complex media for growth is inexpensive and many different strategies for expression exist due to its well documented physiology^{54,55}. Proteins that are sourced from another organism, or produced from manipulated DNA, and grown in another organism such as *E. coli* are called recombinant proteins. Extraction varies between each system. *E. coli* cells may be manipulated to secrete the enzyme of interest into media, or be broken through lysis to expose the enzyme. Following extraction, enzymes may be purified through affinity chromatography, size exclusion chromatography, and charge or hydrophobic based chromatography.

2.1.2 Kinetic characterization

Following purification, enzyme characterization may be performed. This can include studies on topics such as: substrate specificity, the effects of pH on enzyme activity, enzyme half-life, stabilities at increased temperatures and structural analysis. Characterization of an enzyme for use in a bioprocess tends to focus on kinetic based

properties, which may be detected through various methods such as spectroscopy or radioactive decay. Biocatalytic reactions *in vitro* are most often simplified and examined using the model proposed by Michaelis and Menten found in Equation 1⁵⁶:



Where E represents enzyme, S is substrate, ES is the enzyme-substrate complex, P is product, K_S is the formation rate of the ES complex and K_{cat} is the formation rate of product. This scheme makes several assumptions, a few of which are:

- 1) The enzyme concentration is negligible in comparison to substrate.
- 2) The substrate is always at equilibrium due to rapid diffusion, resulting in a constant concentration which ignores transport effects.
- 3) K_S , or the formation rate of the enzyme-substrate complex is reversible and rapid with no chemical changes occurring, resulting in a steady state concentration of the ES complex.
- 4) The concentration of product is negligible.
- 5) There is no spontaneous creation of product without enzyme.
- 6) The discrete nature of the particles is ignored and replaced with mean-field concentrations⁵⁷.

K_{cat} is the second step rate constant, and is assumed to only occur in the forward reaction. It indicates the number of substrate molecules that one enzymatic site converts to product per unit of time, and is called the enzymatic rate constant. Under the assumed conditions above, the reaction rate follows saturation kinetics. The reaction rate is the rate of consumption of substrate per unit of time, and is considered zero-order. These conditions are only valid during a short window of time, when the product has not accumulated in significant amounts, and where the enzyme-substrate complex is assumed to not change. These conditions are also assumed to be *in vitro*, as *in vivo* kinetic modeling has been found to not agree with these assumptions⁵⁷. At this steady state, the

initial reaction rate, or v_0 , is what is typically measured and used in characterizing the reaction. This term is used interchangeably with activity. An equation describing the rate may be derived from Equation 1 and is found below⁵⁸:

$$v_0 = \frac{V_{max}[S]}{K_m + [S]} \quad (2)$$

Where v_0 is the initial reaction rate, V_{max} is the maximal reaction rate and K_m is the concentration of substrate where the reaction may reach half of V_{max} under saturating substrate conditions. K_m is generally known as the Michaelis constant, and is commonly used as a relative measurement of substrate binding efficiency. A small value of K_m indicates a high affinity of substrate to the enzyme.

Modeling kinetic characteristics by the Michaelis-Menten method is used in bioprocesses; however, there are some shortcomings to this model⁵⁰. The assumptions listed do not hold true in realistic situations. Diffusion limitations are present in a real world application, such as a bioprocess incorporating immobilized enzymes⁵⁹. Some product will likely be present prior to addition of enzyme, either due to spontaneous conversion or due to an impure feedstock. More appropriate and complex modeling equations may be adopted, to include other factors such as enzyme deactivation and equilibrium effects⁶⁰.

2.1.3 Coupled assays and calculation methods

For some enzymatic reactions, direct measurement of either consumption of substrate or formation of product is not possible. These reactions are often coupled with one or more auxiliary enzymes, which consume a product of the reaction of interest (the intermediate), and are directly measurable. Several assumptions are made for these systems: the rate constant (K_{cat}) of the initial reaction of interest is zero-order and irreversible, the coupled reactions are irreversible and first-order with respect to the concentration of the product of the initial reaction⁶¹. As a condition, the initial enzyme must be the rate-limiting step in the sequence in order to be accurately measured⁶². As a

linear rate is dependent on a steady state of the intermediate, a transient lag phase is typically present in coupled systems, as intermediate substrate must accumulate in significant amounts.

Cleland (1979) demonstrated that the observed rate of reaction approaches 99 % of the v_0 at a point 4.6 times the length of the induction, or lag phase⁶³. This entire phase is called the total lag phase. The length of the phase is related to the amount of secondary enzymes present, as well as the characteristics of the secondary enzymes. Some may form non-active oligomers at storage concentrations, only to dissociate into active monomers under working assay concentrations⁵⁸. Following this lag phase, v_0 may be measured at varying concentrations of substrate, and should be found to be at a steady state. In the past, the range of collected data, initial velocities and substrate concentrations, would be linearized and plotted against each other. There are several methods of linearization, the most used of which was proposed by Lineweaver and Burk (1934)⁶⁴. After applying a linear fit, the kinetic constants K_m and V_{max} are determined from the slope and intercept. This method is heavily reliant on calculated velocities at low substrate concentration, which is where the relative errors of gathered data are likely to be greatest⁶⁵. These associated errors can result in biased and indirect constants for maximum velocity and K_m . The non-linear least squared method of kinetic constant determination has been presented as a superior method in comparison to the double-reciprocal methods⁶⁶.

Following these calculations, and knowing the concentration of enzyme added, the rate constant K_{cat} may be calculated by dividing V_{max} by the number of catalytic sites of E present in the solution. The rate constant is also referred to as the turnover number, which provides the number of conversions of substrate to product that a single catalytic site may perform per unit of time (typically seconds). Another unit to represent the purity and activity of an enzyme is specific activity. This gives the amount of product formed in moles, in a certain amount of time, per milligram of enzyme, and should remain constant for pure enzyme. Specific activity may decrease if the some of the enzymes become inactive or denatured. Finally, enzyme activity may also be denoted by the term enzyme

unit. One unit (U) is the amount of enzyme that will catalyze the conversion of one micromole of substrate in one minute. The conditions are of the conversion are needed, as pH and temperature will affect the reaction.

2.1.4 Enzyme lifetime

The operational stability of an enzyme may be estimated by its half-life, which is the amount of time that has passed when the catalytic activity, or reaction rate v_0 , is reduced to half its original amount⁶⁷. This parameter governs the feasibility of using the enzyme in a bioprocess. It also allows greater control over the process step, as one may accurately estimate the amount of active enzyme remaining, and establish lower thresholds to prevent a bottleneck in the process. For one enzyme, estimation of this point in time will vary depending on a variety of factors such as enzyme concentration, temperature and pH conditions and stabilizing factors such as inhibitors or protecting agents. Different complex models of deactivation have been proposed for these factors and others⁶⁸. For deactivation of soluble enzymes, assuming no factors besides intrinsic degradation over time are involved, the single-step, first order deactivation scheme shown in Equation 3 is most often employed:



where E is the initial, active enzyme, E_d is the inactivated enzyme, and K is the enzyme deactivation rate constant. The assumption is made that the initial state of E is homogenous, and that at time (t)=0 all enzyme present is in the active state. An equation of normalized activity at time=t may be derived⁶⁸:

$$A = A_0 e^{-Kt} \quad (4)$$

where A is measured activity, A_0 is activity at time=0, e is Euler's number and t is time. Assuming a constant deactivation rate, the time taken by the enzyme to lose half of its activity is expression by the equation:

$$t_{\frac{1}{2}} = \frac{\ln 2}{K} \quad (5)$$

A common, less time intensive method of demonstrating operational stability is to use thermal deactivation. By increasing the temperature above the enzymes normal operating range, the enzyme will deactivate at a faster rate. The variation in enzyme activity was typically described using Equation 6⁶⁹:

$$V_{\max} = K_{\text{cat}} \times [E_0] \times e^{-k_{\text{inact}} \times t} \quad (6)$$

where V_{\max} is the maximal reaction rate, K_{cat} is the formation rate of product, E_0 is total concentration of enzyme, e is Euler's number, k_{inact} is the thermal inactivation rate constant and t is assay time. Activities are typically reported as a percentage of the enzymatic activity at $t=0$. The Equilibrium model was recently proposed, wherein a third temperature dependent property of enzymes was introduced by Peterson *et al.* (2004)⁶⁹. They modeled and demonstrated through experimentation, that active enzymes exist in a reversible equilibrium at a certain temperature (T_{eq}) with inactivated enzymes. Below this temperature the previous thermal deactivation model holds true. Above T_{eq} , the inactive enzyme will irreversibly denature, to remain permanently inactive. This rate in decrease may be up to two orders or magnitude greater than thermal denaturation below T_{eq} , and should be taken into consideration when using thermal deactivation information based on the outdated model.

Lifetime of an enzyme may also be quantified by a number of cycles. A cycle involves the enzymes activity being measured during a process or assay, followed by the separation of products from the enzyme, to begin a new separate cycle. This may be presented as a variation of half-life, as activity is typically reported for each cycle and compared to the initial cycle. Immobilized enzyme systems often report effective activity over a number of cycles. Camila *et al.* (2011) reported that 70 % of the enzyme lipase was active following 10 cycles of use when immobilized on chitosan microcapsules⁷⁰.

Wang *et al.* (2012) created a polymersome Pickering emulsion system with encapsulated lipase that retained up to 89 % of its initial activity following eight cycles over a period of eight days⁷¹. Reporting lifetime in this fashion will include the inactivation of the enzyme over time as well as loss of enzyme during product or enzyme removal.

2.1.5 Ribose 5-phosphosphate isomerase

Ribose 5-phosphate isomerase (Rpi) catalyzes the reversible conversion between ribose 5-phosphate (R5P) to ribulose 5-phosphate (Ru5P), and plays a crucial role in cell metabolism⁷². The enzyme is present in all three kingdoms of life, and is found in both the Calvin cycle in plants, as well as the pentose phosphate pathway in plants and animals. The enzyme has been sequenced from more than 60 species, and several protein structures have been solved^{73,74}.

Species	K_m (R5P mM)	K_{cat} (s^{-1})	Assay conditions
<i>Trypanosoma cruzi</i> ⁷⁵	4 ± 1	12 ± 5	pH 8.4, 25 °C
<i>Escherichia coli</i>	4.4 ± 0.5 ⁸¹	2100 ± 300 ⁷³	pH 7.5, 37 °C
<i>Pyrococcus horikoshii</i> ⁷⁶	1.2 ± 0.4	330 ± 29	pH 6, 50 °C
<i>Spinacia oleracea</i> ⁷⁷	0.63 ± 0.05	3440 ± 60	pH 8, 25 °C
<i>Clostridium thermocellum</i> ⁷⁸	17 ± 0.4	51998 ± 1423	pH 7.5, 65 °C
<i>Mycobacterium tuberculosis</i> ⁷⁹	1.0 0.4	50 ± 20	pH 7.5, 37 °C

Table 2.1 Selected kinetic parameters of Rpi from different species

In *E. coli*, there are two forms, RpiA, which is constitutively expressed, and RpiB which is a redundant protein formed via inductive pathways. *E. coli* RpiA has been previously shown to be more resistant to heat inactivation than RpiB, indicating that is likely more stable than RpiB due to its intrinsic properties^{80,81,82}. As such, this enzyme was chosen for study in this work, and henceforth the abbreviated Rpi will refer to the *E. coli* RpiA enzyme unless otherwise stated.

When catalyzing the reaction toward Ru5P, the enzyme binds to the open form of R5P, and moves a proton from the C2 carbon, generating an intermediate *cis*-1,2-enediol(ate), and releases the proton at the C1 carbon. At the same time, the protein group opposite the active site transfers a proton from O2 to O1 of the sugar, which results in the

final form of Ru5P (Figure 2.1). The stabilization of the transient enediolate intermediate via protein group interactions is paramount in reducing the activation energy barrier⁸³.

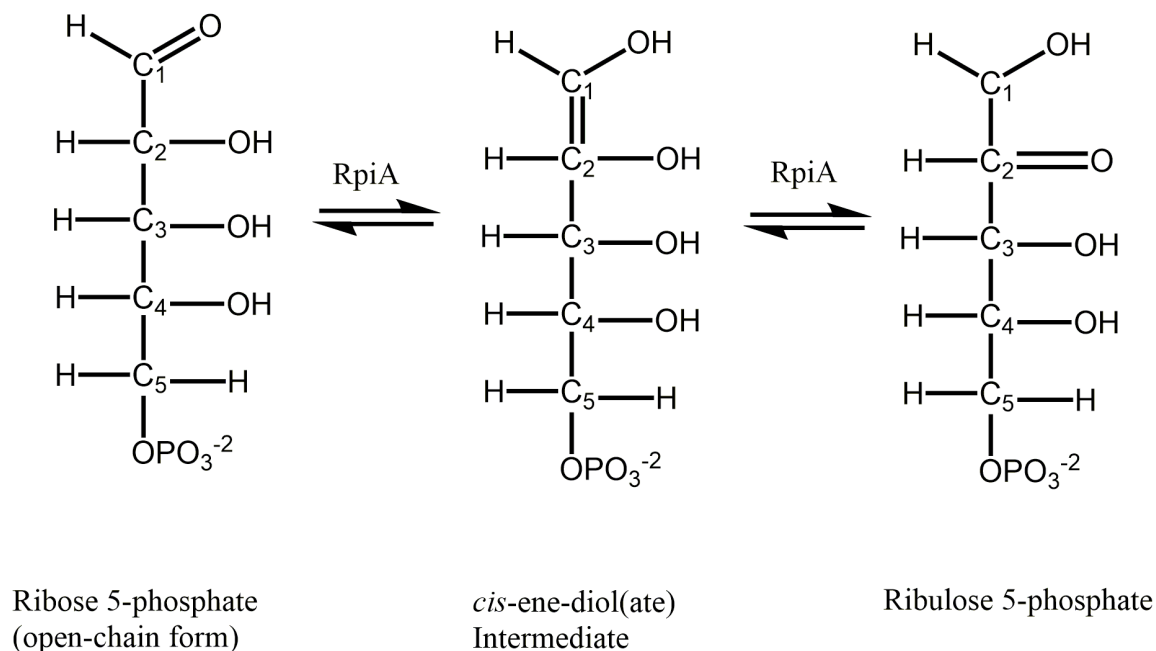


Figure 2.1 Reaction mechanism for RpiA catalysis.

Process requirements

The 22 kilodalton (kDa) unit must form a homodimer to enable functionality⁸⁰. It has been shown to be functional over a range of pHs, from 7 to 7.5, as well as a range of temperatures, from a low of 20 °C to a high of 37 °C^{83,84,85}. Several inhibitors have been found to reduce activity of the forward reaction to form Ru5P. Adenosine monophosphate (AMP) has been found to inhibit Rpi kinetic activity by approximately 30 %^{80,81}. Glucose-6-phosphate inhibits the kinetic activity by 17 %⁸¹. Several other molecules have been reported, along with their respective inhibitor constants (K_i), which is the concentration required to produce half-maximum inhibition⁷³. These molecules include D-erythrose-4-phosphate (0.67 mM), D-erythronic acid (0.32 mM) and D-4-phosphoerythronic acid (4 μM). As the reaction catalyzed by Rpi is reversible, with an increase in product concentration, the enzyme will catalyze the reverse reaction of Ru5P to R5P. Equilibrium between the two molecules at room temperature and *in vitro* is reached when Ru5P constitutes 24.4 % of the sugars, with R5P forming the remainder⁸⁶.

A variety of buffering agents have been employed in published Rpi kinetic results, such as sodium borate⁸¹, Tris-HCL⁷³ and potassium phosphate⁸⁴. There has been no investigation into the effects of differing buffer agents on the apparent kinetic activity.

Alternative enzymes

In the Calvin cycle, Ru5P is an intermediate product, which may be formed from either of two pathways in the regeneration of RuBP (Figure 1.1). Phosphopentose epimerase (also known as ribulose-phosphate 3-epimerase or PPE) catalyzes the reversible conversion of xylulose 5-phosphate (X5P) to Ru5P. Both PPE and Rpi are required to fully convert the 5 triose-phosphates formed following the fixation of six molecules of CO₂, during the regeneration of RuBP. If one enzyme were to not be present, a metabolic dead end would occur, severely reducing the effectiveness of the conversion process, as RuBP would not be fully replaced following a cycle. In addition, without the removal of products that would occur if both enzymes were present, product inhibition could reduce the reaction rate of the remaining enzyme.

PPE sourced from *Oryza sativa*, and grown recombinantly in *E. coli*, was used to convert X5P to Ru5P by Bhattacharya *et al.* (2004) in the regeneration of RuBP⁵⁰. The enzyme was immobilized on nylon beads, and was found to be active at a pH of 8 and temperature of 25 °C. Only one PPE variant, sourced from *Spinacia oleracea* (spinach), has a faster turnover rate than *E. coli* Rpi, reported at 7100 molecules/second compared to Rpi at 2100 molecules/second. While this more rapid turnover rate appears attractive, this PPE protein which was produced recombinantly in *E. coli* has been shown to have an extremely limiting half-life of approximately 25 minutes at 2 °C without the presence of additives⁸⁷. The sole additive that was found to effectively stabilize the enzyme is the competitive inhibitor G3P. This molecule is a product of the earlier reduction pathway portion of the Calvin cycle (see section 1.4). Using this highly unstable enzyme in place of Rpi would thus require separation from G3P prior to use, to prevent inhibition.

Factors affecting enzyme activity

As mentioned throughout section 2.1, a variety of factors may affect the operating stability of an enzyme. There have been no published reports on *E. coli* Rpi stability at

storage (~4 °C) or ambient (~20 °C) temperature; however, a report on the thermal stability of *E. coli* Rpi at elevated temperatures has been previously published by Essenberg *et al.* (1975), who incubated Rpi and measured activity retention⁸¹. After 30 minutes at 45 °C, Rpi retained 90 % of its initial activity. At 60 °C the enzyme retained ~30 % of its initial activity after 30 minutes. This indicates that Rpi is susceptible to increased temperatures, and will retain partial activity at temperatures well above those found *in vivo*.

The same group also briefly reports that at concentrations below 0.026 units/mL and above 2.6 units/mL, all activity was lost after a 15 minute exposure at 60 °C, while intermediate concentrations between (0.13-1.9 units/mL) the enzyme retained ~30 % activity. This suggests that enzyme concentration plays a role in the stability of Rpi. This was the case with Rpi purified from tobacco plants reported by Kawashim and Tanabe (1976)⁸⁸. They report that when Rpi was incubated in the presence of both magnesium (Mg²⁺) and a variety of proteins, Rpi could retain all of its initial activity. No further factors have been investigated in literature concerning factors that may affect the stability of *E. coli* Rpi.

2.1.6 Phosphoribulokinase

Phosphoribulokinase, or PRK, is one of the two unique enzymes involved only in Calvin cycle processes (the other being RuBisCO). It catalyzes the conversion of Ru5P to Ribulose 1,5-bisphosphate (RuBP). The enzyme has been prepared from both eukaryotic and bacterial sources, with a sequence identity of conservation of approximately 10 % between all sources⁸⁹. This diversity is further evident in the quaternary forms, as some enzymes form dimers, tetramers and others octomers. One structure has been solved, for PRK from *Rhodobacter sphaeroides*⁹⁰. Three recombinant forms of PRK have been expressed successfully thus far in *E. coli*, from *Rhodobacter sphaeroides*, *S. oleracea* and *Synechococcus elongatus*^{91,92,93}. Of these three, published specific activities are known only for *S. oleracea* and *S. elongatus* at 410 and 230 $\mu\text{mol}/\text{min}/\text{mg}$ respectively^{94,95}.

Species	K_m (ATP, μM)	K_m (Ru5P, μM)	K_{cat} (Ru5P s^{-1})	Assay Conditions
<i>Chlamydomonas reinhardtii</i> ⁹⁶	33.8 ± 6.0	87.5 ± 5.2	262 ± 4.3	25 °C
<i>Synechococcus elongatus</i> ¹⁰³	90	270	11.4 ^a	pH 8, 25 °C
<i>Odontella sinensis</i> ⁹⁷	84 ± 6.5	118 ± 13	110 ± 5^b	pH 8
<i>Heterosigma carterae</i> ⁹⁸	208	226	37 ^c	pH 8, 25 °C
<i>Spinacia oleracea</i>	625	222	100 ^d	pH 8, 25 °C

Table 2.2 Selected kinetic parameters of PRK from different species. a, b, c and d are approximations of K_{cat} using specific activity data, and were calculated⁹⁹ using molecular weights of 37.7⁹⁵, 44⁹⁷, 41.3⁹⁸ 38.9 kDa¹⁰⁰ respectively.

PRK will catalyze the transfer of the γ -phosphoryl group from an ATP molecule to Ru5P, with no enzyme intermediate being involved in the in-line transfer (Figure 2.2)¹⁰¹. The reverse reaction will occur in the presence of RuBP and ADP¹⁰². Wadano *et al.* (1998) suggest that the enzyme binding follows an ordered bi bi mechanism, with the Mg-ATP complex binding before Ru5P in PRK from *S. elongatus*¹⁰³. Lebreton *et al.* (1997) propose an ordered reaction where Ru5P first binds, followed by ATP¹⁰⁴. Other studies have suggested that a stable PRK-ATP complex forms prior to Ru5P binding, leading Mizioroko to suggest that it is unclear whether substrate binding must follow an ordered fashion³⁵.

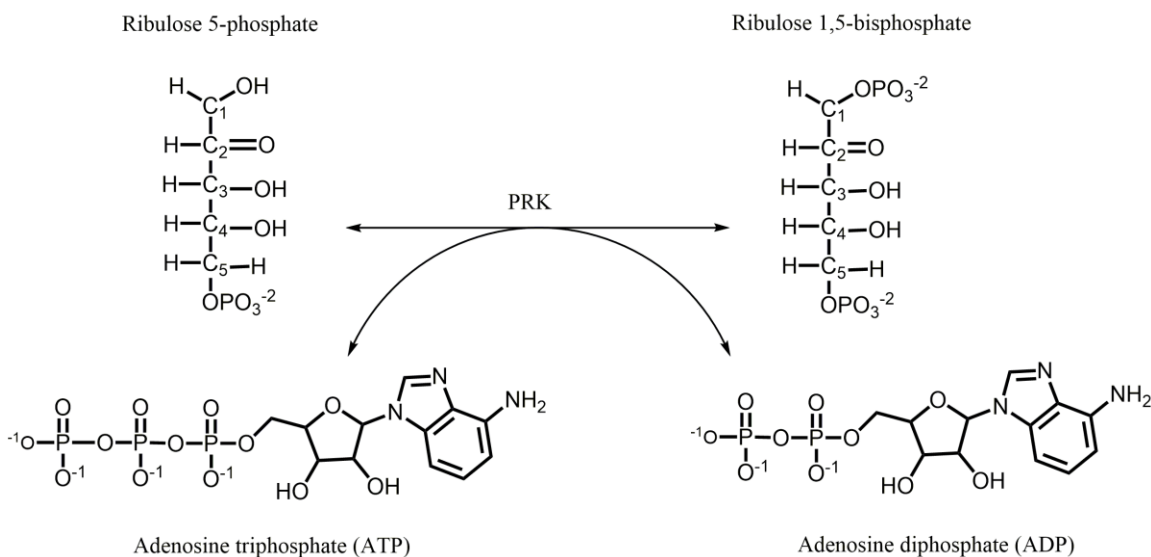


Figure 2.2 Reaction mechanism of PRK

Process requirements

The effects of pH on spinach PRK was investigated by Hurwitz *et al.* (1956)¹⁰⁵. They found that the optimum pH was 7.9, and its activity was severely affected by either an increase or decrease by as little as a 0.5 units. MacElroy *et al.* (1972) investigated the effects of the substrates used in a coupled assay for PRK, with the protein being sourced from *Halothiobacillus neapolitanus*¹⁰⁶. They found that when the secondary component phosphoenolpyruvate was added, the pH optimum of PRK shifted from 7.9, to 8.4. When this was investigated in PRK from spinach, no such shift occurred from the established pH level of 7.9. Surek *et al.* (1985) demonstrated that PRK from *Triticum spelta* exhibited optimal activity over a short range from pH 7.75 to 8.4¹⁰⁷. The temperature used to assay PRK is typically set at 25 °C¹⁰³. No works were found which reported on the effects of temperature on PRK activity.

Cyanobacterial PRK contains two consensus cysteine residues that correspond to regulatory residues in higher plant PRK variants such as spinach. This regulatory site is highly sensitive in higher plants, and oxidation leading to thiol bond formation precludes activity. In cyanobacterial PRK, the use of a reducing agent, such as dithiothreitol (DTT), was shown to not be a necessary factor for enzymatic activity by Tamoi *et al.* (1997)¹⁰⁸. Kobayashi *et al.* (2003) incubated *Synechococcus* PRK in the presence of 5,5'-dithiobis-(2-nitrobenzoic acid), an oxidation agent for five minutes⁹⁵. This action led to a complete inactivation of the enzyme, which was then nearly completely recovered following incubation with DTT to reduce the disulfide bond. These findings suggest that a reducing agent is not necessary for bulk activity; however, if complete oxidation is to occur, the enzyme will become inactivated. As such, a reducing agent is typically included to ensure complete activity of cyanobacterial PRK, and is necessary for PRK sourced from higher plants. In addition, the metal cofactor magnesium is essential for the activity of PRK, and no reaction will occur in its absence¹⁰⁹. This is likely due to ATP existing largely as an Mg-ATP complex in the cell¹¹⁰.

Several inhibitors of PRK activity have been reported on. In the presence of 6 mM 3PG, PRK exhibited a 74 % loss in activity¹⁰⁷. 6-phospho-D-gluconate and AMP

have K_i values of 0.22 mM and 80 μ M respectively^{111,112}. The products of the forward reaction, ADP (0.32 mM¹⁰³, 4.2 mM¹¹²) and to a lesser extent, RuBP (10 mM), are inhibitors of the forward reaction. No equilibrium constant between the products RuBP and Ru5P have been reported from *in vitro* studies. *In vivo* equilibria will vary depending on regulatory factors influenced by the cells environment. One group reported a concentration of 5.2 ± 1.1 mM RuBP in relation to 0.06 mM Ru5P¹¹³. Phosphoenolpyruvate (PEP) has been reported to be an allosteric inhibitor (binds at a location other than the active site) in some bacterial PRK's. PRK from *Rhodospseudomonas acidophila* has a K_i of 0.32 mM, and from *Chlorogloeopsis fritschii* there was complete inhibition at 1 mM¹¹⁴.

Alternative enzymes

RuBisCO has been found to be expressed in some forms of anaerobic archaea, without the presence of homologue genes for PRK¹¹⁵. This pathway requires an alternative method to replace RuBP. Finn and Tabita (2004) suggest that two enzymes convert precursor molecules to RuBP¹¹⁶. The first enzyme, encoded by the gene *Mj0601* found in *Methanocaldococcus jannaschii* is suggested to be an isomerase, and converts ribose 1,5-bisphosphate (R15P) to RuBP. The second, encoded by *Ma2851* in *Methanosarcina acetivorans* converts 5-ribose-1,2-cyclic phosphate to RuBP as a synthase homolog. These two enzymes were not successfully purified in their active forms, although they were successfully expressed in *E. coli* and were found to be active in the cell extract. No further research has been produced on either of these enzymes.

Another archaeal species, *Thermococcus kodakarensis* also exhibits RuBisCO activity. Imanaka *et al.* (2007) were able to isolate the enzyme ribose 1,5-bisphosphate isomerase, which produces Ru5P¹¹⁷. It followed the reaction proposed for *Mj0601* by Finn and Tabita, catalyzing the conversion of R15P to RuBP. The substrate R15P is a product of AMP degradation, as Archaea use AMP forming kinases in glycolysis. This large pool of AMP is recycled into another metabolic pathway. R15P isomerase would not make for an ideal enzyme to produce Ru5P. This is because the precursor, R15P, is

not commercially available, and needs to be synthesized either enzymatically using AMP and the enzyme AMP phosphorylase, or via chemical synthesis¹¹⁸. This would not allow for a cyclical CO₂ conversion process.

Factors affecting stability

Racker (1957)¹⁰² reported that a solution of purified spinach PRK from lost 50 % of its activity following a 3 hour incubation at room temperature. When this solution had a supplemental reduction agent and 0.1 % serum albumin added, the activity was not lost. Kamber *et al.* (1998)¹¹⁹ report that PRK measured in spinach cell extract lost the same amount of activity after 68 minutes when kept at a temperature of 25 °C. They report that the addition of the substrate ATP and a reducing agent contributed to enhanced stability of the enzyme. PRK from these reports would be highly susceptible to oxidative inactivation in the absence of a reducing agent. This inactivation can be reversed, and does not represent true denaturation, which is typically what is meant by stability¹²⁰. Recent work has shown that PRK and another CBB cycle enzyme, glyceraldehyde-3-phosphate dehydrogenase, form a supramolecular complex in the presence of the regulatory peptide CP12¹²¹. The study suggests that this is for regulation of activity. After dissociation, PRK retained 100 % of its initial activity after several hours at 4 °C. Association with these proteins and others such as albumin in solution, along with the substrate ATP, appear to stabilize the enzyme over time.

2.2 Optimization methods

To establish the local optimal, one may perform what is referred to as a method of steepest ascent to find an approximated optimum. This method reveals which factors are significant enough to warrant further investigation, based on the effects of the chosen factor levels. This gradient method was first proposed by Augustin-Louis Cauchy, who used it to solve a non-linear regression problem in relation to his astronomical works¹²². This is a first order regression model, which does not investigate the interaction of individual factors, only the main effects of their levels on the outcome. It allows one to find the general approximation of direction, which will lead towards the vicinity where the subsequent second order experiment will take place.

An example of this first order method was employed in the immobilization of the enzyme β -galactosidase by Guowei Shu *et al.* (2014), when binding the proteins onto chitosan beads¹²³. The group made use of a Plackett-Burman design to first screen for important factors, which influenced the activity. This was followed by a steepest ascent experiment, which resulted in an overall increase of activity of approximately 37.6 % when compared to their initial rates.

Srivastava *et al.* (2011) investigated the effect of both pH and temperature on the activity of urease immobilized onto gold nanoparticles using the gradient method¹²⁴. They were able to show that the bound enzyme exhibited greater activity, at a threshold 5 °C higher than the free enzyme. The method also revealed that bound enzyme had greater activity when compared to the free enzyme from pH 5-6.5. They followed up on their findings with a second order model, in this case using a response surface factorial design to find the global maximum rate.

As the local maximum is approached using the gradient method, the model used will require step increments to decrease. This will either yield diminishing results, or produce a model that demonstrates a lack of fit. This could be due to second order (quadratic) effects which are present in the system. These effects can be investigated by expanding the one-dimensional gradient method into two dimensions by employing axial runs. This leads into the realm of response surface methodology (RSM), which provides statistical insight into the relationship between several factors and the response, while reducing the number of runs needed compared to full factorial methods when investigating many factors and levels.

There are two dominant response surface designs that are routinely used in optimization: Box-Behnken and Box-Wilson central composite design (CCD). The differences between the two methods are very minor at a glance. Box-Behnken (Figure 2.3) requires fewer runs when there are up to four factors being investigated. It also avoids runs with extreme settings by limiting runs to three levels per factor, whereas CCD requires five, of which the two extremes could be costly under some circumstances.

Box-Behnken does not contain a factorial design, so one must begin a new experiment if this follows a gradient method.

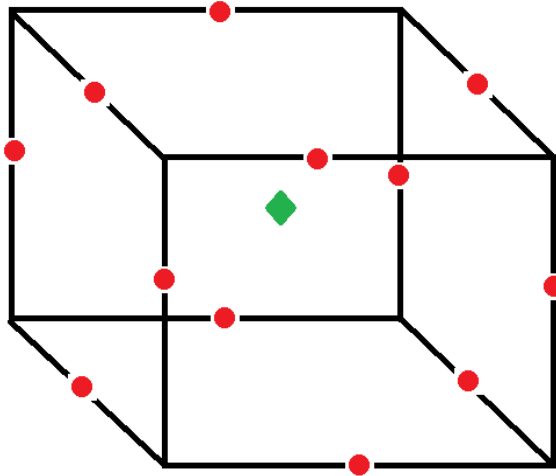


Figure 2.3 Geometry of a Box-Behnken design. Collection points are located at the midpoint of the designed edges, with a centre point to aid in prediction of variance.

This design method was successfully employed by Su *et al.* (2010) who had non-covalently bonded lipase with polyethylene glycol¹²⁵. The group optimized the activity of the lipase by first investigating the variables using the gradient method. Having found the relevant factors, they followed up with a Box-Behnken designed experiment.

Circumscribed central composite design is a continuation along the theme of the gradient method. It allows one to use the relevant data along the factorial corner points, followed by a design that includes central and axial points. Axial distances are determined as a function of the number of factorial runs, which is defined as α , in order to establish rotatability. Rotatability ensures constant predictability, as all axial points are now equidistant from the centre point. The circumscribed design can be troublesome if the axial points are at an extreme level, such as being close to zero or very high. It may be difficult to simulate these extreme environments, in which case there are two alternate

versions of the CCD, namely inscribed and face-centered. These versions offer the benefit of less extreme axial points kept within the established factorial limits of ± 1 , which are now located on the "face" of the square of the factorial square. These alternate versions will not be discussed further, in favour of the augmented circumscribed design.

Responses at each point are collected, and with the aid of computer software, regression equations are estimated to fit a second-degree statistical model. This yields information relative to the linear effect of the factors, curvilinear effects, and interactive effects between factors. The generated model must be tested for accuracy in its predictive outcomes.

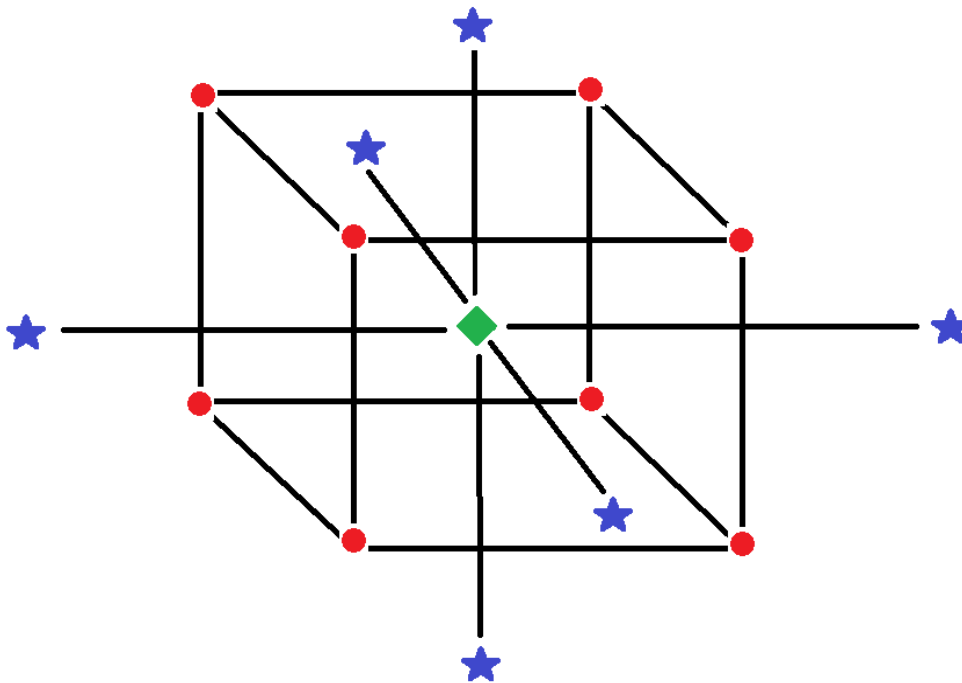


Figure 2.4 Geometry of a circumscribed central composite design. The diamond is the centre point, with stars representing axial points. Circles are factorial points on the corner of the box.

Hamsaveni *et al.* (2001) investigated the effects of process condition levels on the activity of immobilized lipase using a central composite designed experiment¹²⁶. Their model achieved a high coefficient of determination, indicating the suitability of the model in predicting the relationship between factor levels. The synthesis of the product was

optimized, and the group achieved a 325 % increase in product over the central (control) points.

2.3 Improving enzymatic stability

Enzymatic reactions take place within the interior of an organelle, cytoplasm of a cell, or in an extracellular environment. Many enzymes have come about through evolution to play very specific roles, which are necessary for the organism's survival. As such, they are produced as needed, and often maintained in environments where they may operate efficiently and for as long as needed. These contained microenvironments in the cells are often specific organelles. Within an organelle such as a chloroplast, the protein concentration can be up to 400 mg/mL. This tight packing affects reaction equilibria, as and has been linked to increased stability of enzymes¹²⁷. There are conflicting reports as to how confinement affects activity of enzymes¹²⁸.

Within the concentrated volume of an organelle, sequential reactions are able to occur much quicker than if a substrate had to diffuse to the other end of the cell for the next reaction¹²⁹. This is highly dependent on locality of enzymes involved in a sequential reaction, as diffusion rates are slower. This can prove to be a boon for reactions that require more than the substrate alone, such as organic or inorganic cofactors. The products themselves may be then competed for by several different enzymes, such as is the case with the molecule malonyl-coenzyme A, which is a precursor in both fatty-acid and flavonoid biosynthesis¹³⁰. By containing the metabolite within one location, it can then be accessed equally by the two separate enzymatic pathways. By compartmentalization of these reactions, nature has provided an optimal location for both the enzyme to reside, the reaction to occur, for products to be contained and used¹³¹.

As enzymes are typically removed from this stabilizing environment for use in downstream processes, their new environment is drastically different when compared to *in vivo* conditions. Being placed in aqueous or organic solutions, the stabilizing effects of ionic molecules and various proteins may be missing, with their benefits being entirely unrecognized unless having been previously studied. The enzymes very nature may also

be short lived, on the order of minutes for some¹³². The enzyme may not be thermostable at the temperature required by the downstream process, or the temperature required by the enzyme to optimally function may be cost inhibitive to the process. These, and other issues associated with stability can potentially be overcome in several ways.

Enzymes may be screened from thermal tolerant species, which often contain thermostable enzyme variants. This is commonly carried out using bioinformatics software for genomic library screening to search for variants with conserved homology, or through directed evolution of enzymes, where mutations are induced in hopes of producing enzymes with desired properties^{133,134}. Screening is a time consuming effort, and gambles with the prospects of decreased activity, less specific reactions and difficulty in expression and purification. If ample enzyme of interest has been previously purified, is it possible to enhance its stability *in vitro*, and ameliorate shortcomings, through modification techniques collectively titled immobilization.

2.4 Immobilization

Technique	Enzyme	Advantages	Disadvantages
Binding via affinity tag	β -galactosidase ¹³⁵	Simple, cost effective.	Requires genetic modification, may affect enzyme structure and function
Covalent binding	Oxygenase ¹³⁶	Simple, cost effective	Inactivation, orientation must be controlled
Cross linking	Penicillin G acylase ¹³⁷	Stability, increased turnover rate	Denaturation may occur under harsh conditions, difficulty in recovery
Entrapment	Lipase ¹³⁸	Stability, easy recovery	Enzyme leakage, low immobilization efficiency, substrate diffusion difficulties
Encapsulation	Peroxidase ¹³⁹	Retain natural conformation, resistant to proteolysis	Difficult to scale up to large volumes, low encapsulation efficiency (maximum of 40 %)

Table 2.3 Comparison of immobilization techniques.

Immobilization has been described by Brena and Batista-Viera as "enzymes physically confined or localized in a certain defined region of space with retention of

their catalytic activities"¹⁴⁰. Immobilization can take many forms, from covalent attachment to nanoparticles to cross-linked enzyme aggregates^{141,142}. A few are briefly highlighted in Table 2.3. The various techniques cover a large selection of materials and enzymes, with varying degrees of success. There is no clear, unified solution to the question of which immobilization method to employ. Methods vary in apparent strengths and weaknesses depending on the process of interest and desired enzyme trait improvements. There is no scheme to predict the results of enzyme immobilization, results at present may only be obtained through experimentation.

For a process in which natural enzyme activity must be retained as much as possible, entrapment and encapsulation would be ideal choices, as they do not require modification of the enzyme itself, and preserve mobility¹⁴³. Entrapment involves enclosing the enzymes "in a surrounding lattice/matrix structure" while encapsulation sees enzymes captured within a type of small capsule¹⁴⁴. Entrapment typically uses polymer gels and beads to entrap enzyme. Reliance on a porous network can present diffusion limitations on substrate entering and product leaving through intricate structures¹⁴⁵. The molecules may suffer from a reduction in mass transfer. This can be overcome by increasing the surface area to volume ratio, which is naturally higher in nano-sized encapsulation techniques when compared to typically micro-sized entrapment structures¹⁴⁶. Entrapment also suffers from long gelation times, from hours to weeks, and the method of structure synthesis must be biocompatible¹⁴⁴ or may require robust enzymes which can endure solvents used in the reaction¹⁴⁷. Finally, they commonly encounter leaching problems and make use of carrier materials which are ill suited for reactor processes^{148,149}.

2.5 Encapsulation

Encapsulation of enzymes was the immobilization method which was ultimately chosen for the work in this thesis. As mentioned in sections 2.1.6 and 2.3, stability is dependent on protein concentration. Enzyme encapsulation takes place under milli to micromolar concentrations of enzyme. Following purification steps, the internal concentration will remain at these more stabilized, initial levels. Working assay

concentrations of enzymes are typically in the nano-molar range. Dilution of encapsulated enzymes will not affect these interior concentrations. Nasseau *et al.* (2001) showed that diluted, encapsulated acetylcholinesterase (AChE) could retain 100 % activity after 5 hours, compared to the diluted free enzyme which lost up to 50 % at a concentration of 0.1 nM¹⁵⁰. Vamvakaki *et al.* (2007) later demonstrated that encapsulated AChE, independent of concentration factors, retained nearly 100 % activity after 50 days of storage, compared to the 44 % of the free enzyme¹⁵¹.

Encapsulation involves the use of either biological or polymeric materials. Lipid encapsulation has been in use since 1971, and is a well-established method of encapsulation¹⁵². As carriers, they have been used for drug loading and release, receptor mediated endocytosis, nucleic acid delivery and enzyme compartmentalization¹⁵³. Liposomes have been found to increase the stability of enzymes, and are able to be formed under ambient conditions with encapsulation efficiencies approaching 30-40 %^{148,154}.

Lipids in nature are used as barriers for separation of environments and protection. As such, they have a low tolerance for passive diffusion of large molecules. Permeability may be modulated by varying the composition of lipids, and by adding detergents. Well defined ratios are needed, and small changes due to dilution can negate permeability. Biomimicry may again serve as inspiration in this case, as several methods are found in nature to overcome this problem. Endo and exocytosis are two methods for large molecule transport across lipid membranes in nature; however, these active transport forms require cell signaling pathways and protein machinery to function¹⁵⁵. Membrane spanning channel proteins also allow transport of molecules, either through facilitated diffusion or active transport. These proteins have been successfully purified and incorporated into liposomes, making them permeable. This has allowed for the creation of nanoreactors.

Synthetic polymers have also been demonstrated in the encapsulation of enzymes¹⁵⁶. They are comparable to lipid based systems in that both are composed of

amphiphilic diblock or triblock molecules, which enclose an aqueous compartment (Figure 2.5)¹⁵⁷. A review by Discher *et al.* (2009) highlights the differences in use between the two types of polymer¹⁵⁸. These polymers excel over their lipid counterparts in several regards. Greater control over their properties is granted due synthesis. You can functionalize surfaces with different entities¹⁵⁹, change block composition, length and weight. Molecular weights of up to 100 kDa are possible, when compared to less than 1 kDa for lipids. The higher weight building blocks impart superior chemical and physical stabilities to polymersome over liposomes¹⁶⁰. These higher weights correspond with a greater thickness of the membrane. This further reduces the permeability through the membrane. Discher *et al.* (1999) found that the membrane of polymersomes was 10 times less permeable to water when compared to liposomes¹⁶¹. Thicker membranes also result in less leakage over time compared to liposome systems¹⁶².

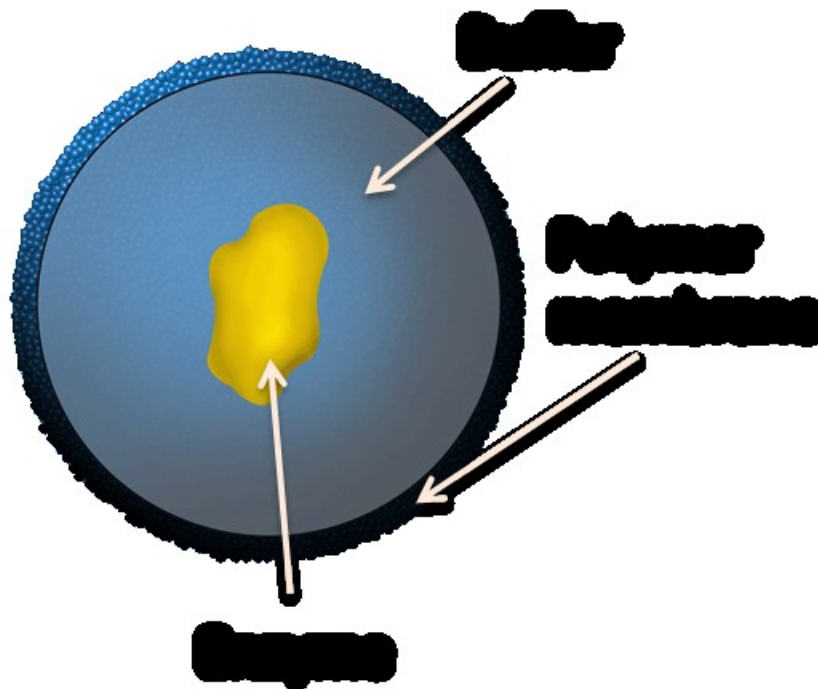


Figure 2.5 Schematic of enzyme encapsulation within polymersome

To overcome permeability issues, properties may be introduced into the polymer which allows for permeabilization. Vriezema *et al.* (2003) synthesized a diblock polymer which was naturally permeable to materials¹⁶³. They created polystyrene-*b*-poly(L-

isocyanoalanine-(2-thiophene-3-yl-ethyl)amide (PS-PIAT). They later used this polymer to encapsulate glucose oxidase¹⁶⁴. They report that the free enzyme was 59 % active after 15 days, while the encapsulated enzyme retained 98 % of its initial activity. Wang *et al.* (2014) demonstrated a stimuli triggered block copolymer polymersome system¹⁶⁵. Upon UV exposure, primary amine release occurs, leading to crosslinking and a transition from hydrophobicity to hydrophilicity within the bilayer. The group encapsulated an enzyme, and showed retention of activity, diffusion of substrate into the polymersome, and retention of enzyme.

For polymers which are not intrinsically permeable, such as the triblock Poly(2-methyloxazoline)-block-poly(dimethylsiloxane)-block-poly(2-methyloxazoline) (PDMS-PMOXA-PDMS), the membrane must be made permeable through other means. As with liposomes, a biomimetic approach involving membrane spanning transport proteins has been demonstrated several times^{32,166}. A published photoreactive technique by Spulber *et al.* (2013)¹⁶⁷ involved permeabilizing the membrane through post-assembly modification of the membrane via a photoreactant. The photoreactant will form a radical following UV light exposure, and it was hypothesized that in the presence of the triblock polymer and under chosen conditions, that the radical would react with the surface, increasing the hydrophilicity of the membrane. It is planned to use this triblock polymer in the regeneration of ATP in the bioprocess described in section 1.4¹⁶⁸. Due to its past success in enzyme encapsulation, well characterized properties such as mechanical strength and flexibility and availability, it was decided to employ this polymer in the research¹⁶⁹.

Materials and Methods

The first objective of the work in this thesis was to find a source of PRK. The experimental work for this objective can be found in sections 2.7 and 2.8. Following purification, kinetic characterization of the enzymes PRK and Rpi was obtained through experimental procedures to find their: Michaelis constants, stabilities at both room temperature (22 °C) and following UV light exposure. These procedures are found in sections 2.9.3 and 2.10.3. Experiments focused on the optimization of conditions affecting the kinetic performance of the enzymes are found in sections 2.11.1 and 2.11.2 . Experiments were performed to synthesize the triblock polymer (2.12), form enzyme-laden polymers (2.13) and characterize polymersomes (2.14). Procedures focused on the investigation into the protection afforded the enzymes following encapsulation as well as the efficiency of encapsulation are found in section 2.15. An outline of the experiments and procedures carried out may be found in Table 0.1.

Objective of thesis research	Experimental Techniques	Expected outcome	Section
Expression of PRK	PCR, DNA and SDS gel electrophoresis, fermentation	Enzyme expression in <i>E. coli</i>	2.7, 2.8
Purification of PRK	Cell lysis, Centrifugation, Chromatography	Pure, active PRK	2.8
Kinetic properties of the enzymes Rpi and PRK	Spectrophotography, Michaelis-Menten modeling,	Calculate K_m of Rpi and PRK at room temperature	2.9, 2.10
Investigate stability of Rpi and PRK	Spectrophotography, non-linear least squares curve fitting	Calculate half-life of enzymes, investigate effects of UV light	2.9.3, 2.10.3
Optimization of reaction rate conditions	Non-linear regression, ANOVA, spectrophotography	Measure apparent reaction rate increase under new conditions	2.11.1, 2.11.2
Encapsulation of enzymes	Thin film rehydration, chromatography, protease digestion, FCS, spectrophotography	Verify encapsulation of enzyme and determine efficiency	2.13, 2.15
Characterize polymersomes	DLS, SEM and TEM	Determine the size and morphology of polymersomes	2.14

Table 0.1 Summary of experiments used in this study

2.6 Ribose 5-phosphate isomerase from *E. coli*

2.6.1 Expression and purification procedure

The gene encoding the *E. coli* ribose-5-isomerase A (Rpi) subunit was sourced from UniProt, PRIDE entry P0A7Z0. The sequence in Table 0.2 was submitted to Integrated DNA Technologies for synthesis as a custom gene fragment. The gene was successfully cloned into the pET-15b vector using Xho and NcoI restriction endonucleases and T4 ligase.

```
5'ACCCAGGATGAACTGAAAAAAGCGGTGGGCTGGGCGGCGCTGCAGTATGTGCAGCCGGGC
ACCATTGTGGGCGTGGGCACCGGCAGCACCGCGGCGCATTATTTATTGATGCGCTGGGCACCATG
AAAGGCCAGATTGAAGGCGCGGTGAGCAGCAGCGATGCGAGCACCGAAAACTGAAAAGCC
TGGGCATTCATGTGTTTGATCTGAACGAAGTGGATAGCCTGGGCATTTATGTGGATGGCGCGG
ATGAAATTAACGGCCATATGCAGATGATTAAAGGCGGCGGCGCGCGCTGACCCGCGAAAAA
ATTATTGCGAGCGTGGCGGAAAAATTTATTTGCATTGCGGATGCGAGCAAACAGGTGGATATT
CTGGGCAAATTTCCGCTGCCGGTGGAAAGTGATTCCGATGGCGCGCAGCGCGGTGGCGCGCCA
GCTGGTGAAACTGGGCGGCCCGCCCGGAATATCGCCAGGGCGTGGTGACCGATAACGGCAACG
TGATTCTGGATGTGCATGGCATGGAAATTCTGGATCCGATTGCGATGGAAAACGCGATTAACG
CGATTCCGGGCGTGGTGACCGTGGGCCTGTTTGCGAACC GCGGCGCGGATGTGGCGCTGATTG
GCACCCCGGATGGCGTGAAAACCATTTGTGAAA-3'
```

Table 0.2 Genetic sequence of Rpi

Transformed *E. coli* cells were grown at 37 °C in LB broth media which contained 100 ug/mL of the antibiotic ampicillin. When the optical density at 600 nm (OD₆₀₀) reached 0.6 using the spectrophotometer, the cells were induced by adding Isopropyl β-D-1-thiogalactopyranoside (IPTG) to a final concentration of 1 mM. The media was incubated for 18 hours at 20 °C. Following incubation, the cells were collected via centrifugation at 5000xG for 20 minutes at 4 °C. Cells were then resuspended in lysis buffer.

Lysis buffer is composed of 25 mM Tris-HCL, pH 8, 1 mM DTT, and one protease inhibitor tablet. One litre of 25 mM Tris-HCL was made by combining 3.03 g of tris base, 1.17 mL of HCl and bringing it to close to 1 L in volume with distilled water. DTT was then added to a final concentration of 1 mM, and the pH of the solution was adjusted, and brought to 1 L with water.

Following suspension in this lysis buffer, cells were lysed via sonication on ice at 45 % amplitude, pulsed for 20 seconds four times and centrifuged at 25,6631xG for 2

hours at 10 °C. The supernatant was applied onto a custom packed anion exchange column, with a column volume of 60 mL, which was pre-equilibrated with lysis buffer. Two column volumes of washing occurred, with lysis buffer containing 50 mM NaCl. A linear gradient elution was applied using lysis buffer containing 1 M NaCl at a flow rate of 2 mL/minute for a total of 120 mL. Fractions were collected at 2 mL intervals. Fractions were applied onto an SDS-polyacrylamide gel for analysis (Figure 0.1).

The gel cassette was loaded into an electrophoresis cell. The cassette was immersed in running buffer and run at 180 volts for 45 minutes. Running buffer is composed of 3 g of Tris base, 14 g glycine, 1 g of SDS into 1 L of water. The gels were imaged with a cell phone camera. Fractions found to contain Rpi were pooled and placed in dialysis tubing with a 3.5 kDa molecular weight cut-off (MWCO) against 1 L of lysis buffer, with four 1 L buffer exchanges over the course of a day, at 4 °C. Purified enzyme activity was tested following the procedure in section 2.9.1.

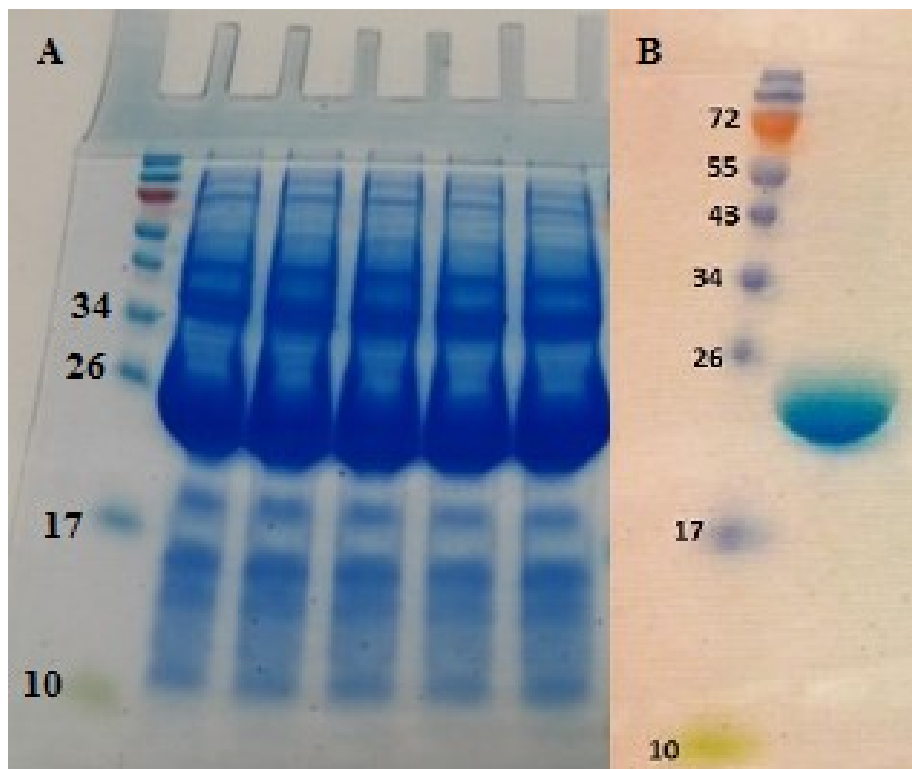


Figure 0.1 Gel images of the expression and purification of Rpi (A and B respectively).

2.6.2 Materials and equipment

Material	Supplier	Catalogue number	Purity	Molecular weight	CAS number
pET-15b plasmid	Novagen	69661-3	n/a	n/a	n/a
BL-21 (DE3) <i>E. coli</i> cells	New England Biolabs	C2527H	n. a	n/a	n/a
LB broth media	ThermoFisher	12780-052	n/a	n/a	n/a
Ampicillin	ThermoFisher	BP1760-25	≥98 %	371.4 g/mol	69-52-3
IPTG	ThermoFisher	FERR0392	≥99 %	238.3 g/mol	367-93-1
Tris base	ThermoFisher	BP152-1	≥99.8 %	121.1 g/mol	77-86-1
DTT	Sigma	D9779	≥98 %	154.3 g/mol	3483-12-3
Protease inhibitor	ThermoFisher	88266	n/a	n/a	n/a
Q-sepharose fast flow	GE Healthcare Sciences	17-0510-01	n/a	n/a	n/a
Sodium chloride	Sigma	S9888	≥99 %	58.4 g/mol	7647-14-5
Sodium dodecyl sulfate	Bio-Rad	1610302	≥98 %	288.4 g/mol	151-21-3
SDS-polyacrylamide gel. 10% SDS.	Bio-Rad	161-0302	n/a	n/a	151-21-3
Dialysis tubing	Fisherbrand	21-152-10	n/a	n/a	n/a
Distilled Water	n/a	n/a	Resistivity at 22° C: 18.2MΩ•cm	18.0 g/mol	7732-18-5
Glycine	Sigma	G8898	≥99 %	75.1 g/mol	56-40-6
FastDigest NcoI	ThermoFisher	FD0573	n/a	n/a	n/a
FastDigest XhoI	ThermoFisher	FD0694	n/a	n/a	n/a
T4 DNA ligase	ThermoFisher	EL0014	n/a	n/a	n/a
1cm disposable cuvette	ThermoFisher	14-955-125	n/a	n/a	n/a
Hydrochloric acid	Ricca Chemicals	3780-5PT	18.8-12.2N at 20° C	36.5m g/mol	7647-01-0

Table 0.3 Materials used in the expression and purification of Rpi

Equipment	Make	Model	Catalogue number	Supplementary information
Centrifuge	Optima	L-100XP	392052	Ti-70 rotor, part number 337922
Incubator	New Brunswick	Innova 4330	M1193-1010	Temperature range: 4-60 °C Agitation: 25-500 rpm
Sonicator	Fisher Scientific	Dismembrator Model 500	15-338-550	Tip: Model 102-C Branson Sonifier, catalogue number BR-101-135-066R.
Spectrophotometer	Thermo Scientific	BioMate 3S	840208300	Range: 190-1100 nm Accuracy: ± 1 nm
Chromatography system	Bio-Rad	Bio-Logic LP	7318300	n/a
Electrophoresis cell	Bio-Rad	Mini-PROTEAN Tetra Cell	1658005EDU	n/a
Electrophoresis power supply	Bio-Rad	PowerPac HC	1645052	n/a
Purification column	Fisher Scientific	Kimble Flex	4204001530	53 mL column

Table 0.4 Equipment used in the expression and purification of Rpi

2.6.3 Bradford assay

The Bradford assay is a spectroscopic method of determining protein concentration¹⁷⁰. It is a colourmetric assay, performed following a reaction between the protein and dye solution, resulting in an absorbance shift in the dye. A 1 mg/mL BSA stock is dissolved in the same buffer as the protein of interest. From this, a standard curve is prepared using Bovine serum albumin (BSA) over the linear range, from 0.05 mg/mL-0.5 mg/mL.

Bradford dye reagent is prepared by dissolving 50 mg of coomassie dye in 50 mL of ethanol and 100 mL of 85 % (w/v) phosphoric acid, bringing the solution to 1 L and filtering undissolved dye out of the solution. 10 μ L of six protein standards and a blank are added to a 96 well plate in triplicate (0.05, 0.1, 0.2, 0.3, 0.4 and 0.5 mg/mL). The

protein of interest is also added in triplicate. 190 μ L of Bradford reagent is added to every well, followed by intermittent shaking, allowing the solution to equilibrate over 5 minutes.

The absorbance of the cells was read in the microplate reader at 595 nm, and the data was transferred to Microsoft Excel for analysis. The absorbance of the blank is subtracted from the averages of the 3 standards and 3 unknown wells. A standard curve is made, with absorbance on the Y-axis and concentration on the X-axis using the absorbance readings of the standards. Using the equation of the slope, the concentration of the unknown can be found by substituting absorbance for the variable Y. Dilution factors of the unknown were taken into account for the final concentration.

Materials and equipment

Material	Supplier	Catalogue number	Purity	Molecular weight	CAS number
Coomasie Brilliant Blue R-250 dye	ThermoFisher	20278	$\geq 90\%$	226.0 g/mol	6104-59-2
Bovine serum albumin	Sigma	A4503	$\geq 96\%$	66 kDa	9048-46-8
96-Well microplate	ThermoFisher	8404	n/a	n/a	n/a
Phosphoric acid	Sigma	345245	$\geq 99.9\%$	98.0 g/mol	7664-388-2
Methanol	ThermoFisher	A412P	$\geq 99.8\%$	32.0 g/mol	67-56-1
Corning sterile filter	ThermoFisher	430770	n/a	n/a	n/a

Table 0.5 Materials used in the Bradford assay

Equipment	Make	Model	Catalogue number	Supplementary information
Microplate absorbance reader	Bio-Rad	iMark	1681130	Wavelength range: 400-750 nm Photometric range: 0-3.5 OD Resolution: 0.001 OD Microplate manager software version 6.3

Table 0.6 Equipment used in the Bradford assay procedure

2.7 Phosphoribulokinase from *Spinacia oleracea*

2.7.1 Expression and purification procedure

The sequence in Table 0.7 was submitted to Integrated DNA Technologies for synthesis as a custom gene fragment. Primers were also designed for polymerase chain reaction (PCR) amplification of the gene. The synthesized gene was dissolved in milliQ water and amplified via PCR. The PCR solution contained 1 μ L DNA polymerase, 1 μ M of each forward and reverse primers complementing the gene and 200 μ M deoxyribose nucleoside triphosphates (dNTPs) in a final volume of 50 μ L. The dNTPs were composed of 2'-deoxy(adenosine, cytidine, guanosine, thymidine) 5'-triphosphate (dATP, dCTP, dGTP, dTTP). An annealing temperature of 55 $^{\circ}$ C was used over 35 cycles with a final extension step at 68 $^{\circ}$ C for 5 minutes.

Following the last extension, the PCR solution was applied to a 1 % agarose gel with a voltage of 140 V being applied for 25 minutes. This gel was made by dissolving 1g of agarose into 100 mL of TE buffer. TE buffer consists of 10 mM Tris-HCL, 1mM (ethylenedinitrilo)tetraacetic acid (EDTA) with a pH of 8, brought to volume with water. The gene fragments were excised from the gel and purified using a PCR purification kit, using the microcentrifuge to spin the components. The fragments and pET-15b vector were then digested at 37 $^{\circ}$ C using NcoI and XhoI FastDigest restriction endonucleases for one hour (same materials as section 2.6.2). The digested gene and vector were further purified through gel electrophoresis using a 1 % agarose gel (Figure 3.1), with the addition of 5 μ L of SYBR green stain. Images were taken on the imager using the UV transilluminator settings, with the Cy2 profile selected on automatic acquisition. The appropriate bands were excised and purified using a gel extraction kit

```

5'-AGCCAGCAGCAGACCATTGTGATTGGCCTGGCGGCGGATAGCGGCTGCGGCAAAAGCACCT
TTATGCGCCGCTGACCAGCGTGTGGCGGCGCGGCGGAACCGCGAAAGGCGGCAACCCG
GATAGCAACACCCTGATTAGCGATAACCACCACCGTGATTTGCCTGGATGATTTTCATAGCCTG
GATCGCAACGGCCGCAAAGTGAAAAAGTGACCGCGCTGGATCCGAAAGCGAACGATTTTGA
TCTGATGTATGAACAGGTGAAAGCGCTGAAAAGAAGGCAAAGCGGTGGATAAACCGATTTATA
ACCATGTGAGCGGCCTGCTGGATCCGCCGGAAC TGATTCAGCCGCCGAAAATTCTGGTGATTG
AAGGCCTGCATCCGATGTATGATGCGCGCGTGCGCGAACTGCTGGATTTTAGCATTTATCTGG
ATATTAGCAACGAAGTGAAATTTGCGTGGAAAATTCAGCGCGATATGAAAGAACGCGGCCAT
AGCCTGGAAAGCATTAAAGCGAGCATTGAAAGCCGCAAACCGGATTTTGATGCGTATATTGA
TCCGCAGAAACAGCATGCGGATGTGGTGATTGAAGTGCTGCCGACCGAACTGATTCGGATG
ATGATGAAGCAAAGTGCTGCGCGTGCGCATGATTTCAGAAAAGAAGGCGTGAAATTTTTAAC
CCGGTGTATCTGTTGATGAAGGCAGCACCATGATTGGATTCCGTGCGGCCGCAAAGTACC
TGCAGCTATCCGGGCATTAAATTTAGCTATGGCCCGATACCTTTTATGGCAACGAAGTGACC
GTGGTGAAATGGATGGCATGTTTGATCGCCTGGATGAACTGATTTATGTGGAAAGCCATCTG
AGCAACCTGAGCACCAAATTTTATGGCGAAGTGACCCAGCAGATGCTGAAACATCAGAACTT
TCCGGGCAGCAACAACGGCACCCGGCTTTTTTCAGACCATTATTGGCCTGAAAATTCGCGATCT
GTTTGAACAGCTGGTGGCGAGCCGCAGCACCCGCGACCGCGACCGCGGCGGCAAAGCG-3'

```

Table 0.7: Genetic sequence of PRK from *S. oleracea*, as expressed in *E. coli*

The digested gene and vector were incubated in the presence of T4 ligase for three hours. Following ligation, 1 μ L of solution was added to a 50 μ L aliquot of *E. coli* DH5- α cells (same material as in section 2.6.2). Electroporation was carried out on an Eppendorf 2510 electroporator using a voltage of 2500 V. The solution was diluted to 1 mL with LB media (see section 2.6.2 for material), followed by incubation at 37 $^{\circ}$ C with shaking set at 225 rpm. Following 1 hour of incubation, the media was diluted 1:5 with LB media. This dilution was spread on warmed LB agar plates and incubated at 37 $^{\circ}$ C overnight in a lab oven.

The agar plates were made by adding 1.5 g of agar to 100 mL of LB broth (same material as in section 2.6.2). Following a cycle in the autoclave, the flask was allowed to cool prior to the addition of antibiotic. Kanamycin stock which had been dissolved in water was added to a final concentration of 30 μ g/mL. The plates solidified overnight and were then stored at 4 $^{\circ}$ C.

A single colony was used to inoculate 5 mL of LB media containing 30 μ g/mL of kanamycin. The following day, plasmid was harvested from the cells using the PureLink Quick Plasmid Miniprep Kit using the microcentrifuge. The concentration of DNA was estimated using the absorbance of the solution at 260 nm, multiplied by the dilution factor and constant 50 ng/ μ L, using the spectrophotometer and 50 μ L microcuvettes¹⁷¹.

Approximately 10 ng of plasmid was added to 50 μ L the cells for heat shock transformation. After a 15 minute period of incubation on ice, the cells were placed in a 42 °C water bath for 30 seconds, followed by 2 minute incubation on ice. 200 μ L of 37 °C LB media was added and the solution was incubated at 37 °C in a shaking incubator at 225 rpm. The solution was then diluted 1/20 into more LB media, with 100 μ L of this dilution being spread on an LB agar plate containing 30 μ g/mL kanamycin and incubated at 37 °C overnight.

A full factorial experimental design was used to determine optimal growing conditions for maximum PRK expression in culture. Three variable factors were chosen in addition to the cell types: growth temperature, the concentration of the inducing agent IPTG and the harvest time (Table 0.8).

Order	Cell Type	Temperature (°C)	IPTG (mM)	Growth time (Hours)
1	C43	18	0.1	3
2	C43	18	0.1	6
3	C43	18	0.1	24
4	C43	18	0.5	3
5	C43	18	0.5	6
6	C43	18	0.5	24
7	C43	18	1	3
8	C43	18	1	6
9	C43	18	1	24
10	C43	30	0.1	3
11	C43	30	0.1	6
12	C43	30	0.1	24
13	C43	30	0.5	3
14	C43	30	0.5	6
15	C43	30	0.5	24
16	C43	30	1	3
17	C43	30	1	6
18	C43	30	1	24
19	C43	37	0.1	3
20	C43	37	0.1	6
21	C43	37	0.1	24
22	C43	37	0.5	3
23	C43	37	0.5	6

24	C43	37	0.5	24
25	C43	37	1	3
26	C43	37	1	6
27	C43	37	1	24
28	T7	18	0.1	3
29	T7	18	0.1	6
30	T7	18	0.1	24
31	T7	18	0.5	3
32	T7	18	0.5	6
33	T7	18	0.5	24
34	T7	18	1	3
35	T7	18	1	6
36	T7	18	1	24
37	T7	30	0.1	3
38	T7	30	0.1	6
39	T7	30	0.1	24
40	T7	30	0.5	3
41	T7	30	0.5	6
42	T7	30	0.5	24
43	T7	30	1	3
44	T7	30	1	6
45	T7	30	1	24
46	T7	37	0.1	3
47	T7	37	0.1	6
48	T7	37	0.1	24
49	T7	37	0.5	3
50	T7	37	0.5	6
51	T7	37	0.5	24
52	T7	37	1	3
53	T7	37	1	6
54	T7	37	1	24
55	BL21	18	0.1	3
56	BL21	18	0.1	6
57	BL21	18	0.1	24
58	BL21	18	0.5	3
59	BL21	18	0.5	6
60	BL21	18	0.5	24
61	BL21	18	1	3
62	BL21	18	1	6
63	BL21	18	1	24
64	BL21	30	0.1	3

65	BL21	30	0.1	6
66	BL21	30	0.1	24
67	BL21	30	0.5	3
68	BL21	30	0.5	6
69	BL21	30	0.5	24
70	BL21	30	1	3
71	BL21	30	1	6
72	BL21	30	1	24
73	BL21	37	0.1	3
74	BL21	37	0.1	6
75	BL21	37	0.1	24
76	BL21	37	0.5	3
77	BL21	37	0.5	6
78	BL21	37	0.5	24
79	BL21	37	1	3
80	BL21	37	1	6
81	BL21	37	1	24

Table 0.8 The factorial design to maximize PRK expression

Each cell type was used to inoculate 100 mL of Terrific Broth (TB) containing the antibiotic kanamycin. This was grown on a shaking incubator at 225 rpm until the OD₆₀₀ of the culture reached 0.8. At this point, the media was split into 5 mL tubes, inducing agent was added and the tube was placed into the shaking incubator at the appropriate temperature, at a shaking speed of 225 rpm. At the determined time, samples were centrifuged to collect a pellet of cells with the media being decanted. Pellets were lysed using 4 mL of BPER protein extraction agent. This was applied to a vortex shaker for 20 seconds, followed by incubation at room temperature for 15 minutes. The tubes were then applied to the microcentrifuge at 15,000xG for 5 minutes. The soluble supernatant was applied to an SDS-PAGE cell for visualization (procedure as laid out in section 2.6.1). Images were captured using the imager, with the plate set at position 1 and acquisition set to automatic in the software (Figure 3.2). The molecular weight and width of the protein bands were estimated using the program ImageQuant.

Following expression optimization, BL-21 (DE3) cells which were transformed with the vector were selected and used to inoculate 25 mL of LB media with 30 µg/mL of

kanamycin, and incubated at 37 °C overnight at 225 rpm in a shaking incubator. The following day, 10 mL was used to inoculate 500 mL of TB media. When the OD₆₀₀ reached 0.8, the culture was induced with IPTG (as in 2.6.2), to a final concentration of 0.5 mM. This was measured using the spectrophotometer with disposable 1 cm cuvettes. The temperature was reduced to 30 °C, with the culture being left to grow for another 12-16 hours. The culture was collected via centrifugation at 10,000xG at 4 °C using a JLA-9.1000 rotor for 10 minutes. Cells were then frozen at -20 °C, and then thawed 24 hours later for enzyme purification.

Purification was adapted from the method of Hudson *et al.* (1992)¹⁷². The 500 mL pellet of cells was suspended in 20 mL of cell breaking buffer. Cell breaking buffer consisted of 25 mM Tris-HCl, 20 mM EDTA, 10 mM DTT (same material as section 2.6.2), 1 mM phenylmethanesulfonyl fluoride (PMSF). The suspension was applied on a French press using a maximum cell pressure of 1100 psi.

The cell lysate was centrifuged in an ultracentrifuge at 150,000xG for 30 minutes at 4 °C. Ammonium sulfate salt was added slowly with stirring to the decanted supernatant, to a final concentration of 35 % weight/volume (w/v). This was allowed to stir at 4 °C for 10 minutes to form a homogenous solution. The slurry was centrifuged at 17,200xG for 20 minutes at 4 °C using a JA-30.50 rotor in the Avanti centrifuge. The supernatant was decanted, and ammonium sulfate was again added to a final concentration of 60 % w/v¹⁷³. The previous centrifugal step was repeated, the pellet was collected and suspended in 10 mL of cell breaking buffer. 50 % w/v polyethylene glycol in water was added with stirring to a final concentration of 20 % w/v at room temperature to further precipitate unwanted proteins in conjunction with a final centrifugal step at 17,200xG.

The supernatant was dialyzed against 2 litres of Buffer A overnight, which was composed of 25 mM Tris-HCl, 1 mM DTT, 0.5 mM EDTA (materials found in section 2.6.2). Following dialysis, 10 mL of sample was applied to a 5 mL weak anion exchange column using a chromatographic pumping system at 4 °C. The sample was washed with

two column volumes of Buffer A, followed by a linear gradient of Buffer A with added 1 M NaCl. The majority of the PRK eluted at 12%, or 120 mM NaCl (Figure 3.5).

The fractions containing PRK were then applied to a centrifugal device with a MWCO of 10 kDa, and centrifuged at 4000xG using the benchtop centrifuge. After 25 minutes of spinning, the filtrate was discarded. Buffer A was added to the concentrate in the device to remove salts and remove the contaminating lower molecular weight proteins. After a total of three spins, the concentrated sample was applied onto a 5 mL HiTrap Blue column. A gradient elution of Buffer A, by addition of adenosine triphosphate (ATP) was applied to the column. PRK eluted with two contaminating bands, at a gradient of 1 mM ATP. Purity was assessed using the same equipment and procedure outlined for SDS-Page analysis in section 2.6, and imaged (Figure 3.6). The lower molecular weight contaminant at ~27 kDa was later removed using a centrifugal device with a MWCO of 30 kDa, prior to activity assessment.

2.7.2 Materials and equipment

Material	Supplier	Catalogue number	Purity	Molecular weight	CAS number
Phusion DNA polymerase	New England Biolabs	M0530S	n/a	n/a	n/a
Agarose	Sigma	A5304	≥93 % due to moisture impurities	n/a	9012-36-6
dNTP mixture (dATP, dCTP, dGTP, dTTP)	New England Biolabs	N0446S	≥99 %	464.1-504.2 g/mol	1927-31-7, 102783-51-7, 93919-41-6, 18423-43-3
EDTA	Sigma	431788	≥99.99 %	292.2 g/mol	60-00-4
PCR purification kit	ThermoFisher	K3100-01	n/a	n/a	n/a
Petri dishes	ThermoFisher	FB0975713	n/a	n/a	n/a
Agar	ThermoFisher	BP1423	n/a	n/a	n/a
PureLink gel extraction kit	ThermoFisher	K2100-12	n/a	n/a	n/a

GeneRuler 1kb DNA ladder	ThermoFisher	SM1331	n/a	n/a	n/a
Kanamycin	Sigma	K4000	≥95 %	582.6 g/mol	25389-94-0
C43 OverExpress <i>E. coli</i> cells	Lucigen	60446-1	n/a	n/a	n/a
Electroporation cuvettes, 0.1cm	ThermoFisher	P410-50	n/a	n/a	n/a
T7 Express <i>E. coli</i> cells	New England Biolabs	C2566H	n/a	n/a	n. a
PureLink Plasmid miniprep kit	ThermoFisher	K2100-11	n/a	n/a	n/a
B-PER	ThermoFisher	78248	n/a	n/a	n/a
SYBR Green I nucleic acid stain	ThermoFisher	S-7563	n/a	n/a	n/a
Terrific Broth	ThermoFisher	BP2468-10	n/a	n/a	n/a
1 cm disposable cuvette	ThermoFisher	14-955-125	n/a	n/a	n/a
PMSF	ThermoFisher	36978	≥99 %	174.2 g/mol	329-98-6
Ammonium sulfate	Sigma	A4418	≥99 %	132.1 g/mol	7783-20-2
Polyethylene glycol BioUltra 3350	Sigma	88276	Contains insoluble matters, passes filter test	3000-3700 g/mol	25322-68-3
Centrifugal filter 10kDa	Amicon	UFC901024	n/a	n/a	n/a
ATP	Sigma	A2383	≥99 %	551.1 g/mol	34369-07-8
Centrifugal filter, 30kDa	Amicon	UFC903024	n/a	n/a	n/a

Table 0.9 Materials used in experiments to purify PRK from *S. oleracea*

Equipment	Make	Model	Catalogue number	Supplementary information
PCR Thermal cycler	ThermoFisher Scientific	ProFlex PCR system	4484073	Denaturation set at 95° C Annealing set at 55° C
Electroporator	Eppendorf	2510	940000009	Voltages: 200-2500V
Autoclave	Tuttnauer	3870EA		Temperature: 121° C Time:45 minutes Pressure range: 0.2 to 31psi
Shaking Incubator	New Brunswick	Innova 44	M1282-0000	
Incubator	Fisher Scientific	Isotemp 637G	13-247-625G	Temperature range: 20-200° C
Vortex mixer	VWR	Vortex Mixer Mini	58816-123	
Gel Imager	GE Life Sciences	ImageQuant LAS 4000	28-9558-10	Software: ImageQuant TL 8.1
Spectrophotometer	Beckman Coulter	DU 720	A23615	Range: 190-1100nm Resolution: 1nm Holders: 50µL single cell holder, 523382. 1 cm cell holder, A24211 Cuvette: 50µL quartz cuvette, A23622.
Benchtop Centrifuge	Eppendorf	5810R	5810 000.130	Rotor: Swing bucket rotor, A-4-81
Microcentrifuge	Eppendorf	5427R		Rotor: Aerosol-tight rotor, 05-100-157
Centrifuge	Beckman Coulter	Avanti J-30I	363118	<i>Rotors: JLA-</i>

				9.1000, 969328. JA-30.50, 363420.
Ultracentrifuge	Beckman Coulter	Optima XPN- 100		<i>Rotors:</i> Ti-70 rotor, 337922.
French Press Cell	Thermo Scientific	FA-078A	PC-180	40K cell body was used
Electrophoresis power supply	Life Technologies	250EX	14577	Voltage: 0-250 V Current: 0-500 mA
Chromatography system	GE Healthcare Life Sciences	ÄKTA Pure	29-0182- 24	UV detector: U9-M, 28-9563-78 Fraction collector F9-R, 29011362
Chromatography column	GE Healthcare Life Sciences	DEAE fast flow weak anion	17-5055- 01	5mL bed volume
Chromatography column	GE Healthcare Life Sciences	HiTrap Blue	17-0412- 01	5mL bed volume
SDS-gel Imaging software	GE Healthcare Life Sciences	ImageQuant	29000737	Version 8.1

Table 0.10 Equipment used in the expression and purification of PRK from *S. oleracea*

2.8 Phosphoribulokinase from *Synechococcus elongates*

2.8.1 Expression and purification procedure

Materials, equipment and procedure used in this procedure match what was listed in section 2.7 unless stated. The second PRK contained a 6-histidine tag and was a gift from the lab of Ichiro Matsumura. Plasmid was harvested from 5 mL LB culture of *E. coli* containing the plasmid using the PureLink Quick Plasmid Miniprep Kit. Plasmid concentration was determined as in section 2.7.1. 10 ng of plasmid was added to 50 μ L of BL21 *E. coli* cells on ice. Heat shock transformation, dilution, plating and colony growth conditions methods were the same as in section 2.7.1. The antibiotic chloramphenicol was used in place of kanamycin, at a concentration of 25 μ g/mL.

Colonies grew overnight at 37° C, and the next day an individual colony was selected and used to inoculate 50 mL of LB media supplemented with 25 µg/mL chloramphenicol. This inoculum grew overnight in a shaking incubator at 37 °C, 225 rpm, and was used to inoculate 500 mL of TB media. The flask was shaken at the same speed and temperature as the inoculum. When the media reached an OD₆₀₀ of 0.8 using, the cells were induced by addition of L-arabinose to a final concentration of 0.2 %. 10 % L-arabinose stock was made by dissolving 1 g of arabinose in 9 mL of distilled water. The flask was then moved to an incubator at 18 °C and shaken at 225 rpm overnight.

The culture was then centrifuged at 8000xG for 30 minutes to pellet the cells (using the JLA-9.1000 rotor), and frozen at -20 °C overnight. The frozen cell culture was then resuspended in 25 mM Tris-HCL buffer, 125 mM NaCl, pH 8 at room temperature, supplemented with 5 mM imidazole. The solution was passed through a homogenizer three times at a pressure of approximately 12,000 PSI. The homogenized solution was then centrifuged at 18,000xG for 30 minutes to collect cellular debris (using the JA-30.50 rotor).

The supernatant was decanted, and passed through a 0.22 µm syringe filter. A 5 mL chromatography column was washed with the previously mentioned Tris-HCl buffer, at a rate of 2 mL/minute, for a total of 3 column volumes. Approximately 10 mL of the filtered supernatant solution was then applied at the same flow rate. An elution buffer, of Tris-HCl, containing 0.5 M imidazole, was then applied as a gradient to the column. The initial wash was 2 % elution buffer, or 5 mM imidazole, which removed a portion of the contaminating proteins that were bound to the column. After 4 column volumes of wash, the concentration was increased to 10 % for several column volumes to remove more protein impurities, followed by elution at 20 %, with fractions being collected at 1 mL/fraction. The last increase saw 100 %, or 500 mM imidazole being applied to the column. Collected fractions were assayed for activity. Active fractions were combined and applied onto a centrifugal device with a MWCO off 30 kDa (same material as in section 2.7.2). The solution was washed three times with 25 mM Tris-HCl buffer, pH 8 at

4000xG. The concentrated enzyme was quantified via Bradford assay, was supplemented with 15 mM DTT for storage. Purity was assessed via SDS-polyacrylamide gel as in section 2.6 (Figure 3.8).

2.8.2 Materials and equipment

Material	Supplier	Catalogue number	Purity	Molecular weight	CAS number
PRK Plasmid	Addgene	41041	n/a	n/a	n/a
BL21 (DE3) <i>E. coli</i> cells	New England Biolabs	C2527H	n/a	n/a	n/a
Chloramphenicol	Sigma	C0378	≥98 %	323.1 g/mol	56-75-7
L-(+)-Arabinose	Sigma	A91906	98 %	150.1 g/mol	5328-37-0
Imidazole	ThermoFisher	10522765	≥99 %	68.1 g/mol	288-32-4
Syringe filter (0.22µm)	ThermoFisher	09-720-004	n/a	n/a	n/a

Table 0.11 Materials used in the purification of PRK from *S. elongates*

Equipment	Make	Model	Catalogue number	Supplementary information
Homogenizer	Avestin	Emulsiflex C5	n/a	Pressure range: 500-30000psi
Chromatography column	Clontech	His60 Ni Superflow column	635679	Bed volume: 5 mL
Chromatography system	GE Healthcare Life Sciences	ÄKTA Start	29-0220-94	UV module for ÄKTA Start: 29-0240-18

Table 0.12 Equipment used in the purification of PRK from *S. elongates*

2.9 Kinetic characterization of Rpi

2.9.1 Procedure

Rpi activity was assayed following the method of Wood (1970)¹⁷⁴. This spectroscopic method measures an increase in absorbance at 290 nm over time. This absorbance is due to the product Ru5P containing a ketone group, whilst the substrate

contains a terminal aldehyde group, which does not exhibit this absorbance. Ribose 5-phosphate (R5P) was dissolved in 25 mM Tris-HCl pH 7.5 to a final concentration of 55 mM, and stored on ice. 99 μ L of this solution was added to three or four wells in a microplate (same material as in section 2.6.3) and left to equilibrate for five minutes at 37 $^{\circ}$ C within the plate reader. The wells were then read as a blank, if there was more than 10% difference between the wells, they would be discarded. Following this blank, 1 μ L of Rpi from a stock solution is added, to a final concentration of 1.76 nM in each well. The wells were read immediately after.

Softmax Pro was opened with the kinetics program being selected. The absorbance wavelength was set at 290 nm. The well areas to be read were selected, with minimal read times of 2 seconds for all three wells. The read length was set between 3-5 minutes with the data being exported to Excel 2010 following acquisition. The time was set as the x-axis, with absorbance on the y-axis. To find the concentration of product formed in a 1 cm path length, the Beer-Lambert law would be used:

$$A = \epsilon cl \quad (7)$$

A is absorbance, ϵ is the extinction coefficient of the molecule of interest measured in $M^{-1} \cdot cm^{-1}$, c is the concentration of the molecule of interest and l is the path length. The data recorded by the microplate reader does not have a path length of 1 cm. This limits the comparison of the data to other works, as the concentration of product is not known. Concentration is a more standard number to report over absorbance, which can vary between machines and materials used. To convert to a 1 cm path length following equations were used¹⁷⁵:

$$d(\text{cm}) = \frac{\text{plate reader}(OD_{1000} - OD_{900})}{k} \quad (8)$$

where d is the path length in cm, OD_{1000} and OD_{900} are the optical densities at 1000 nm and 900 nm as measured on the plate reader, and k is the water constant. The water constant k is based on the difference in absorbance of water in the near infrared region in a 1 cm cuvette as found in equation 9:

$$k = \text{cuvette}(\text{OD}_{1000} - \text{OD}_{900}) \quad (9)$$

25 mM Tris-HCl buffer was used in place of water for consistency between the solutions being used in assays and calculations. Using the spectrophotometer and disposable cuvettes from section 2.7, k was found to be 0.265 ± 0.008 for a pathlength of 1 cm. The numerator in equation 8 was measured using a 96 well from section 2.6.3, and found to be 0.156 ± 0.003 . The path length, $d(\text{cm})$ was calculated to be $0.57 \pm 0.03\text{cm}$ when 100 μL was pipetted into a well. To convert plate reader data to a 1 cm path length absorbance, equation 10 was used:

$$\frac{\text{OD}}{\text{cm}} = \frac{\text{OD}_{\text{Sample}}}{d(\text{cm})} \quad (10)$$

To calculate v_0 (section 2.1.1), the optical densities are first plotted against time (Figure 0.2). Due to the rapid catalytic activity of Rpi, at a maximum, the first 30 seconds were assumed to occur under saturating substrate conditions (Figure 0.2). The slope is calculated from the time period 0-30 seconds.

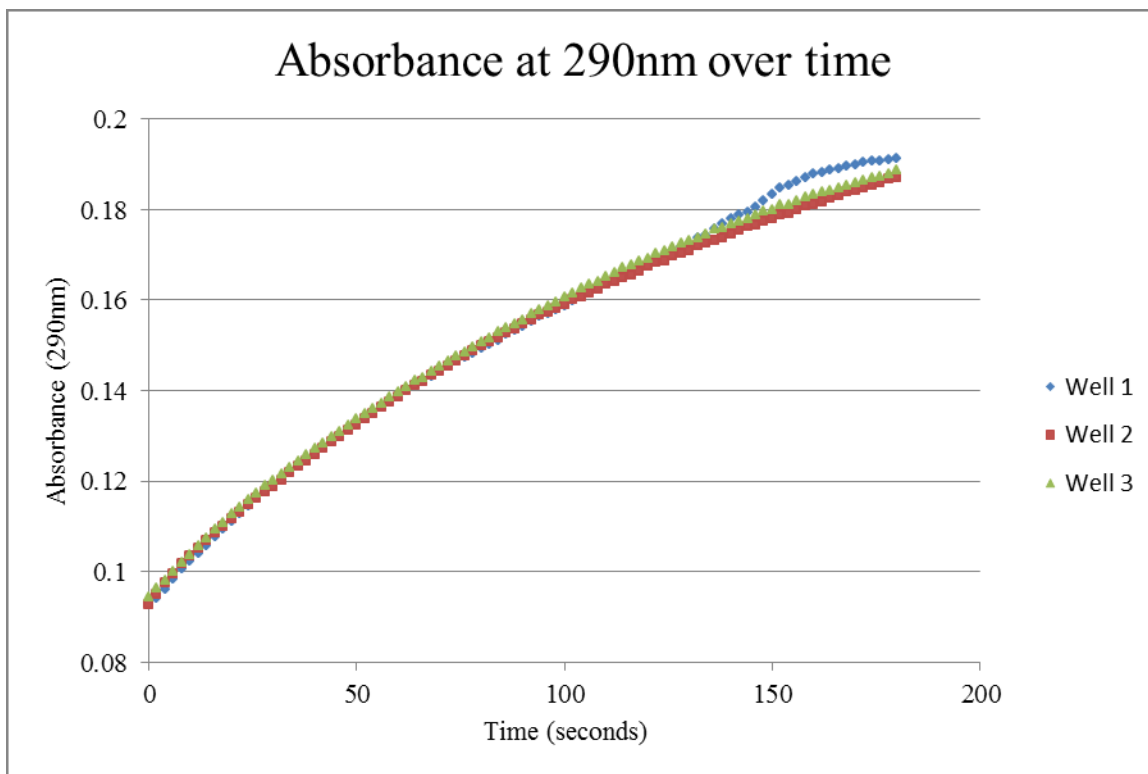


Figure 0.2 Example of raw data from Rpi kinetic assay, $n=3$.

Using Excel, the three replicates were analyzed individually using the LINEST function. This function returns several useful statistics of a line. It uses the least squares method to fit the line, and calculates both the slope and standard error, represented by equations 11 and 12 respectively¹⁷⁶:

$$m = \frac{\sum(x - \bar{x})(y - \bar{y})}{\sum(x - \bar{x})^2} \quad (11)$$

$$SE_y = \frac{\sqrt{\frac{1}{N} \sum_{i=1}^N (y_i - \mu)^2}}{\sqrt{N}} \quad (12)$$

The calculated slope, m , is equal to v_0 . As the concentration of substrate is known at this initial rate, a plot may be made of various reaction rates against their respective concentrations. Using non-linear regression of Equation 2, parameters such as K_m and

V_{\max} may be determined. Kinetic reactions involving Rpi were sourced from the same batch of Rpi.

2.9.2 Michaelis-Menten kinetic modeling

The Michaelis constant of Rpi was found by varying the substrate concentrations, measuring the v_0 and performing non-linear regression using the software GraphPad Prism. The substrate concentrations used were: 70.4, 54.46, 40, 20, 10, 8 and 6 mM R5P. The v_0 was calculated using the method in section 2.9.1, and in each trial the number of replicates was $n=4$. The assay was run using the optimal conditions found in section 3.4.1, with the temperature at 35.3 °C, concentration of Tris-HCl buffer at 10 mM, and a final pH of 7.7.

All concentrations were tested with the same amount of enzyme (1.76 nM final concentration), from the same purified batch of Rpi. The mean and standard error of the mean of v_0 for each concentration assay were calculated using Equations 11 and 12. For the 20, 10 and 8 mM assays, the first 15 seconds were considered saturating conditions. For the 6 mM assay, v_0 was calculated from the first 10 seconds of data. The data was entered into the GraphPad software by selecting Michaelis-Menten data, and formatting the Y data table to have mean and the standard error of the mean entered.

2.9.3 Stability of Rpi

Stability over time

The stability of Rpi at room temperature was investigated by calculating the half-life of enzymatic activity. The reaction rate v_0 was measured at an initial time point, $t=0$, when a solution of enzyme stock (176 nM) had reached room temperature using the method in section 2.9.1. The solution was then stored in a dark drawer. The reaction rate was measured intermittently, using the same stored stock solution of enzyme over a period of a week. Each data point at a measured time point consists of $n=4$ replicates. Only the mean average of the four was entered into the GraphPad software, which was entered as a percentage of the original activity. This original activity was assumed to be 100 % at $t=0$.

Stability under UV conditions

A 1 mL stock solution of Rpi (176 nM) was placed in a sealed quartz vial. Several of these vials were prepared in total. The solutions were bubbled with argon for 5 minutes to displace the air. The control vial was covered with tin foil following argon bubbling. The vials were placed under an 8-watt UV lamp at a distance of approximately 5 cm, for either 1 or 5 minutes at a wavelength of 254 nm. Halfway into the allotted time, vials were shaken gently to ensure homogeneous exposure. The enzyme solution was then assayed following procedure in section 2.9.1, with n=3 replicates. The v_0 of each solution was compared to the v_0 of the control (assumed to contain 100 % activity).

2.9.4 Material and equipment used in kinetic characterization of Rpi

Material	Supplier	Catalogue number	Purity	Molecular weight	CAS number
D-ribose 5-phosphate disodium salt	Sigma	R7750	≥98 %	274.07	18265-46-8
Quartz vial	Postnova	Z-VIA-VIA-016	n/a	n/a	n/a

Table 0.13 Materials used in the kinetic characterization of Rpi

Equipment	Make	Model	Catalogue number	Supplementary information
Microplate reader	Molecular Devices	FlexStation 3	FLEX3	Temperature control: 2-45° C Wavelength range: 200-1000 nm Wavelength accuracy: ±2 nm Photometric Range: 0-4.0OD Software: Softmax Pro version 5
Modeling software	GraphPad	GraphPad Prism	n/a	Version 6.01.
UV lamp	UVP	3UV, 8 watt lamp	95-0343-01	254, 302, 365 nm

Table 0.14 Equipment used in the kinetic characterization of Rpi

2.10 Kinetic characterization of PRK

2.10.1 Procedure

PRK was assayed as described by Harihan *et al.* (1998)¹⁷⁷. The assay involves coupling the production of ADP to a secondary reaction which can be directly quantified (see section 2.1.3). ADP is first converted to ATP via pyruvate kinase in combination with PEP. This reaction leads to the formation of both ATP and pyruvate. Pyruvate is then catalysed to lactate by lactate dehydrogenase, whilst oxidizing NADH to NAD⁺.

NADH has an absorbance peak at approximately 340 nm, which is absent in NAD⁺. As NADH is oxidized by lactate dehydrogenase, a decrease in absorbance can be measured via absorbance spectroscopy. This indirect method of measurement provides a 1:1 molar ratio of ATP and ribulose 5-phosphate (Ru5P) conversion, to the oxidation of NADH. Absorbance was measured using the same materials and equipment found in 2.9.4, with n=3-4 replicates in a volume of 100 μ L. The assay is performed in 4 steps, with the final concentrations listed, as follows:

1. Add 25 mM Tris-HCl buffer, pH 8 to the well. Add 1 μ M of Rpi, 15 mM DTT (same material from section 2.6.2), 4.5 mM magnesium chloride (MgCl₂) and 2 μ L of lactic dehydrogenase/pyruvate kinase stock (LD/PK). The LD/PK commercial stock solution equates to 6-10 units of LD, and 9-14 units of PK. 0.1 mM NADH is also added. This stock (5 mM) was made fresh by dissolving NADH in 2-(*N*-morpholino)ethanesulfonic acid (MES) buffer. This buffer was made by adding 1.95 g of MES solid to 900 mL of distilled water, with the pH being titrated with HCl (same material from section 2.6.2), and brought a volume of 1 L. When all materials were added, they were allowed to come to equilibrium with the set temperature for 5 minutes. The absorbance was measured at 340 nm to ensure there no more than 10% difference between the wells.
2. 3 mM of ATP (same material from section 2.7.2) and 2 mM of PEP were added to the well next. Fresh stocks were made by dissolving the materials in distilled water.

The absorbance was measured over time until reaching equilibrium (typically 1-2 minutes). This step removes the excess ADP from the ATP solution, and identifies any contaminating sources of ATPase.

3. PRK is added to a final concentration of 3.7 nM. This is a control step, as no activity should be seen.

4. The substrate R5P is added last, bringing the volume to 100 μ L. Absorbance is measured over a period of 5 minutes at 340 nm using the same software settings as in section 2.9.1. The kinetic data was transferred to Microsoft Excel 2010 for analysis. Raw absorbance data is found in Figure 0.3.

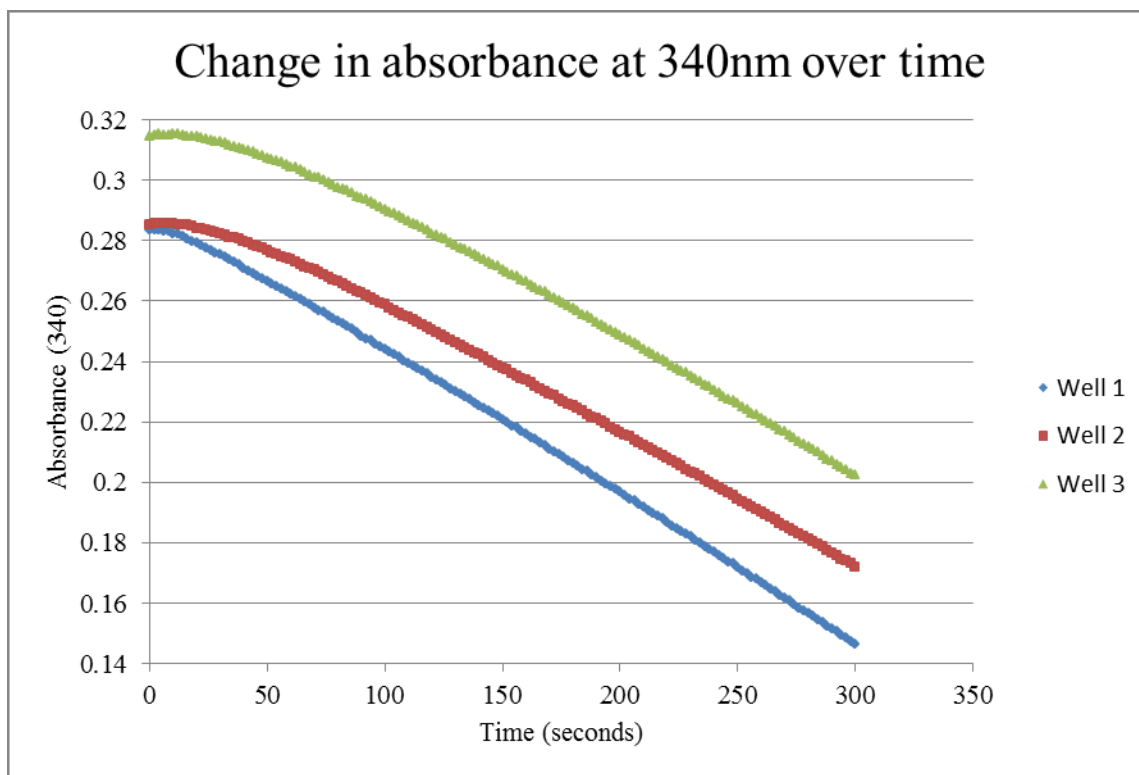


Figure 0.3 Example of absorbance data from a PRK kinetic assay, n=3.

As there is a period of lag before the reaction reaches a steady rate, v_0 was only calculated after a period of two minutes. The v_0 was found to have little variance after this point in the assay, and was assumed to have reached its steady state. The v_0 was calculated using the LINEST method as found in section 2.9.1.

Due to the presence of coupling enzymes and the various substrates, a standard curve of the NADH stock was made using the PRK buffer to aid in the conversion of absorbance data to concentration (Figure 3.11). A blank well would also be measured containing all reagents, save NADH, with buffer in its place for each set of $n=3$ readings. To convert absorbance data generated using this NADH stock to the concentration of product formed, equation 13 (from the standard curve) was used:

$$\text{Concentration} = \frac{((\text{Activity}_{340\text{nm}} - \text{Blank}_{340\text{nm}}) - b)}{m} \quad (13)$$

where b is equal to the y-intercept of the standard curve, m is the slope of the curve, blank is the absorbance of the blank well containing all reagents except NADH and activity is measured absorbance of the kinetic assay. PRK was prepared fresh for experiments which were not performed in the same day (Table 0.15). No normalization took place between batches, as such, comparison between experimental results of different batches was not made in this work.

Batch number	Experimental section	Experiment
1	2.10.2	K_m ATP
2	2.10.2	K_m Ru5P
3	2.10.3	Stability over time and under UV conditions
4	2.11.2	Optimization of reaction conditions, first model
5	2.11.2	Optimization of reaction conditions, second model

Table 0.15 Batches of PRK prepared for experimental procedures

2.10.2 Michaelis-Menten kinetic modeling

The Michaelis constants of PRK for ATP and Ru5P were found by varying the substrate concentrations, measuring the v_0 (as in section 2.10.1) and performing non-linear regression using the software GraphPad Prism (equipment listed in section 2.9.4). The concentrations of ATP used were: 22.5, 45, 90, 135, 180, 450 and 900 μM . The concentrations of Ru5P used were: 0.1, 0.3, 0.355, 0.5, 0.75, 1, 2.5 and 5 mM . In each trial the number of replicates was $n=4$. The assay was run using the optimal conditions found in section 3.4.2, with a temperature of 39.9 $^{\circ}\text{C}$, 20 mM DTT, 6 mM MgCl_2 and 2 mM ATP (materials found in section 2.10.4).

All concentrations were tested with the same amount of enzyme (3.7 nM final concentration), from the same purified batch of PRK. The mean and standard error of the v_0 for each concentration assay was calculated using Equations 11 and 12, entered into the GraphPad software by selecting Michaelis-Menten data, and formatting the Y data table to have mean and the standard error of the mean entered.

2.10.3 Stability of PRK

Stability over time

The stability of PRK at room temperature was investigated by calculating the half-life of enzymatic activity. The reaction rate v_0 was measured at an initial time point, $t=0$, when a solution of enzyme stock (370 nM) had reached room temperature, following the method outlined in section 2.10.1. The solution was then stored in a dark drawer. The reaction rate was measured intermittently, using the same stored stock solution of enzyme over a period of a week. Each data point at a measured time point consists of $n=4$ replicates. Only the mean average of the four was entered into the GraphPad software (equipment from section 2.9.2), and was entered as a percentage of the original activity, which was assumed to be 100% at $t=0$.

Stability under UV conditions

A 1 mL stock solution of PRK (370 nM) was placed in a 1.5 mL quartz vial, and sealed with the screw top and septa included with the vial. The procedure for measuring PRK stability followed the procedure used for Rpi, as laid out in section 2.9.3. The same equipment and materials were used, while the kinetic assay largely followed the procedure found in section 2.10.1 with the v_0 being measured from the time point 250 seconds instead of 120.

2.10.4 Materials used in kinetic characterization of PRK

Material	Supplier	Catalogue number	Purity	Molecular weight	CAS number
NADH	Sigma	N8129	≥97 %	709.4 g/mol	606-68-8
MgCl ₂	Sigma	M8266	≥98 %	95.2	7786-30-3
LD/PK	Sigma	P0294	n/a	n/a	n/a
PEP	Sigma	860077	99 %	206.1 g/mol	4265-07-0
MES	FisherScientific	BP300-100	≥98 %	213.2 g/mol	145224-94-8
Ru5P	Sigma	R9875	≥90 %	230.1	93-87-8

Table 0.16 Materials used in the kinetic characterization of PRK

2.11 Optimization of enzymatic reaction conditions

2.11.1 Rpi Optimization

The conditions affecting Rpi reaction kinetics were optimized using the software Minitab (version 17.1.0)¹⁷⁹. Using the design of experiment builder, a central composite surface design was selected. Four conditions of the enzyme assay from section 2.9.1, or factors, were investigated: pH, temperature, ionic strength of the buffer and concentration of substrate. The experiment had 3 replicates, with 28 assays, or runs to be measured in total. The range and levels of this experiment are outlined in Table 0.17.

		Range and Levels (coded)				
Factor	Factor Code	- α	-1	0	+1	+ α
Temperature (°C)	<i>A</i>	22	27	32	37	44
pH	<i>B</i>	6.5	7	7.5	8	8.5
R5P (mM)	<i>C</i>	10	32.5	55	77.5	100
Buffering strength (mM)	<i>D</i>	10	32.5	55	77.5	100

Table 0.17 The experimental domain for the local optimization of Rpi. α represents axial points. 0 represents centre points, and 1 is representative of factorial points.

The v_0 was calculated for each of the runs following the LINEST method (section 2.9.1). The average v_0 was entered into the software. Polynomial regression was performed by the software, which modeled a predicted outcome of an experiment based on the operating conditions of interest. This model was then subjected to analysis of variance (ANOVA) to analyze the variance between the predicted model kinetic means, and the actual kinetic means which were originally collected.

		Range and Levels (coded)				
Factor	Factor Code	$-\alpha$	-1	0	+1	$+\alpha$
Temperature (°C)	<i>A</i>	35.4	37	41	45	46.6
pH	<i>B</i>	7.69	8	8.75	9.5	9.81

Table 0.18 The experimental domain for the second Rpi response surface experiment

Following the first experiment, a second RSM experiment was conducted, to further investigate improved levels of the temperature and pH factors. The range and levels for this are outlined in Table 0.18.

2.11.2 PRK optimization

PRK reaction kinetics was optimized using the same methodology and software as Rpi (section 2.11.1). The six conditions of the enzyme assay investigated were: pH, temperature, ATP concentration, DTT concentration, R5P and MgCl₂. The experimental design included 46 runs, with each being performed in triplicate. The range and levels of this experiment are outlined in Table 0.19.

		Range and Levels (coded)				
Factor	Factor Code	$-\alpha$	-1	0	+1	$+\alpha$
Temperature (°C)	<i>A</i>	29.9	34	37	40	44.1
pH	<i>B</i>	6.3	7	7.5	8	8.7
R5P (mM)	<i>C</i>	1.3	4	6	8	10.7
DTT (mM)	<i>D</i>	3.2	10	15	20	27
MgCl ₂ (mM)	<i>E</i>	1	3	4.5	6	8
ATP (mM)	<i>F</i>	0.6	2	3	4	5.4

Table 0.19 Experimental domain for the local optimization of PRK.

The v_0 was calculated, model predicted and tested through ANOVA as in section 2.11.1. Following the initial round of optimization, a second investigation was run to further investigate improved conditions of temperature and pH factors (Table 0.20).

		Range and Levels (coded)				
Factor	Factor Code	$-\alpha$	-1	0	+1	$+\alpha$
Temperature (°C)	<i>A</i>	36	37	39.5	42	43
pH	<i>B</i>	7.9	8	8.25	8.5	8.6

Table 0.20 Experimental domain for the second surface response optimization of PRK. activity

2.12 Polymer preparation

2.12.1 Procedure

(PMOXA-PDMS-PMOXA) triblock copolymer was produced in house following the protocol outlined by Nardin *et al.* (2000)¹⁵⁶. 34.2 g of ω -bis(3-hydroxypropyl) poly(dimethylsiloxane) (PDMS) was dissolved in 90 mL of hexane. This was added to a rotary evaporator to remove all traces of water. A vacuum pump was used to lower pressure. Pressure was set at 350 mBar, at ambient temperature, rotating at 100 rpm for 17 hours. After this, the solid was cooled to ~ 0 °C by placing the flask in an ice bucket, followed by the addition of 3.6 g of dry pyridine and 12.4 g of trifluoromethanesulfonic acid anhydride. This solution was stirred for 30 minutes at 0 °C, after which 20 mL of chloroform was added. This was filtered using a filter funnel connected to the vacuum pump, with the solution being evaporated on the rotovaporator after. The yield was then dissolved in 40 mL of hexane, 2 g of activated charcoal was added to remove organic impurities, the solution was stirred by hand for 2 minutes. After being filtered, the solution was again evaporated, yielding a clear oil.

8.05 g of the PDMS oil was collected, which was then combined with 5.04 g of 2-methyl-2-oxazoline. 15 mL of 1,2-dichloroethane was added to this mixture at room temperature, with the solution being stirred for 1.5 hours. After being heated for 48 hours at 40° C, the solution was then cooled to room temperature, and 5.5 mL of a 0.5 M potassium hydroxide solution dissolved in ethyl alcohol was added. This was stirred for 1

hour, then the solution was evaporated using the vacuum pump to yield the triblock polymer.

The molecular weight distribution was estimated by size-exclusion chromatography (SEC) using a Malvern system equipped with refractive index, ultraviolet and light scattering detectors at 40 °C. The permeation column was composed of hydrophilic vinyl polymer-based gel. 1 mg of triblock polymer was dissolved in chloroform and placed in the sample tray. The system was operated at the flow rate of 1.0 mL/min using chloroform as the eluent. Polystyrene standards (Malvern) ranging from 850 to 50000 g/mol were used for calibration of the column. The retention time of the polymer was compared to these standards by the software to estimate the molecular weight.

2.12.2 Materials and equipment

Material	Supplier	Catalogue number	Purity	Molecular weight	CAS number
PDMS	Sigma	481246	n/a	~5,600 g/mol	156327-07-0
Hexane	Sigma	33117	≥99.5 %	84.2 g/mol	110-82-7
Pyridine	Sigma	270970	≥99.8 %	78.1 g/mol	110-86-1
Trifluoromethane sulfonic anhydride	Sigma	176176	≥99 %	282.1 g/mol	358-2306
Chloroform	Sigma	288306	≥99 %, with 0.5-1 % ethanol	119.4 g/mol	67-66-3
Activated charcoal	Sigma	05105	Contains variable cation traces	12 g/mol	7440-44-0
Dichloroethane	Sigma	284505	≥99.8 %	99.0 g/mol	107-06-2
KOH	Sigma	484016	≥90 %	56.1 g/mol	1310-58-3
Ethyl alcohol	Commercial Alcohols	P016EAAN	≥99.9 %	46.1 g/mol	64-17-5
2-Methyl-2-oxazoline	Sigma	137448	≥98 %	85.1 g/mol	1120-64-5
Whatman Grade 1 filter paper	VWR	28450-070	n/a	n/a	n/a
GPC standards	Malvern	TDS3000	n/a	n/a	n/a

Table 0.21 Materials used in the preparation of polymer

Equipment	Make	Model	Catalogue number	Supplementary information
Rotary evaporator	Büchi	Rotavapor R-205	n/a	Accessory: Vacuum semi-automatic controller V-800
Vacuum pump	Edwards/Savant	VLP200 RV8	M90-0283-16	n/a
Stir plate	IKA	C-MAG HS7	0003581201	ETS-D5 thermometer, 0003378000.
GPC	Malvern	GPCmax	n/a	Triple detector array: TDA 305 Software: OmniSEC version 4.7
GPC column	Malvern	T2500	CLM3002	Dimensions 30x0.8 cm column 13 μ m bead size, exclusion limit 20 000 Da

Table 0.22 Equipment used in the preparation of polymer

2.13 Polymersome formation and purification

2.13.1 Procedure

Thin film rehydration was used to form polymersomes. If enzyme is added to the solution, a portion will be encapsulated during the self-assembly of polymersomes. 30 mg of PMOXA-PDMS-PMOXA was dissolved in 5 mL of chloroform in a 25 mL round bottom flask. The solution was evaporated using the rotary evaporator (equipment in section 2.12.2), at a pressure of 350 mBar, at ambient temperature and rotating at 100 rpm. Following a minimum of eight hours, the flask was applied to the in-house vacuum system and was left for 3 hours to remove lingering solvent.

The film was rehydrated by the addition of 5 mL of distilled water. To make enzyme-laden polymersomes, water was replaced with either 25 mM Tris buffered solution containing 11 μ M Rpi at pH 8 (same buffer as in section 2.6.1), or 25 mM phosphate-buffered saline (PBS) with the same pH and enzyme concentration. PBS is composed of the following concentrations: NaCl 137 mM, 2.7 mM potassium chloride

(KCl), 10 mM sodium phosphate dibasic (Na_2HPO_4), 1.8 mM potassium phosphate (KH_2PO_4), with the pH adjusted to 7.5. As Tris-HCl is not compatible with the fluorescent tagging protocol (section 1.1.1), PBS was used in some cases, as Rpi had been found to be active in both buffers.

The aqueous solution would be stirred at 4 °C for 12 hours. The cloudy, resuspended solution was then applied onto a Lipex 10 mL thermobarrel extruder equipped with a 0.2 μm membrane filter. This was connected to a compressed air cylinder, set to emit a maximum pressure of 200 psi. Following extrusion, the flow through was again filtered, repeated for a total of three extrusions until a more transparent solution was obtained. It was then applied onto a gel filtration column, equilibrated with water, at a flow rate 1.3 mL/minute at 4 °C. The column was attached to the chromatography system in section 2.8.2. Elution of polymersomes occurred approximately 1 hour following sample application (Figure 3.22).

When encapsulating enzyme, the column would be equilibrated with at least one column volume of buffer in place of water, and an additional purification step would take place before application on the gel filtration column. The solution would be spun at 4,000xG for 30 minutes in a spin column with a MWCO of 30 kDa. After a spin, the solution would be brought back to volume with buffer, and the spin would be repeated (same material and equipment as used in section 2.7.2). Following three spins, it was hypothesized that much of the free enzyme would have been removed. The gel purification would separate any remaining enzyme and free polymer from the polymersomes.

2.13.2 Materials and equipment

Material	Supplier	Catalogue number	Purity	Molecular weight	CAS number
Polycarbonate membrane	GE Health Sciences	110606	n/a	n/a	n/a
KCl	Sigma	P9541	≥99 %	74.6 g/mol	7447-40-7
Na ₂ HPO ₄	Sigma	S9390	≥98 %	268.1 g/mol	7782-85-6
KH ₂ PO ₄	Sigma	P0662	≥99.0 %	136.1 g/mol	7778-77-0

Table 0.23 Materials used in the formation and purification of polymersomes

Equipment	Make	Model	Catalogue number	Supplementary information
Extruder	Northern Lipids Inc	Lipex, 10mL thermobarrel	T.001	n/a
Chromatography column	GE Healthcare Sciences	HiPrep Sephacryl S-100 HR	17-1194-01	320mL

Table 0.24 Equipment used in the formation and purification of polymersomes

2.14 Characterization of polymersomes

2.14.1 Dynamic light scattering (DLS)

A Zetasizer Nano was used to measure the light scattering of polymersomes in solution. The polymersomes were diluted by adding 10 μ L of purified solution from section 2.13.1 into 990 μ L of distilled water, to a final concentration of 5 μ M. The zetasizer was set at 25 °C, viscosity at 0.8872 centipoise, the dispersant refractive index at 1.330. These were the internal levels the instrument had on file for water at this temperature (due to the diluteness of the solution). As only intensity size distribution was being measured, the refractive index of the material was not needed as it would not influence the intensity measurements¹⁸⁰. Disposable cuvettes (from section 2.6.2) were used, with 15 measurements taken per run over three runs total. The zetasizer software analyzed and calculated the intensity-weighted size distribution, to produce the final z-average and PDI (polydispersity index).

2.14.2 Scanning electron microscopy (SEM)

Procedure

Copper grids were prepared for SEM work by both cleaning, and making them hydrophilic, through a exposure to a glow discharge system over 10 seconds. Polymersomes were diluted to approximately 1.6 μM using PBS buffer, and stained with 1.5% uranyl acetate. Uranyl acetate was prepared by dissolving 0.15 g of solid in 10 mL distilled water, with stirring in a fume hood, at room temperature overnight. It was then filtered with a 0.22 μm filter (same filter from section 2.8.2).

To stain the polymersomes, 5 μL was placed on copper grid surface for 10 seconds, followed by gently drying of the sample by blotting using filter paper (material found in 2.12.2). 5 μL of the uranyl acetate solution was then added to the grid, and removed in the same fashion. The samples were dried overnight in a vacuum oven at room temperature. Samples were then viewed using a scanning electron microscope running in TEM mode at 30.0 kV with a current of 20 μA .

2.14.3 Cryogenic transmission electron microscopy (Cryo-TEM)

Polymersomes were diluted following purification (see section 2.13.1), to approximately 50 μM , using PBS buffer. Carbon TEM grids were placed in a glow discharger to prepare the grid surface for sample application (as in section 2.14.2). 10 μL of solution was placed on the grid and allowed to stand for 2 minutes. The grid was mounted on the freezing plunger, and chilled in liquid ethane. Following chilling, a cryo-transfer holder was used to load the grid. The samples were imaged at 200 kV, with a 10 eV energy slit being applied for improved contrast.

2.14.4 Materials and equipment

Material	Supplier	Catalogue number	Purity	Molecular weight	CAS number
Uranyl acetate	Spectrum Chemicals	U1005	100 % by weight	424.2 g/mol	6159-44-0
Copper grid	Electron Microscopy Sciences	FF400-Cu	n/a	n/a	n/a
Holey carbon grids	Agar Scientific	AGS147	n/a	n/a	n/a

Table 0.25 Materials used in the characterization of polymersomes

Equipment	Make	Model	Catalogue number	Supplementary information
Zetasizer	Malvern	Nano ZS	n/a	Analysis range: 0.6 nm – 6 µm Temperature control range: 0 °C – 90 °C ± 0.1
Glow Discharger	Pelco	easiGlow	91000	GD4 vacuum pumping system, 91040
Vacuum oven	VWR	12.5L vacuum oven	10144-910	Temperature range: 10-220° C
Scanning electron microscope	Hitachi	S-4800		Accelerated voltage range: 0.5-30kV Magnification: 30-800,000X Image capture software: Quartz PCI version 0.9, Image editing software: ImageJ ¹⁸¹
Rapid Immersion Freezer	Electron Microscopy Sciences	EMS-002	37000	Cryo-transfer holder Make: Gatan Model: 914
Rapid Immersion Freezer	Electron Microscopy Sciences	EMS-002	37000	Cryo-transfer holder Make: Gatan Model: 914
Transmission electron microscope	Jeol	JEM-2200FS	n/a	Accelerating voltage: Up to 200 kV Magnification: 100-1,500,000X

Table 0.26 Equipment used in the characterization of polymersomes

2.15 Post-encapsulation experiments

2.15.1 Digestion assay

Polymersomes were formed in the presence of Rpi (procedure outlined in section 2.13.1). A control and an experimental solution of Rpi were both prepared at the same concentration (11 μM), with the same buffer (25 mM Tris-HCl, pH 8- see materials and procedure in section 2.6.1) as the polymersomes. 1 mg of Proteinase K was dissolved in 1 mL distilled water to make a stock solution. 100 μL of this solution added to each of the experimental solutions (one with polymersomes, one with free Rpi), with 100 μL of distilled water being added to the control. A calcium chloride (CaCl_2) stock was prepared by dissolving 14.7 g in 100mL distilled water. CaCl_2 was added to a final concentration of 5 mM to all solutions, followed by incubation with shaking at 37 $^\circ\text{C}$ for 9 hours (using the incubator from section 2.6.2), until the average level of enzymatic activity (v_0) was appeared no different from the background isomerization of R5P in a separate blank well containing R5P in buffer.

PMSF was dissolved in ethyl alcohol (materials found in sections 2.7.2 and 2.12.2 respectively) to a final concentration of 100 mM to create a fresh stock. PMSF was added to the three solutions to a final concentration of 5 mM to inactivate the proteinase. The solutions were gently shaken for 10 minutes to ensure complete inactivation, followed by the addition of 50 μL of surfactant (Polysorbate 20). The solutions were shaken for one minute, gently inverting the tubes to prevent formation of bubbles, for one minute. The procedure for measuring Rpi activity (section 2.9.1) was then followed, assuming that the concentration of Rpi present in solution was equal to the amount calculated through absorbance spectroscopy (section 3.7.3).

The software GraphPad Prism (section 2.9.4) was used to compare the mean v_0 values through ANOVA. This method was also used to determine that the enzymatic activity was not statistically different from the background earlier in the procedure.

2.15.2 Fluorescence correlation spectrophotography

A 2 mL solution of Rpi (55.3 μM) was prepared in PBS buffer, pH 8 (material in section 2.13.1) and tagged with fluorescein 5(6)-isothiocyanate (FitC) using a labeling kit. Sodium carbonate-bicarbonate buffer (0.1 M, pH 9) was prepared from the kit materials by adding 50 mL of distilled water to a capsule combined with shaking to dissolve the materials. 2 mL of this buffer was used to dissolve one capsule of FitC to make a 1 mg/mL stock. 400 μL of this solution was then combined with the 2 mL solution of Rpi in a small vial covered with tinfoil. The solution was stirred at room temperature for 2 hours, using the stir plate found in section 2.12.2. The molecular weight of Rpi was too small to use the materials provided by the kit, which is typically used for labeling much larger biomolecules such as antibodies. Excess, unreacted fluorophores were removed via sedimentation at 4000xG (using the microcentrifuge from section 2.7.2). The solution was decanted and then filtered through a 0.22 μm syringe filter (material in section 2.8.2).

The filtered solution was applied to a desalting column and eluted with PBS buffer to remove the unconjugated FitC from conjugated protein (Figure 3.28). Protein was quantified via Bradford assay (see section 2.6.3). Labeling efficiency was calculated (using the spectrophotometer and cuvettes in section 2.8.2) by way of Equation 14:

$$\text{Labelling efficiency} = \frac{\text{Abs}_{494} \times \text{dilution factor}}{68000 \text{ cm}^{-1}\text{M}^{-1} \times \text{protein concentration (M)}} \quad (14)$$

where 68000 is the molar extinction coefficient of FitC at pH 8 at 494 nm and the dilution factor is included for samples which need to be diluted to be properly measured.

A series of dilutions of the conjugate were measured using the same spectrophotometric method. The extinction coefficient of the Rpi/FitC conjugate was calculated by creating a standard curve of absorbance vs. concentration (Figure 3.31).

The FitC tagged protein was later used in the formation of enzyme-laden polymersomes following the procedure outlined in section 2.13.1. Following encapsulation, enzyme-laden polymersomes, free tagged Rpi and free dye were diluted to approximately 11 nM for polymersomes and 500 nM for the free species in PBS buffer. Solutions of 200 μ L, at room temperature, were loaded into the wells of Lab-Tek II chamber #1.5 slides.

The FitC molecules were excited at a wavelength of 488 nm, with emission measurements being made at 519 nm. FCS mode was selected for these measurements, with a pinhole size of 25 μ m and the triplet state relaxation set to 10 μ s. Ten measurements were made, each over a period of 10 seconds. The average count rates and correlation calculations were performed using the same microscopy software used for FCS capture (Zen 2 Black). The correlation was normalized to a starting value of 1 using Microsoft Excel 2010. A graph of the autocorrelation function $G(\tau)$ vs. the log of lag time (self-similarity at time τ) was prepared (Figure 3.29).

2.15.3 Spectroscopic encapsulation efficiency experiment

Purified polymersomes laden with FitC tagged Rpi in PBS were measured using the spectrophotometer and cuvettes from section 2.7.2. The blank with no polymer was made using the same PBS buffer from section 2.13.1. The blank with polymer was made by forming empty polymersomes in PBS following the procedure in section 2.13.1. The concentration of polymersomes in solution following size-exclusion chromatography was found using the procedure below.

Half of the polymersome solution was combined with three parts chloroform (material found in section 2.12.2) in a separatory funnel. The solution was agitated vigorously to dissolve the polymersomes. The more dense chloroform was carefully removed after phase separation, leaving the aqueous phase. This procedure was repeated twice more on the aqueous phase. The combined chloroform fractions were placed in a previously weighed vial, subjected to rotary evaporation (equipment as found in section 2.12.2) at 190 mBar and 100 rpm for one hour. This resulted in a dried layer of polymer,

which was then weighed. The original concentration of polymer in the remaining half solution of polymersomes was then calculated from this weight. Proper blanks for absorbance spectroscopy of the enzyme-laden polymersomes were prepared from a stock solution (0.71 μ M).

2.15.4 Materials and equipment used in post-encapsulation experiments

Material	Supplier	Catalogue number	Purity	Molecular weight	CAS number
Proteinase K	Sigma	P2308	≥ 90 %	28.93kDa	39450-01-6
CaCl ₂	Sigma	223506	≥ 99 %	147.0 g/mol	10035-04-8
PMSF	Sigma	P7626	≥ 98.5 %	174.2 g/mol	329-98-6
Polysorbate-20	FisherScientific	BP337-100	≥ 95 %	1227.5 g/mol	9005-64-5
FitC labelling kit	Sigma	FITC1	≥ 90 %	389.4 g/mol	3326-32-7
HiTrap desalting column	GE Healthcare Sciences	29-0486-84	n/a	n/a	n/a
Coverglass slides	Sigma	C7182	n/a	n/a	n/a

Table 0.27 Materials used in post-encapsulation experiments

Equipment	Make	Model	Catalogue number	Supplementary information
Dynamic Light Scattering	Malvern	Zetasizer Nano ZS	n/a	Measurement range: 0.3nm-10 μ m Temperature range: 0-90° C Software: Zetasizer DTS software Version 7.0.3
Confocal Microscope	Zeiss	LSM710	n/a	Avalanche photodiode detector: Zeiss Confocor 3 Lens: Objective-C apochromat 40x/1.2 W Corr M27, 421767-9971-000 Software: Zen 2 Black edition software, version 10,0,0,910 Argon laser lines: 458,488 and 514 nm

Table 0.28 Equipment used in post-encapsulation experiments

Chapter 3. Experimental results

3.1 Expression and purification of PRK

3.1.1 PRK from *S. olceracea*

Following the PCR amplification of the synthesized gene insert, the solution was applied to an agarose gel. The amplified gene was visible and corresponded well with the actual size of 1053 base pairs (Figure 3.1).

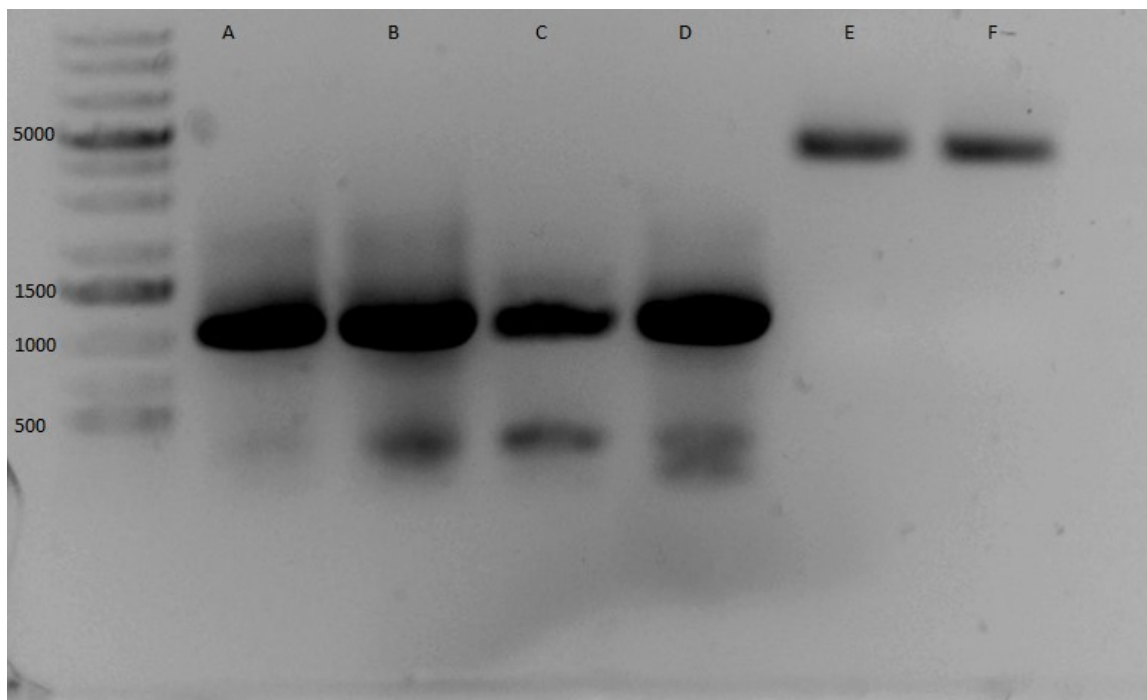


Figure 3.1 Agarose gel of PRK gene and pET-15b vector. Lanes A-D are PRK gene following PCR amplification. Lanes E,F are purified pET-15b vector. Ladder is 1kb Plus DNA ladder with units in base pairs.

The construct was transformed into DH5- α cells. Five isolated colonies were chosen which were used to inoculate 5 mL of media. The cultures were collected and the plasmids were harvested via miniprep protocol. The inserted sequence was verified by Illumina dye DNA sequencing by the Molecular Biology Service Unit (Department of Biological Sciences, University of Alberta). Two forward reads and two reverse reads were conducted for total gene coverage. The raw sequencing files were compared to the actual construct sequence using the online multiple sequence alignment program Clustal

Omega¹⁸², with the reverse sequences being changed to their reverse complement through an online bioinformatics program called Reverse Complement¹⁸³ (Table 3.1). No mutations were present in the sequence alignment.

Forward1	ATTTTGTTTAACTTTAAGAAGGAGATATACCATGGGTAGCCAGCAGCAGACCATTGTGAT
Forward2	-TTTGTTTAACTTTAAGAAGGAGANATACCATGGGTAGCCAGCAGCAGACCATTGTGAT
P09559	-----AGCCAGCAGCAGACCATTGTGAT
Reverse1	-----
Reverse2	-----
Forward1	TGGCCTGGCGGCGGATAGCGGCTGCGGCAAAAAGCACCTTTATGCGCAGCCTGACCAGCGT
Forward2	TGGCCTGGCGGCGGATAGCGGCTGCGGCAAAAAGCACCTTTATGCGCAGCCTGACCAGCGT
P09559	TGGCCTGGCGGCGGATAGCGGCTGCGGCAAAAAGCACCTTTATGCGCAGCCTGACCAGCGT
Reverse1	-----
Reverse2	-----
Forward1	GTTTGGCGGCGCGGCGGAACCGCCGAAAGGCGGCAACCCGGATAGCAACACCCTGATTAG
Forward2	GTTTGGCGGCGCGGCGGAACCGCCGAAAGGCGGCAACCCGGATAGCAACACCCTGATTAG
P09559	GTTTGGCGGCGCGGCGGAACCGCCGAAAGGCGGCAACCCGGATAGCAACACCCTGATTAG
Reverse1	-----AAAAGNNGNCNANNNGNAGCNNNNNCCNNNNNAGC
Reverse2	-----AGCANNNNNGNTTAGN
Forward1	CGATACCACCACCGTGATTTGCCTGGATGATTTTCATAGCCTGGATCGCAACGGCCGCAA
Forward2	CGATACCACCACCGTGATTTGCCTGGATGATTTTCATAGCCTGGATCGCAACGGCCGCAA
P09559	CGATACCACCACCGTGATTTGCCTGGATGATTTTCATAGCCTGGATCGCAACGGCCGCAA
Reverse1	GANNNNNNCCNCCGTGATTTGCCTGGATGNTTTTCATAGNNGNATCGCAACGGCCGCAA
Reverse2	NANCCNCCNCCGTNATTTGNCNNGGATGATTTTCATAGCCTGGATNGCAACNGCCGCAA
	* * * * *
Forward1	AGTGGA AAAAGTGACCGCGCTGGATCCGAAAGCG-AACGATTTTGATCTGATGTATGAAC
Forward2	AGTGGA AAAAGTGACCGCGCTGGATCCGAAAGCG-AACGATTTTGATCTGATGTATGAAC
P09559	AGTGGA AAAAGTGACCGCGCTGGATCCGAAAGCG-AACGATTTTGATCTGATGTATGAAC
Reverse1	AGTGGA AAAAGTGNCCGCGCTGGATCCGAAAGCGNAACGATTTTGATNTGATGTATGAAC
Reverse2	NGTGGA AAAAGTGNCCGCGCTGGATNCGAAAGCG-AACGATTTTGATNTGANGTATGAAC

Forward1	AGGTGAAAGCGCTGAAAGAAGGCAAAGCGGTGGATAAACCGATTTATAACCATGTGAGCG
Forward2	AGGTGAAAGCGCTGAAAGAAGGCAAAGCGGTGGATAAACCGATTTATAACCATGTGAGCG
P09559	AGGTGAAAGCGCTGAAAGAAGGCAAAGCGGTGGATAAACCGATTTATAACCATGTGAGCG
Reverse1	AGGTGAAAGCGCTGAAAGAAGGCAAAGCGGTGGATNAACCGATTTATAACCATGTGAGCG
Reverse2	AGGNNAANCCTGAAAGAAGGCAAAGCGGNGGATAAACCGATTTATAACCATGTGAGCG
	*** * *
Forward1	GCCTGCTGGATCCGCCGGAACGATTCAGCCGCCGAAAATTTCTGGTGATTGAAGGCCTGC
Forward2	GCCTGCTGGATCCGCCGGAACGATTCAGCCGCCGAAAATTTCTGGTGATTGAAGGCCTGC
P09559	GCCTGCTGGATCCGCCGGAACGATTCAGCCGCCGAAAATTTCTGGTGATTGAAGGCCTGC
Reverse1	GCCTGCTGGATCCGCCGGAACGATTCAGCCGCCGAAAATTTCTGGTGATTGAAGGCCTGC
Reverse2	GCNTGCTGGATCCGCCGGAACGATTCAGCCGCCGAAAATTTCTGGTGATTGAAGGCCTGC
	** *****
Forward1	ATCCGATGTATGATGCGCGCTGCGCGAACGCTGGATTTTAGCATTTATCTGGATATTA
Forward2	ATCCGATGTATGATGCGCGCTGCGCGAACGCTGGATTTTAGCATTTATCTGGATATTA
P09559	ATCCGATGTATGATGCGCGCTGCGCGAACGCTGGATTTTAGCATTTATCTGGATATTA
Reverse1	ATCCGATGTATGATGCGCGCTGCGCGAACGCTGGATTTTAGCATTTATCTGGATATTA
Reverse2	ATNCGATGTATGATGCGCGCTGCGCGAACGNTGGATTTTAGCATTTATCTGGATATTA
	** *****
Forward1	GCAACGAAGTAAAATTTGCGTGAAAATTCAGCGCGATATGAAAGAACGCGCCATAGCC
Forward2	GCAACGAAGTAAAATTTGCGTGAAAATTCAGCGCGATATGAAAGAACGCGCCATAGCC
P09559	GCAACGAAGTAAAATTTGCGTGAAAATTCAGCGCGATATGAAAGAACGCGCCATAGCC
Reverse1	GCAACGAAGTAAAATTTGCGTGAAAATTCAGCGCGATATGAAAGAACGCGCCATAGCC
Reverse2	GCAACGAAGTAAAATTTGCGTGAAAATTCAGCGCGATATGAAAGAACGCGCCATAGCC

Forward1	TGGAAGCATTAAAGCGAGCATTGAAAGCCGAAACCGGATTTTGATGCGTATATTGATC
Forward2	TGGAAGCATTAAAGCGAGCATTGAAAGCCGAAACCGGATTTTGATGCGTATATTGATC

Three different *E. coli* host strains were chosen for expression testing of PRK: SHuffle T7, BL-21 (DE3) and C43 cells. The various cell types were transformed with the plasmid vector via heat shock transformation, grown under differing temperatures and subjected to varying amounts of inducing agent concentrations. The soluble portion of the protein lysate was applied onto an SDS-polyacrylamide gel. Expression was estimated by comparing band thickness and the degree of staining at the expected location of PRK against the other soluble protein bands using a relative quantitation method. The gels containing the highest PRK expression for each platform are found in Figure 3.2-4.4. Band widths of PRK bands may be found in the appendix, Table A1. From each cell type, the lane with the most apparent PRK in relation to background was chosen as the local optimum. These are listed in Table 3.2.

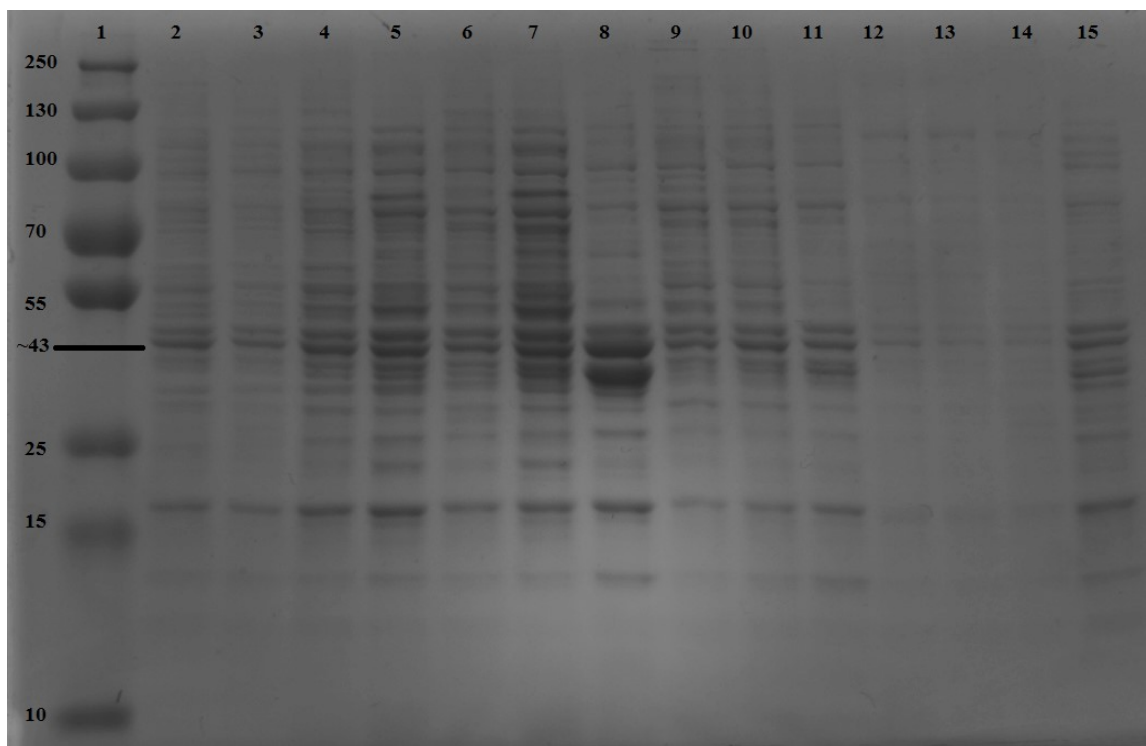


Figure 3.2 SDS-PAGE of PRK expression in BL-21 cells. The growth conditions of the sample run in lane 8 (sample 57) resulted in the highest amount of PRK expression when compared to background proteins. Lanes 2-15 correspond with samples 51-64 in Table 3.8.

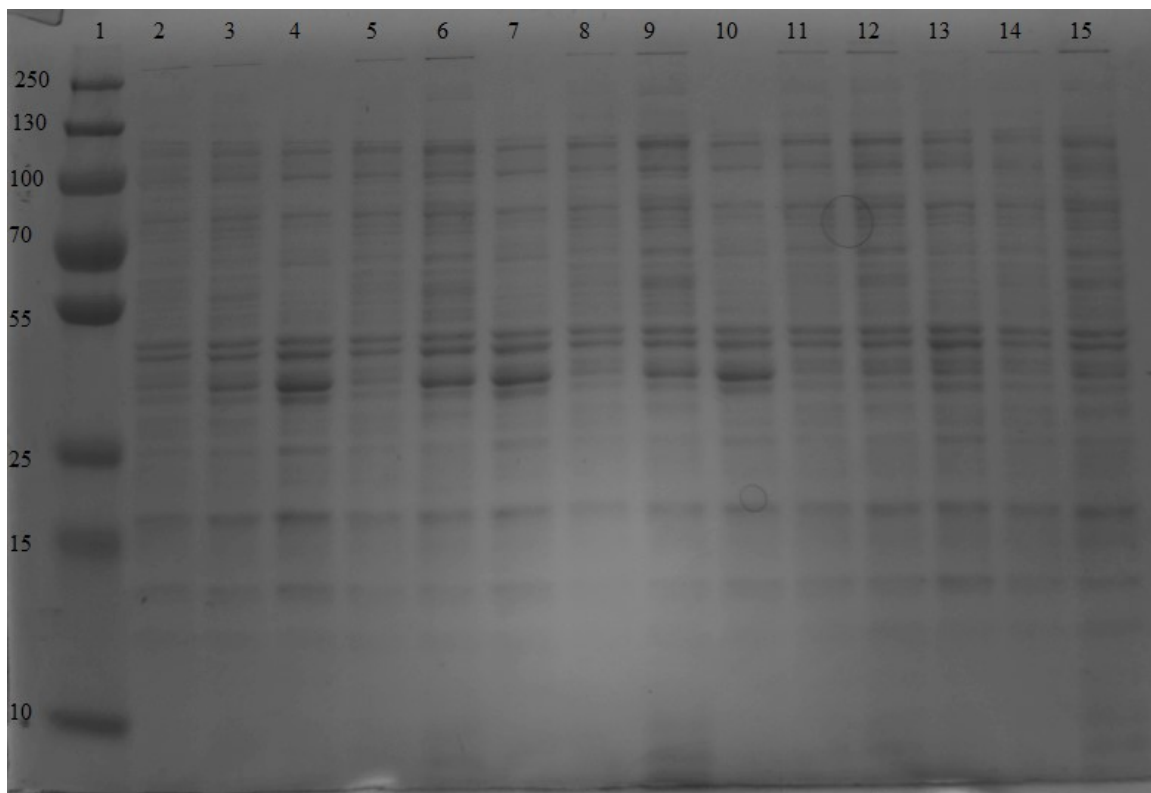


Figure 3.3 SDS-PAGE of PRK expression in C-43 cells. The growth conditions of the sample run in lane 7 (sample 15) resulted in the highest amount of PRK expression when compared to background proteins. Lanes 2-15 correspond with samples 10-23 in Table 3.8.

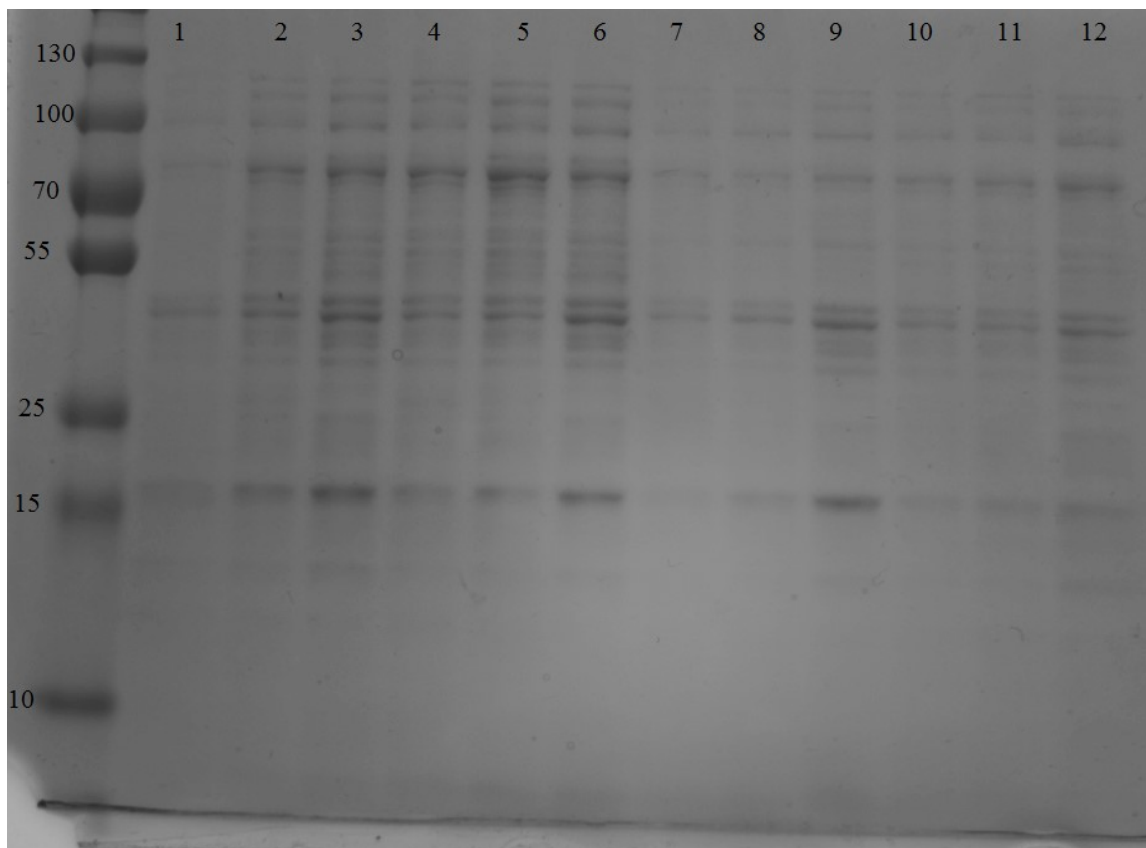


Figure 3.4 SDS-PAGE of PRK expression in T7 cells. The growth conditions of the sample run in lane 6 (sample 33) resulted in the highest amount of PRK expression when compared to background proteins. Lanes 1-12 correspond with samples 28-41 in Table 3.8.

The three optimal cell conditions were further investigated by inoculating 500 mL of TB media, and subsequently allowing the cultures to grow under the local optimum conditions at 225 rpm overnight. These cultures cell density was measured using their OD_{600} values the following day, yielding: 2.331 for BL-21, 2.274 for C43, and 1.76 for T7 type cells.

Local Optimal Condition	T7	C43	BL-21
Temperature (°C)	18	30	18
Growth time (Hours)	24	24	24
[IPTG] (mM)	0.5	0.5	0.1

Table 3.2 Conditions which produced the most apparent PRK once induced, as decided from SDS-polyacrylamide gel results.

BL-21 was ultimately chosen as the cell type to express spinach PRK as it gave the highest cell density using the local optimal growing conditions. These cells were grown, induced and lysed. The soluble lysate solution was applied onto a weak-anion exchange column packed with DEAE bound to the polysaccharide polymer sepharose. Proteins will bind to the column if they contained a net negative charge at the pH of the solution, while the presence of a negative ion in solution (such as Cl^-) will compete with protein binding. The bound protein was eluted using a gradient of buffer, with increasing NaCl (Figure 3.5).

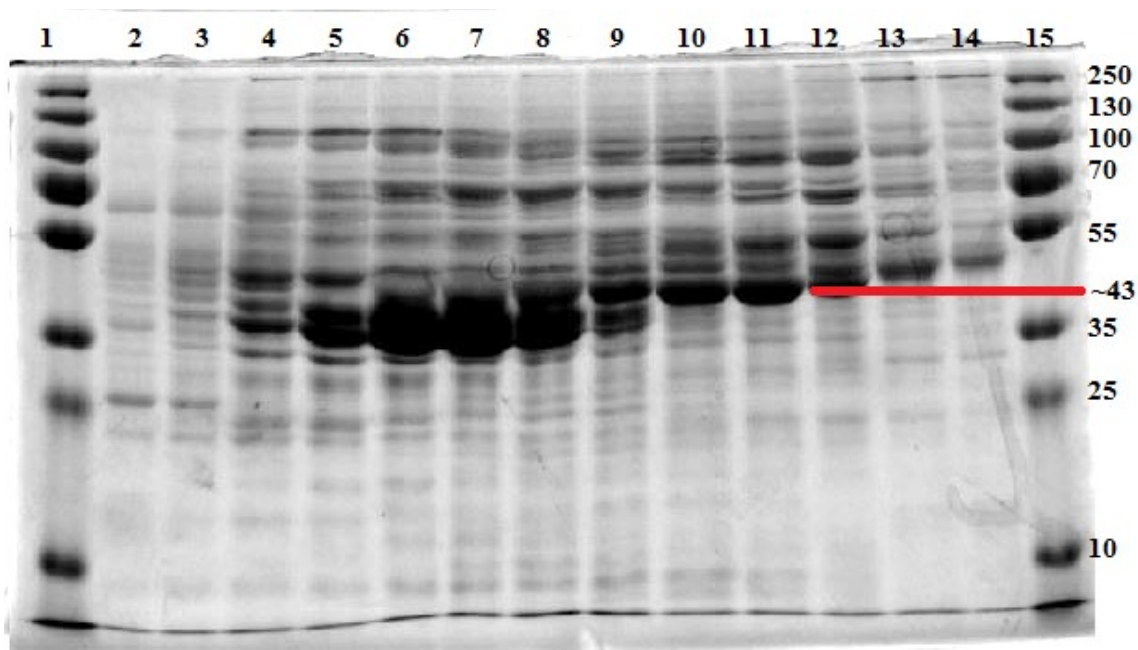


Figure 3.5 SDS-polyacrylamide gel of ion exchange elution fractions. Lanes 8-12 contained the majority of PRK.

The spinach PRK construct had an estimated molecular weight of 37.7 kDa. A large band was observed at this expected size between lanes 4 and 9. One of these were excised and analyzed by the Alberta Proteomics and Mass Spectrometry Facility (Department of Biochemistry, University of Alberta). A second, higher molecular weight band was similarly excised at approximately 43 kDa, as indicated in Figure 3.5, Lane 11.

Description	Coverage	Number of Peptides
Spinach Construct	87.46%	37

Table 3.3 Results of MALDI-TOF protein identification submission

The sequencing of the higher molecular weight band revealed that nearly 90% of the protein in the band consisted of the protein of interest. The number of peptides includes unique peptides cleaved from the protein of origin, as well as from other proteins present in the band. These results are consistent with the apparent molecular weight of spinach PRK in literature, in contrast with the estimated, and smaller molecular weight^{94,184}.

Lane 10 of Figure 3.5 corresponds to the fraction that eluted at a 160 mM NaCl gradient concentration. This lane was combined with lanes 11 and 12, as they had less protein contaminants in proportion to earlier lanes where PRK also appears to have eluted under a less concentrated salt gradient. The combined fractions were desalted and concentrated using a 10 kDa Amicon centrifugal filter. Using a filter with a larger molecular weight cut off allowed for the removal of smaller contaminating proteins. The concentrated solution was applied onto a HiTrap Blue column

Elution was completed with a linear gradient of ATP. Fractions were run on an SDS-polyacrylamide gel, revealing a light band corresponding to the molecular weight of PRK eluted at a concentration of 1 mM ATP (Figure 3.6). This solution was filtered to remove the lower molecular weight contaminant. The spinach PRK, in combination with one contaminating band, yielded 0.8 mg of protein per litre of culture as calculated by a Bradford assay.

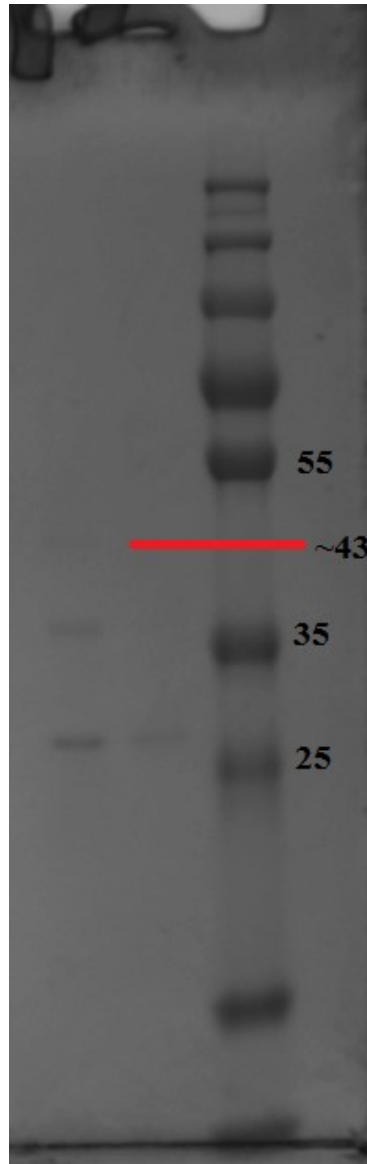


Figure 3.6 Partially purified *S. oleracea* PRK at ~43kDa, with contaminating bands at ~26 and ~36kDa

3.1.2 Purification of PRK from *S. elongatus*

The PRK construct from *S. elongatus* contains a 6xHis-tag, which is a repeated sequence of six histidine molecules that have affinity towards metal ions such as nickel and cobalt¹⁸⁵. These metal ions are in turn bound to a resin that is contained in a column. Following cell lysis, and centrifugation to remove insoluble materials, cell lysate supernatant was applied to a nickel-agarose column. A single chromatographic step (Figure 3.7) removed the vast majority of contaminants from the 6xHis-tagged PRK

(Figure 3.8). The overall yield approached 33 mg/L of culture following the final concentration step as quantified by Bradford assay.

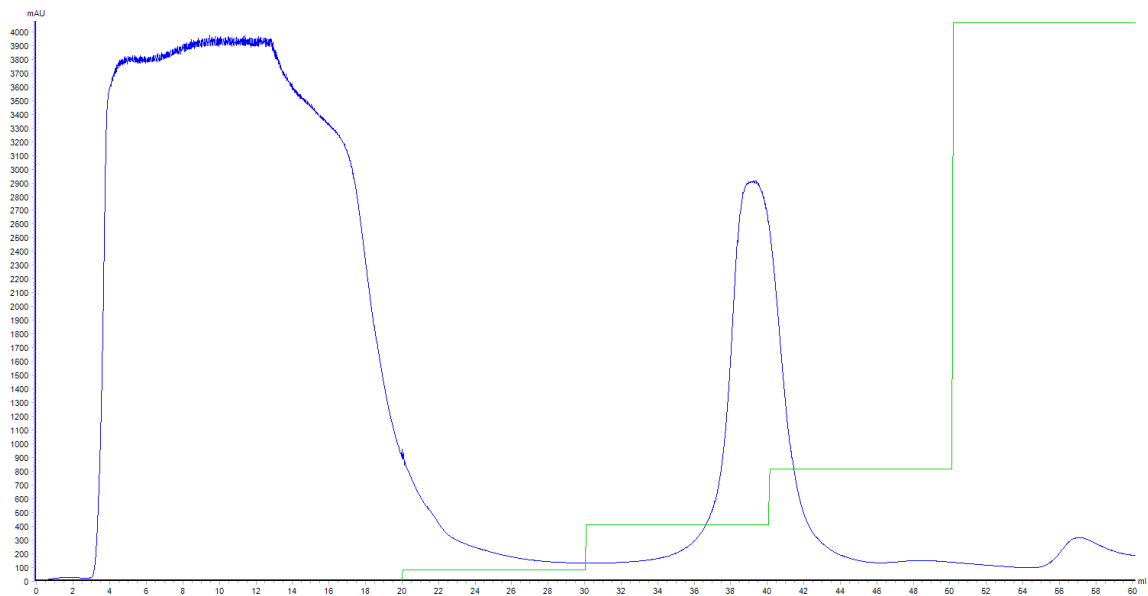


Figure 3.7 Chromatogram showing the elution profile of proteins during 6xHis-tagged PRK purification. The blue line represents the absorbance at 280 nm, while the green is the relative concentration of elution buffer. The final peak contained the tagged PRK.

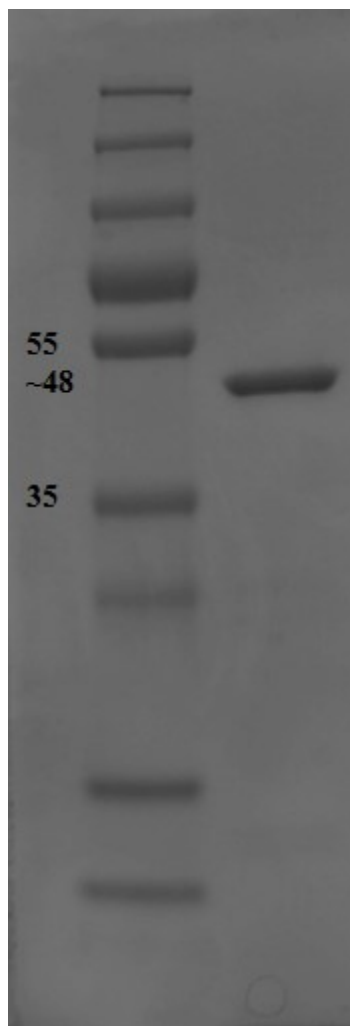


Figure 3.8 SDS-PAGE of 6His-PRK, located at approximately 48 kDa.

3.2 Kinetic characterization of Rpi and PRK

3.2.1 Rpi results

The kinetics of Rpi activity was investigated using absorbance spectroscopy. The initial reaction rate (v_0) absorbance data was converted to a rate of change in concentration using a published extinction coefficient of the substrate in the same buffer used (Figure 3.9)¹⁷⁴.

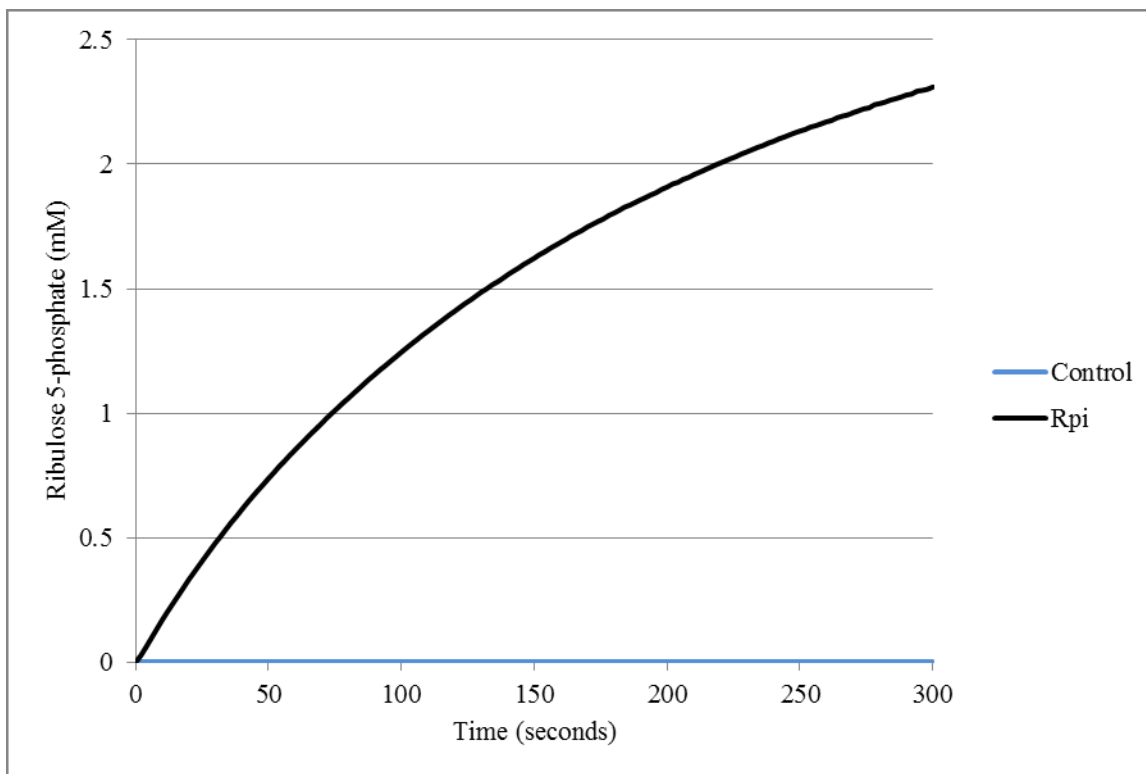


Figure 3.9 Graph of Ru5P product formed over time. The control wells contained substrate, with buffer being added in place of enzyme. N=4 for control and experimental wells.

The kinetics of the two enzymes was characterized through the use of Michaelis-Menten modeling. The optimized levels of factors (found in section 3.4.1) were used in the experimental method, following verification of the local optimization results. The method saw the concentration of substrate varied over seven or eight reactions, plotted against the reaction rate, while the concentration of enzyme between assays remained constant. The reactions were performed in quadruplicate, with the mean and standard error of the four being used in calculations to fit a curved line using least-squares nonlinear regression (Figure 3.10). The K_m of Rpi was found to be 9.4 ± 0.73 mM (Table 3.4).

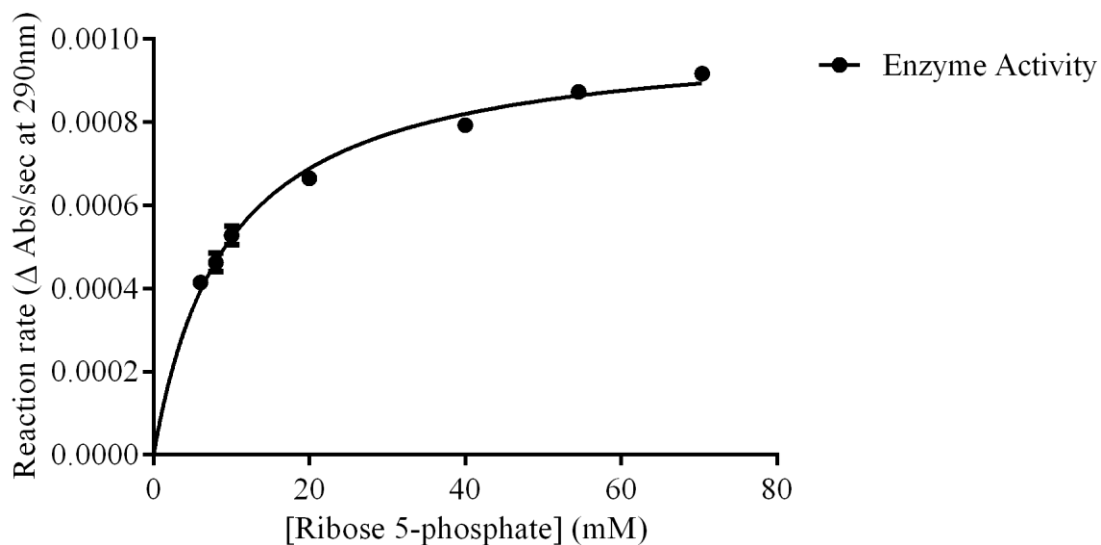


Figure 3.10 Michaelis-menten saturation curve for Rpi

Enzyme	Values in literature	Calculated values and standard error	R^2	Confidence interval (95%)
RpiA	$3.1 \pm 0.2 \text{ mM}^{73}$ $5.9 \pm 0.9 \text{ mM}^{81}$	$9.4 \pm 0.73 \text{ mM}$	0.99	7.5 to 11.3 mM

Table 3.4 Michaelis constants of Rpi found in literature, with the experimentally calculated constant.

3.2.2 PRK results

A standard curve of the substrate NADH was made to facilitate the conversion of absorbance data to molar concentrations (Figure 3.11). The kinetics of PRK activity was investigated using absorbance spectroscopy. The initial reaction rate (v_0) absorbance data was converted to a rate of change in concentration using the equation for line of best fit of this standard curve (Figure 3.12).

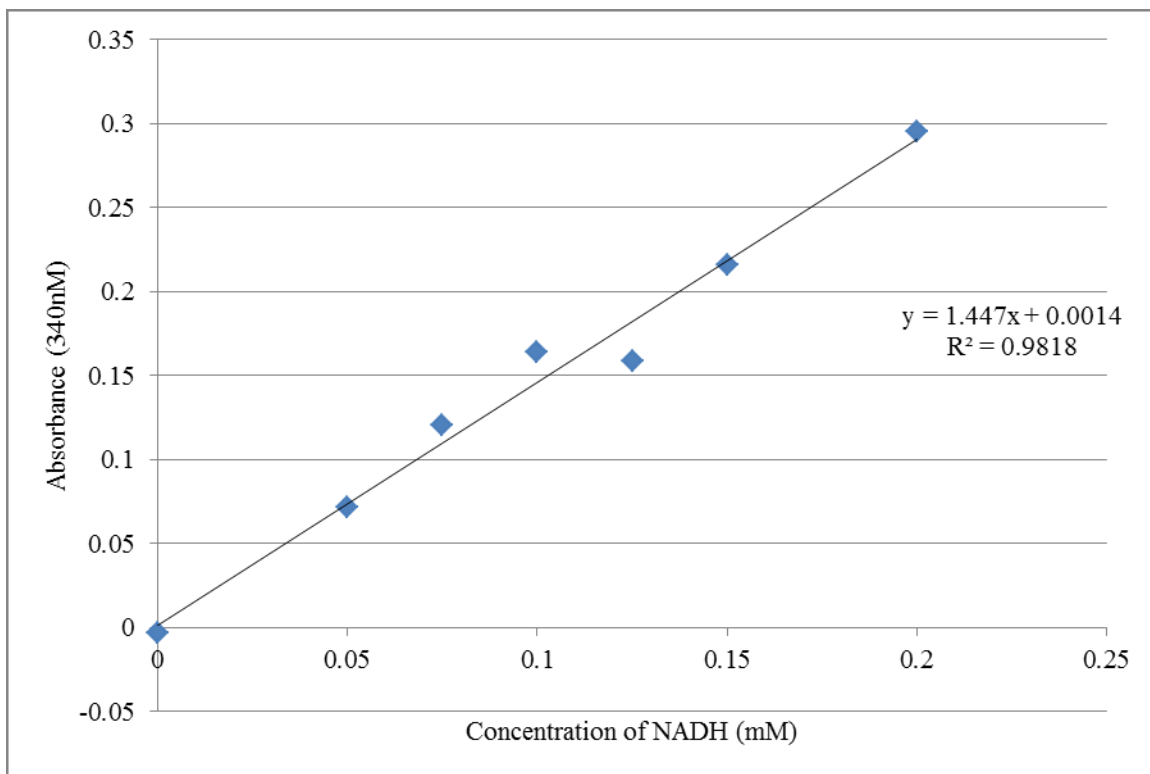


Figure 3.11 Standard curve of NADH stock used in the PRK kinetic assays

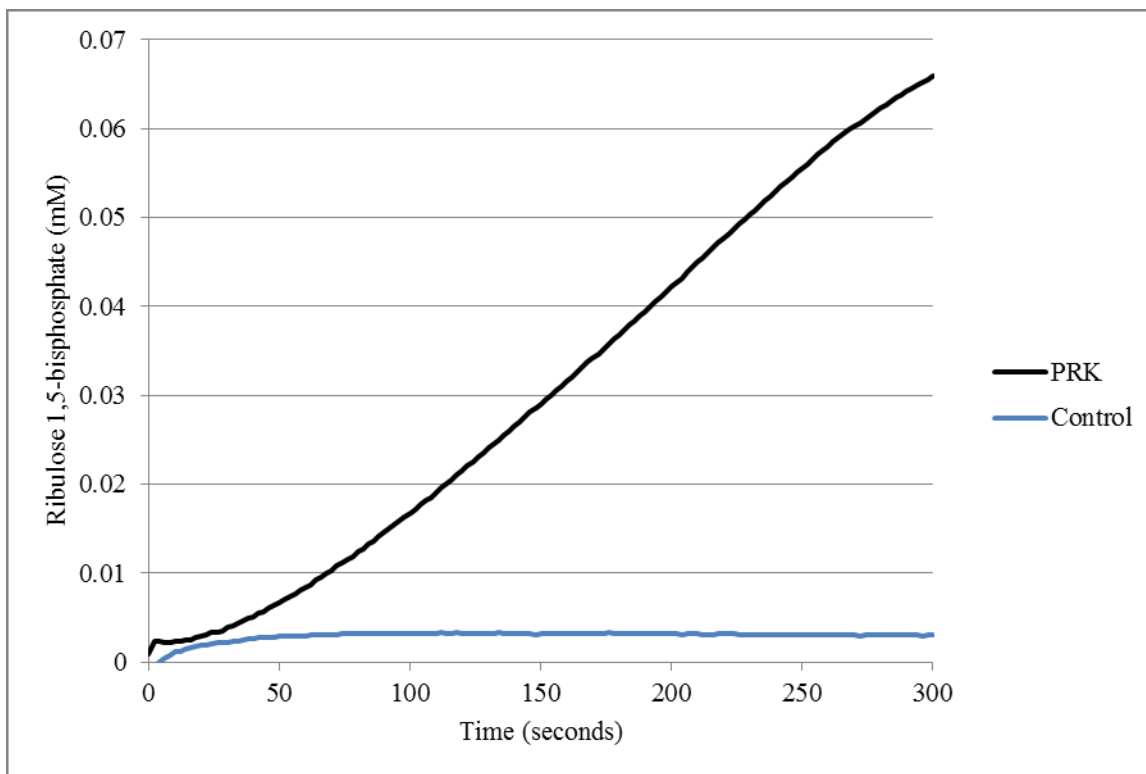


Figure 3.12 Graph of RuBP product formed over time using PRK from *Synechococcus elongatus*. The control wells contained all reagents with the exception of PRK, with buffer being added in place of enzyme. N=4.

The kinetics of the two enzymes was further characterized through the use of Michaelis-Menten modeling. The optimized levels of factors (found in section 3.4.2) were used in the experimental method, following verification of the local optimization results. The method involved varying the concentration of substrate, both Ru5P and ATP, between reactions while the concentration of enzyme remained constant. The reactions were performed in quadruplicate, with the mean and standard error of the four being used in calculations to fit a curved line using least-squares nonlinear regression. The calculated K_m of Ru5P was 0.12 ± 0.02 mM, while the K_m of ATP was 0.069 ± 0.014 mM (Table 3.5).

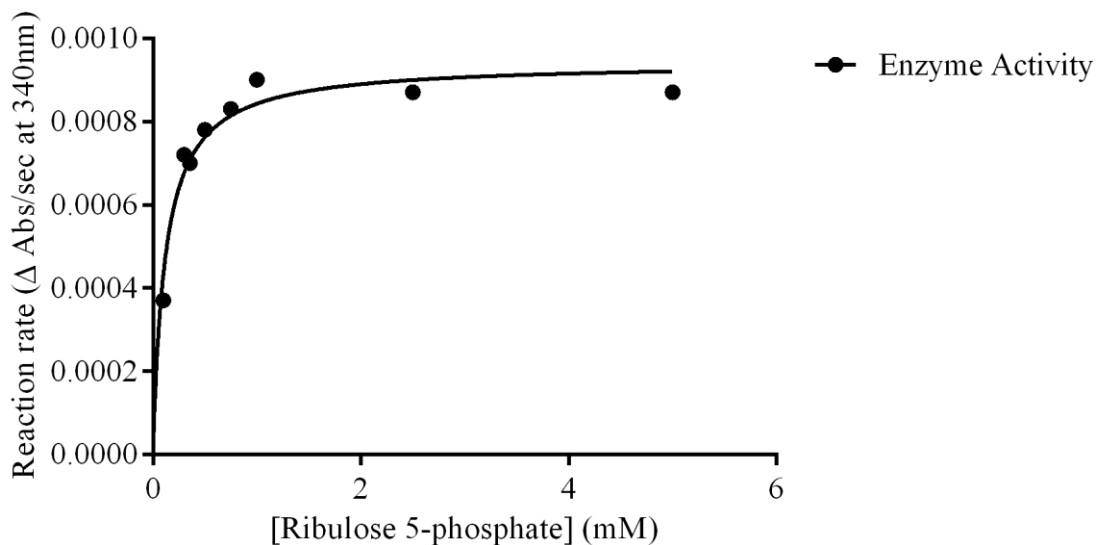


Figure 3.13 Michaelis-Menten saturation curve of PRK activity for the substrate Ru5P

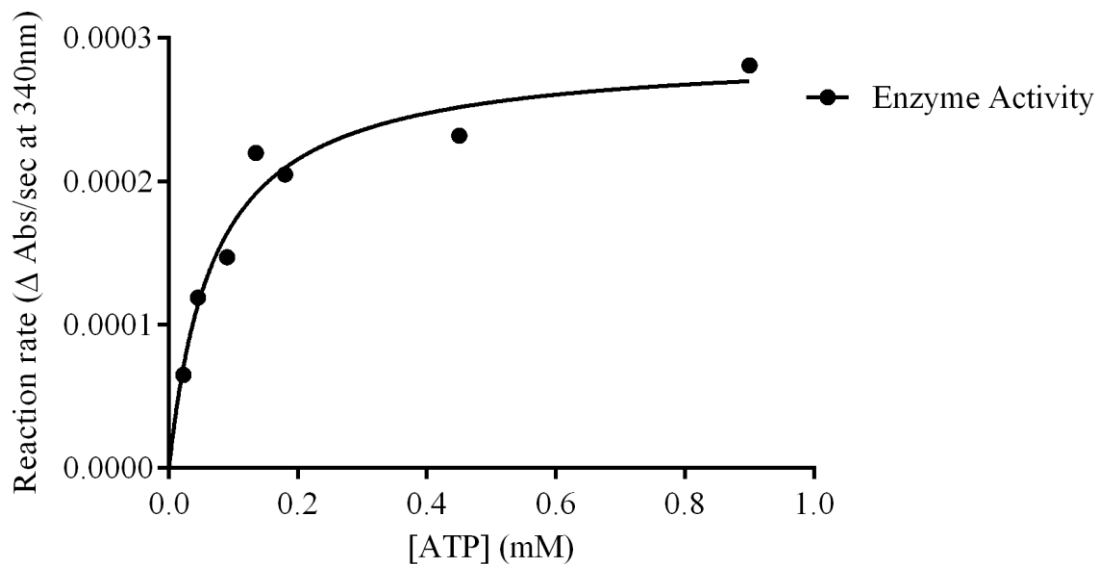


Figure 3.14 Michaelis-menten saturation curve of PRK activity for the substrate ATP

The calculated Michaelis constants of the enzymes Rpi and PRK are compared with constants found in literature (Table 3.5).

Enzyme	Values in literature	Calculated values and standard error	R^2	Confidence interval (95%)
PRK _{ATP}	0.09 mM ¹⁰³	0.069 ± 0.014mM	0.95	0.031 to 0.11 mM
PRK _{Ru5P}	0.27 mM ¹⁰³	0.12 ± 0.02mM	0.94	0.066 to 0.17 mM

Table 3.5 Michaelis constants of PRK found in literature, with the corresponding experimentally calculated constants.

3.3 Stability of enzymes

The durability of the enzymes when exposed to various environmental factors was investigated through two experiments focused on two different factors. These factors were ambient storage temperature over time, and the effect of UV light exposure, and how the activity levels relate to these variables.

3.3.1 Rpi stability

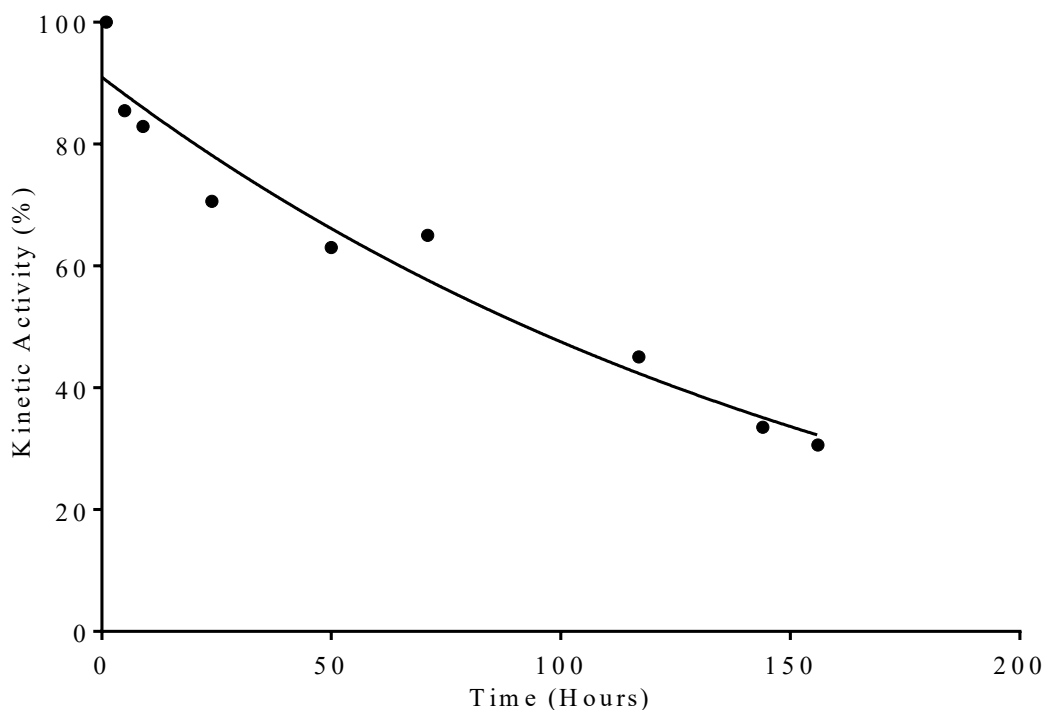


Figure 3.15 Activity of Rpi over time when stored at room temperature. $R^2=0.947$

The stability of Rpi at room temperature was investigated by measuring the enzymes kinetic activity over a period of time. The half-life was calculated to be 89 hours for Rpi (Figure 3.15). The enzyme solution was stored at ambient temperature in the dark between assays.

3.3.2 PRK stability

The stability of PRK at room temperature was investigated by measuring the enzymes kinetic activity over a period of time. The calculated half-life of the kinetic activity was approximately 177 minutes (Figure 3.16). The enzyme solution was stored at ambient temperature in the dark between assays.

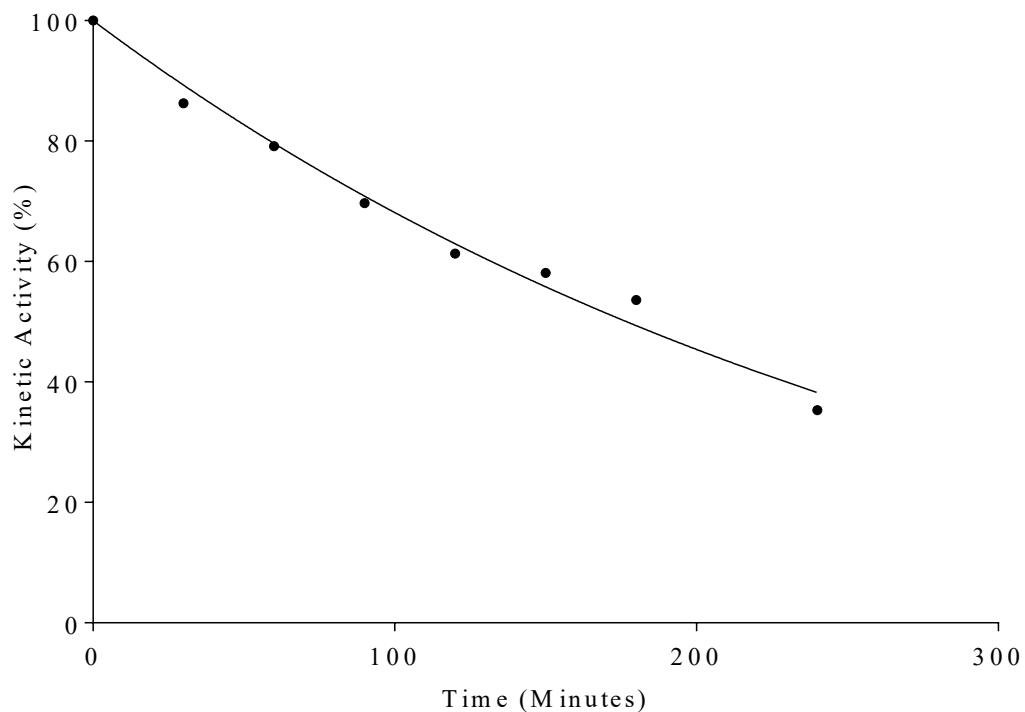


Figure 3.16 Activity of PRK over time when stored at room temperature. $R^2=0.984$

3.3.3 Enzyme stability with UV exposure

The enzymes PRK and Rpi were exposed to UV light, at 254 nm, for a short time (Figures 4.15 and 4.16). Their activity (v_0) was measured at $t = 0$, 1 and 5 minutes. The results are found in Table 3.6, with each assay consisting of $N=3$ replicates.

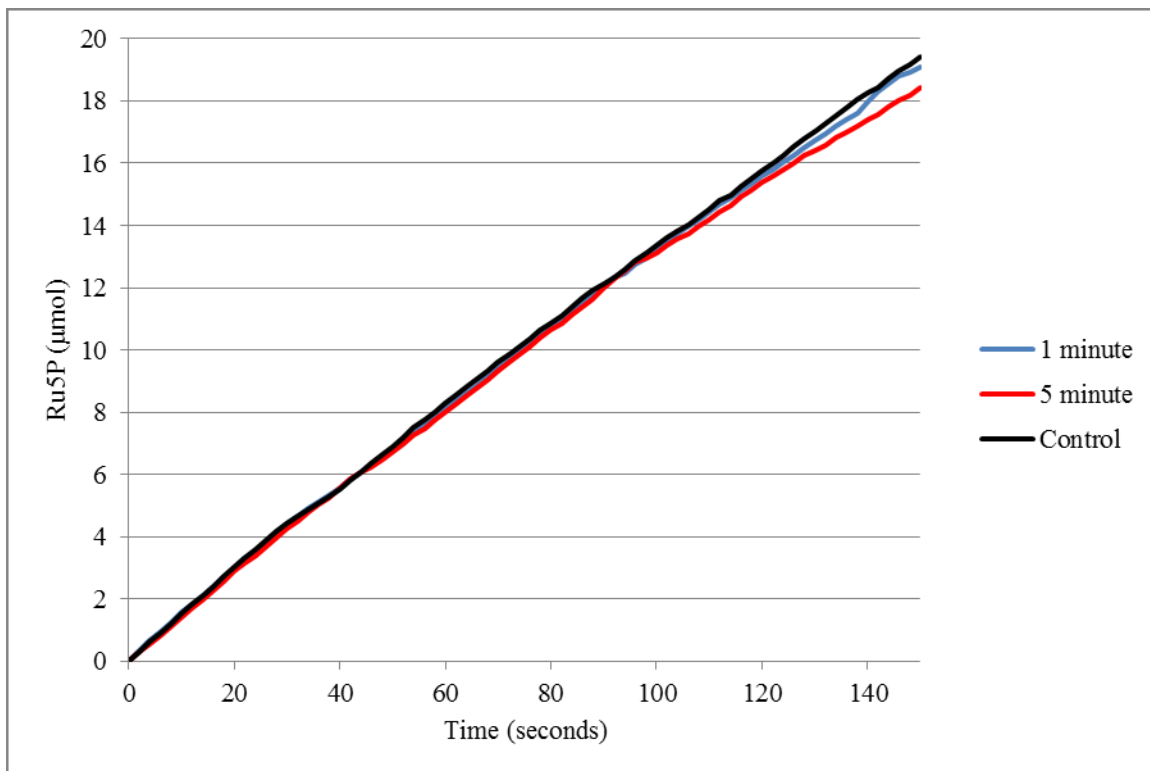


Figure 3.17 Graph of Ru5P formed over time by Rpi exposed to UV light.

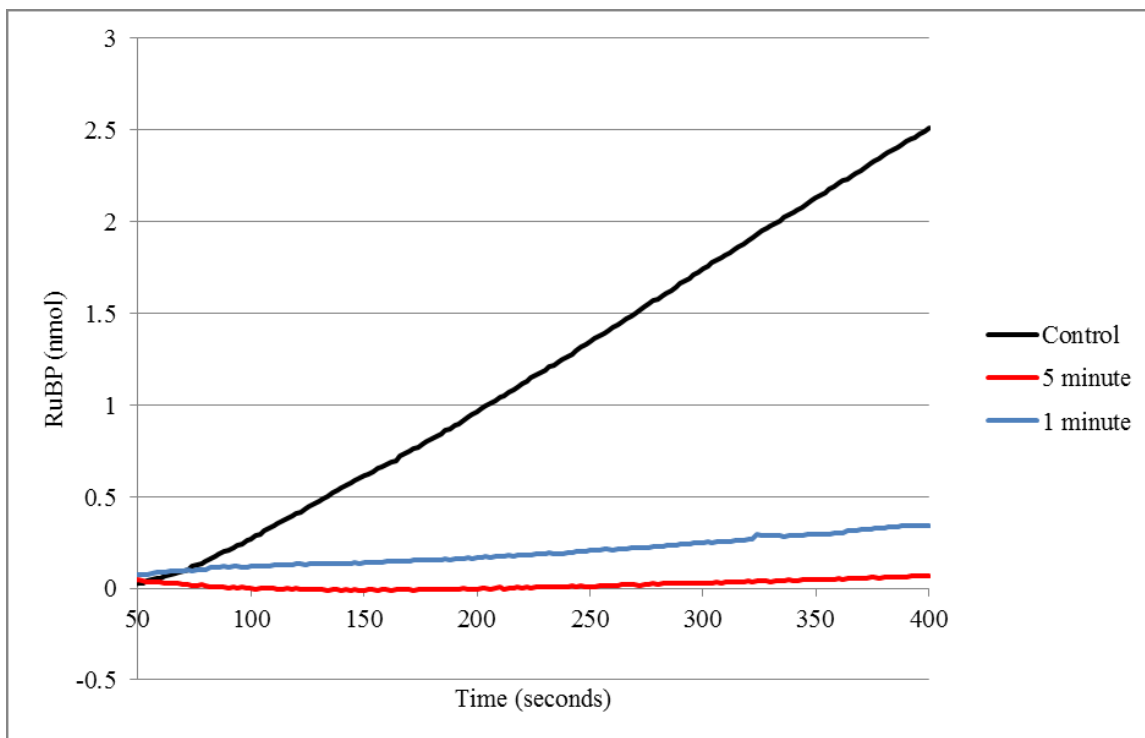


Figure 3.18 Graph of RuBP formed over time by PRK exposed to UV light.

Exposure Time	PRK v_0 (nmols/sec)	Retained activity	Rpi (v_0) (nmols/sec)	Retained activity
Initial Activity	7.80 ± 0.01	100 %	148.27 ± 0.61	100 %
1 minute	0.95 ± 0.01	12.1 %	145.80 ± 0.98	98.3 %
5 minutes	0.38 ± 0.01	4.8 %	141.95 ± 0.52	95.7 %

Table 3.6 Activity of the enzymes following UV exposure

3.4 Local optimization of kinetic activity

3.4.1 Optimization of Rpi

First model:

Optimization of the kinetic rate of Rpi was carried out using surface response methodology. The choice of the central, factorial and axial point levels is discussed further in section 4.3.1. The average v_0 , collected in the form of Δ Absorbance/second at 290 nm, was entered into a central composite designed spreadsheet. Regression analysis was completed using the software, to identify statistically significant factors. A quadratic

model and optimal levels were calculated using the program. The models significance was evaluated using analysis of variance (ANOVA) tests.

Using the software Minitab, an investigative domain was established (Table 0.17), followed by response surface regression analysis being performed on the collected data with a confidence interval set at 95 %.

Term	Coefficient	Standard Error of Coefficient	T-Value	P-Value
Constant	5.4×10^{-4}	1.8×10^{-5}	30.45	0
<i>B</i>	2.3×10^{-5}	6.6×10^{-6}	3.47	0.001
<i>D</i>	-2.4×10^{-4}	6.4×10^{-6}	-3.81	0
<i>C</i>	6.7×10^{-5}	6.4×10^{-6}	10.38	0
<i>A</i>	3.4×10^{-5}	6.6×10^{-6}	5.14	0
<i>B * B</i>	1.1×10^{-5}	7.0×10^{-6}	0.1	0.917
<i>D * D</i>	1.4×10^{-5}	6.8×10^{-6}	2.06	0.043
<i>C * C</i>	-4.0×10^{-5}	6.7×10^{-6}	-5.99	0
<i>A * A</i>	3.0×10^{-6}	7.0×10^{-6}	0.40	0.689
<i>B * D</i>	1.7×10^{-5}	7.9×10^{-6}	2.12	0.038
<i>B * C</i>	5.0×10^{-6}	7.9×10^{-6}	0.63	0.533
<i>B * A</i>	-2.0×10^{-6}	7.9×10^{-6}	-0.22	0.827
<i>D * C</i>	9.0×10^{-6}	7.9×10^{-6}	1.13	0.264
<i>D * A</i>	-1.1×10^{-5}	7.9×10^{-6}	-1.41	0.164
<i>C * A</i>	-1.8×10^{-5}	7.9×10^{-6}	-2.30	0.025

Table 3.7 Coded results of regression analysis of Rpi local activity optimization.

The results of the analysis suggested that all of the modeled linear terms were significant, as the collective p values all fell below the established α value of 0.05 (Table 3.7). Quadratic terms that had significant p values included: buffer*buffer ($p=0.043$), substrate*substrate ($p=0$) and ph*buffer ($p=0.038$). These quadratic terms aid in creating a much more accurate model over one composed solely of linear terms. The full $y=xC+xC^2$ model revealed a clear vertex where maximal activity may be gained at a certain substrate concentration. The $y=xD+xD^2$ model indicated that as buffering strength decreases, the activity rate sees an increase.

The second order quadratic model was calculated, following the results of the regression analysis, of statistically significant factors and interactions is given in coded units below:

$$\begin{aligned} \text{Kinetic Activity (y)} = & \\ & 5.4 \times 10^{-4} + 2.3 \times 10^{-5} B - 2.4 \times 10^{-5} D + 6.7 \times 10^{-5} C \\ & + 3.4 \times 10^{-5} A + 2.8 \times 10^{-5} D^2 - 8.1 \times 10^{-5} C^2 \\ & + 3.3 \times 10^{-5} B * D - 3.6 \times 10^{-5} C * A \end{aligned}$$

ANOVA was used to compare the measured kinetic activity of the chosen factors and levels, against the outcome predicted by the regression model to determine the fitness of the predicted model (Table 3.8).

Order	pH	Buffering Strength	R5P	Temperature	v_0 ($\Delta\text{abs}_{290\text{nm}}/\text{sec}$)	Predicted v_0 ($\Delta\text{abs}_{290\text{nm}}/\text{sec}$)
1	1	-1	-1	-1	4.14×10^{-4}	4.24×10^{-4}
2	-1	1	-1	-1	2.92×10^{-4}	3.40×10^{-4}
3	-1	-1	1	-1	4.68×10^{-4}	5.59×10^{-4}
4	1	1	1	-1	5.57×10^{-4}	6.10×10^{-4}
5	-1	-1	-1	1	5.65×10^{-4}	5.48×10^{-4}
6	1	1	-1	1	5.95×10^{-4}	4.92×10^{-4}
7	1	-1	1	1	7.25×10^{-4}	6.36×10^{-4}
8	-1	1	1	1	5.23×10^{-4}	5.30×10^{-4}
9	0	0	0	0	5.63×10^{-4}	5.40×10^{-4}
10	0	0	0	0	5.77×10^{-4}	5.40×10^{-4}
11	-1	-1	-1	-1	4.44×10^{-4}	4.17×10^{-4}
12	1	1	-1	-1	4.55×10^{-4}	4.13×10^{-4}
13	1	-1	1	-1	5.40×10^{-4}	5.85×10^{-4}
14	-1	1	1	-1	4.63×10^{-4}	5.17×10^{-4}
15	1	-1	-1	1	5.38×10^{-4}	5.47×10^{-4}
16	-1	1	-1	1	5.16×10^{-4}	4.25×10^{-4}
17	-1	-1	1	1	5.85×10^{-4}	6.17×10^{-4}
18	1	1	1	1	6.09×10^{-4}	6.16×10^{-4}
19	0	0	0	0	5.08×10^{-4}	5.40×10^{-4}
20	0	0	0	0	5.38×10^{-4}	5.40×10^{-4}
21	$-\alpha$	0	0	0	5.08×10^{-4}	4.97×10^{-4}
22	2	0	0	0	5.38×10^{-4}	5.89×10^{-4}
23	0	$-\alpha$	0	0	6.20×10^{-4}	6.45×10^{-4}
24	0	α	0	0	5.55×10^{-4}	5.47×10^{-4}
25	0	0	$-\alpha$	0	1.77×10^{-4}	2.45×10^{-4}

26	0	0	α	0	6.14×10^{-4}	5.11×10^{-4}
27	0	0	0	$-\alpha$	5.74×10^{-4}	4.83×10^{-4}
28	0	0	0	α	5.58×10^{-4}	6.20×10^{-4}

Table 3.8 Factors and levels of the first central composite surface design for RpiA activity, with experimental results and results predicted by the proposed regression model. Reaction rate units are in micro absorbance units/second.

Analysis of variance between the predications of the model, and the measured rates was run and is found in Table 3.9. The regression model was deemed significant, with a p -value $< \alpha$. The determination coefficient of how the data fit the modeled line was 79.33 %. The percentage of points outside the line was shown to be statistically significant by the low p value of the lack-of-fit points found through ANOVA modeling.

Source	Adjusted Sum of Squares	Degrees of Freedom	Adjusted Mean of Squares	F-Value	P-Value
Model	6.9×10^{-5}	16	4.3×10^{-6}	14.87	0
Linear	4.8×10^{-5}	4	1.19×10^{-5}	40.81	0
Square	1.7×10^{-5}	4	4.16×10^{-6}	14.29	0
2-Way Interaction	3.6×10^{-6}	6	6.0×10^{-7}	2.07	0.07
Residual	1.8×10^{-5}	62	2.9×10^{-7}		
Lack-of-Fit	1.2×10^{-5}	9	1.4×10^{-6}	12.69	0
Pure Error	5.7×10^{-6}	53	1.1×10^{-7}		
Total	8.7×10^{-5}	78			

Table 3.9 Analysis of variance for the quadratic model of RpiA activity. $R^2=79.33\%$

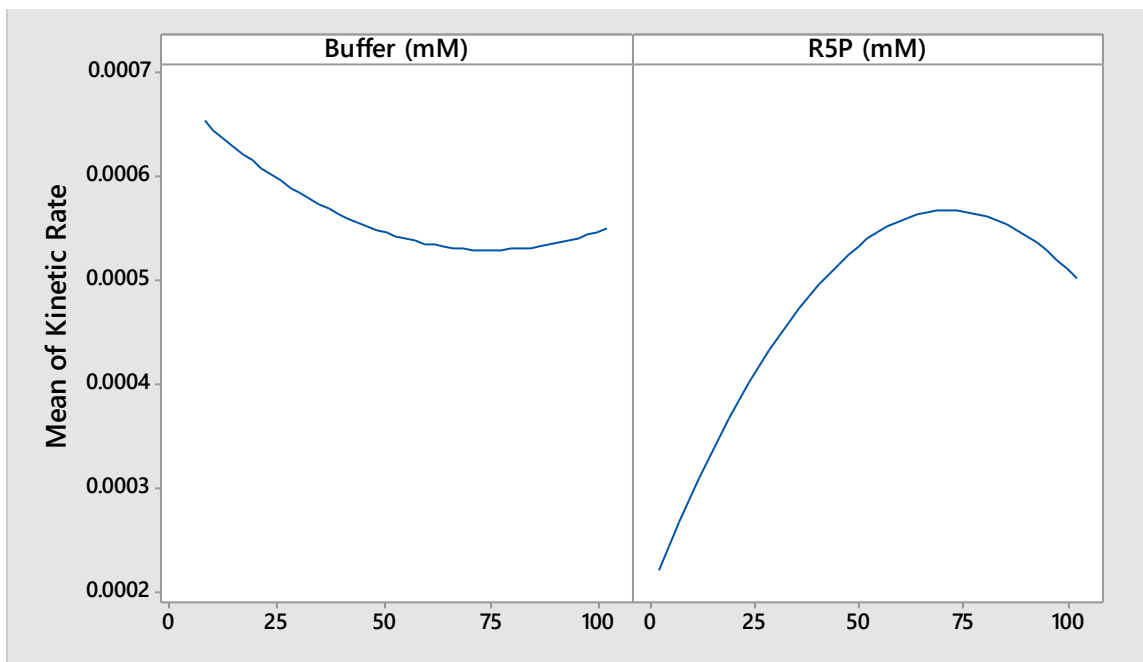


Figure 3.19 Main effects plots of the levels of buffer concentration and R5P (x-axis), with mean activity of Rpi (y-axis) as the response.

Second model:

The second Rpi experiment investigated only pH and temperature, while employing the local optimal levels for R5P and buffer concentration found in the first round of modeling. The choice of these factors and levels is discussed in section 5.2.1. The chosen factors and levels are found in Table 0.18. The experimental results were entered into a Minitab spreadsheet, and were analyzed via surface regression using an α level of 0.05. The calculated model indicated that all terms, linear quadratic, and interactive were significant ($p < \alpha$).

Term	Coefficient	Standard Error of Coefficient	T-Value	P-Value
Constant	5.6×10^{-4}	1.3×10^{-5}	44.58	0
<i>A</i>	-8.0×10^{-5}	4.2×10^{-6}	-18.1	0
<i>B</i>	-2.5×10^{-5}	4.4×10^{-6}	-6.04	0
<i>A</i> * <i>A</i>	3.6×10^{-5}	7.3×10^{-6}	4.97	0
<i>B</i> * <i>B</i>	3.3×10^{-5}	7.3×10^{-6}	4.55	0
<i>A</i> * <i>B</i>	2.5×10^{-5}	5.9×10^{-6}	4.22	0

Table 3.10 Coded results of the second experimental regression analysis of Rpi

The second order quadratic model was calculated, composed of the statistically significant factors and interactions, is given in coded units:

$$\begin{aligned} \text{Kinetic Activity (y)} = & \\ & 5.6 \times 10^{-4} - 8.0 \times 10^{-5}A - 2.5 \times 10^{-5}B + 3.6 \times 10^{-5}A^2 \\ & + 3.3 \times 10^{-5}B^2 + 2.5 \times 10^{-5}A * B \end{aligned}$$

The proposed model was used to predict the measured kinetic activity of the two factors and levels. The experimental design, in addition to the observed reaction rates, is found in Table 3.11.

Order	pH	Temperature	Observed Rate ($\Delta\text{abs}_{290\text{nm}}/\text{sec}$)	Predicted Rate ($\Delta\text{abs}_{290\text{nm}}/\text{sec}$)
1	-1	-1	8.1×10^{-4}	7.6×10^{-4}
2	+1	-1	6.9×10^{-4}	6.6×10^{-4}
3	-1	+1	5.9×10^{-4}	5.5×10^{-4}
4	+1	+1	5.7×10^{-4}	5.5×10^{-4}
5	0	0	6.0×10^{-4}	5.6×10^{-4}
6	$-\alpha$	0	6.6×10^{-4}	6.6×10^{-4}
7	$+\alpha$	0	5.7×10^{-4}	5.9×10^{-4}
8	0	$-\alpha$	7.4×10^{-4}	7.4×10^{-4}
9	0	$+\alpha$	4.9×10^{-4}	5.2×10^{-4}
10	0	0	5.9×10^{-4}	5.6×10^{-4}

Table 3.11 Factors and levels of the second central composite surface design for RpiA activity, with observed and predicted kinetics based on the generated model.

ANOVA was used to compare the measured kinetic activity of the chosen factors and levels, against the outcome predicted by the regression model to determine the fitness of the predicted model (Table 3.12).

Source	Adjusted Sum of Squares	Degrees of Freedom	Adjusted Mean of Squares	F-Value	P-Value
Model	1.8×10^{-5}	6	3.0×10^{-6}	70.54	0
Linear	1.5×10^{-5}	2	7.6×10^{-6}	181.97	0
Square	1.2×10^{-6}	2	5.8×10^{-7}	13.97	0
2-Way Interaction	7.5×10^{-7}	1	7.5×10^{-7}	17.83	0
Error	7.9×10^{-7}	19	4.2×10^{-8}		
Lack-of-Fit	4.0×10^{-8}	2	2.0×10^{-8}	0.45	0.647
Pure Error	8.0×10^{-8}	17	4.7×10^{-9}		
Total	1.8×10^{-5}	25			

Table 3.12 Analysis of variance for the second quadratic model of RpiA activity. $R^2=95.70\%$

Analysis of variance between the predications of the model, and the measured rates was run and is found in Table 3.12. The regression model was deemed significant, with a p -value $< \alpha$. The determination coefficient of how the data fit the modeled line was 95.70 %. The percentage of points outside the line was shown to not be statistically significant, due to the high p value of the lack-of-fit points found through ANOVA modeling.

3.4.2 Optimization of PRK

Optimization of the kinetic rate of PRK was carried out using the same surface response methodology as Rpi (section 3.4.1). The choice of the central, factorial and axial point levels is discussed further in section 4.3.2. The average v_0 , collected in the form of Δ Absorbance/second, was entered into a central composite designed spreadsheet. Regression analysis was completed using the software, to identify statistically significant factors. A quadratic model and optimal levels were calculated using the program. The models significance was evaluated using analysis of variance (ANOVA) tests.

Using the software Minitab, an investigative domain was established (Table 0.19), followed by response surface regression analysis being performed on the collected data with a confidence interval set at 95 % (Table 3.13).

Term	Coefficient	Standard Error of Coefficient	T-Value	P-Value
Constant	2.7×10^{-4}	4.4×10^{-5}	6.12	0
<i>A</i>	5.0×10^{-6}	6.5×10^{-6}	0.76	0.448
<i>B</i>	1.0×10^{-4}	6.3×10^{-6}	16.05	0
<i>E</i>	3.8×10^{-5}	6.5×10^{-6}	5.77	0
<i>D</i>	1.7×10^{-5}	6.3×10^{-6}	2.65	0.009
<i>F</i>	-2.8×10^{-5}	6.5×10^{-6}	-4.23	0
<i>C</i>	3.7×10^{-5}	6.3×10^{-6}	5.85	0
<i>A*A</i>	-9.2×10^{-6}	9.2×10^{-6}	-1	0.318
<i>B*B</i>	-2.8×10^{-5}	8.9×10^{-6}	-3.1	0.003
<i>E*E</i>	-1.8×10^{-5}	9.2×10^{-6}	-1.96	0.052
<i>D*D</i>	3.4×10^{-6}	8.9×10^{-6}	0.38	0.706
<i>F*F</i>	-5.0×10^{-6}	9.2×10^{-6}	-0.54	0.588
<i>C*C</i>	-6.7×10^{-6}	8.9×10^{-6}	-0.76	0.451
<i>A*B</i>	-7.0×10^{-6}	7.4×10^{-6}	-0.95	0.346
<i>A*E</i>	-6.7×10^{-6}	7.4×10^{-6}	0.9	0.368
<i>A*D</i>	1.7×10^{-5}	7.4×10^{-6}	2.3	0.024
<i>A*F</i>	-3.0×10^{-6}	7.4×10^{-6}	-0.41	0.684
<i>A*C</i>	2.0×10^{-5}	7.4×10^{-6}	2.66	0.009
<i>B*E</i>	2.2×10^{-5}	7.4×10^{-6}	3.02	0.003
<i>B*D</i>	1.5×10^{-5}	7.4×10^{-6}	2.07	0.041
<i>B*F</i>	6.7×10^{-6}	7.4×10^{-6}	0.9	0.37
<i>B*C</i>	3.3×10^{-5}	7.4×10^{-6}	4.43	0
<i>E*D</i>	5.6×10^{-6}	7.4×10^{-6}	0.76	0.451
<i>E*F</i>	2.9×10^{-5}	7.4×10^{-6}	3.85	0
<i>E*C</i>	6.0×10^{-6}	7.4×10^{-6}	0.81	0.42
<i>D*F</i>	-8.7×10^{-6}	7.4×10^{-6}	-1.17	0.245
<i>D*C</i>	9.5×10^{-7}	7.4×10^{-6}	0.13	0.898
<i>C*F</i>	-1.3×10^{-5}	7.4×10^{-6}	-1.78	0.079

Table 3.13 Coded regression analysis results of PRK activity.

All of the linear factors were found to have statistically significant effects on the model using $\alpha=0.05$, except for temperature (*A*). Temperature did produce a parabolic curve when viewed as a main effect on activity alone, indicating a broad peak between 37 and 40° C where activity was maximized. The following equation is the resulting modeled equation in coded units, composed of statistically significant terms based on the results of the regression analysis:

$$\text{Kinetic Activity } (y) = 2.7 \times 10^{-6} + 1.0 \times 10^{-6}B + 3.9 \times 10^{-7}C + 1.8 \times 10^{-7}D + 3.6 \times 10^{-7}E - 2.9 \times 10^{-7}F - 2.8 \times 10^{-7}B^2 + 1.9 \times 10^{-7}A * D + 2.2 \times 10^{-7}A * C + 2.2 \times 10^{-7}B * E + 1.8 \times 10^{-7}B * D + 3.5 \times 10^{-7}B * C + 2.6 \times 10^{-7}E * F$$

The proposed regression model was used to predict kinetic rates based on the chosen factors and levels and is found in Table 3.14.

Order	Temperature	pH	MgCl ₂	DTT	ATP	R5P	Measured v_0 ($\Delta\text{abs}_{340\text{nm}}$ /sec)	Predicted v_0 ($\Delta\text{abs}_{340\text{nm}}$ /sec)
1	-1	-1	-1	-1	-1	-1	1.5X10 ⁻⁴	1.6X10 ⁻⁴
2	+1	-1	-1	-1	-1	1	1.3X10 ⁻⁴	1.7X10 ⁻⁴
3	-1	1	-1	-1	-1	1	4.8X10 ⁻⁴	3.4X10 ⁻⁴
4	+1	1	-1	-1	-1	-1	1.2X10 ⁻⁴	1.4X10 ⁻⁴
5	-1	-1	1	1	-1	-1	6.4X10 ⁻⁵	9.6X10 ⁻⁵
6	+1	-1	1	1	-1	1	1.6X10 ⁻⁴	2.2X10 ⁻⁴
7	-1	1	1	1	-1	1	4.9X10 ⁻⁴	4.5X10 ⁻⁴
8	+1	1	1	1	-1	-1	2.9X10 ⁻⁴	3.2X10 ⁻⁴
9	-1	-1	1	-1	1	-1	5.3X10 ⁻⁵	1.4X10 ⁻⁴
10	+1	-1	1	-1	1	1	3.9X10 ⁻⁶	1.3X10 ⁻⁴
11	-1	1	1	-1	1	1	4.6X10 ⁻⁴	4.0X10 ⁻⁴
12	+1	1	1	-1	1	-1	2.0X10 ⁻⁴	2.5X10 ⁻⁴
13	-1	-1	-1	1	1	-1	0.0	2.6X10 ⁻⁵
14	+1	-1	-1	1	1	1	4.4X10 ⁻⁵	3.7X10 ⁻⁵
15	-1	1	-1	1	1	1	1.6X10 ⁻⁴	2.4X10 ⁻⁴
16	+1	1	-1	1	1	-1	2.7X10 ⁻⁴	1.5X10 ⁻⁴
17	0	0	0	0	0	0	3.2X10 ⁻⁴	2.7X10 ⁻⁴
18	-1	-1	1	-1	-1	1	7.2X10 ⁻⁵	1.1X10 ⁻⁴
19	+1	-1	1	-1	-1	-1	2.1X10 ⁻⁴	7.0X10 ⁻⁵
20	-1	1	1	-1	-1	-1	2.1X10 ⁻⁴	2.5X10 ⁻⁴
21	+1	1	1	-1	-1	1	4.3X10 ⁻⁴	4.1X10 ⁻⁴
22	-1	-1	-1	1	-1	1	9.3X10 ⁻⁵	1.2X10 ⁻⁴
23	+1	-1	-1	1	-1	-1	2.0X10 ⁻⁴	1.5X10 ⁻⁴
24	-1	1	-1	1	-1	-1	3.2X10 ⁻⁴	2.6X10 ⁻⁴
25	+1	1	-1	1	-1	1	5.3X10 ⁻⁴	4.4X10 ⁻⁴
26	-1	-1	-1	-1	1	1	1.1X10 ⁻⁵	1.7X10 ⁻⁵
27	+1	-1	-1	-1	1	-1	1.4X10 ⁻⁵	1.9X10 ⁻⁵
28	-1	1	-1	-1	1	-1	2.7X10 ⁻⁴	1.8X10 ⁻⁴
29	+1	1	-1	-1	1	1	3.0X10 ⁻⁴	2.2X10 ⁻⁴
30	-1	-1	1	1	1	1	5.3X10 ⁻⁵	5.6X10 ⁻⁵
31	+1	-1	1	1	1	-1	6.8X10 ⁻⁵	1.3X10 ⁻⁴

32	-1	1	1	1	1	-1	4.6×10^{-4}	3.4×10^{-4}
33	+1	1	1	1	1	1	5.6×10^{-4}	5.1×10^{-4}
34	$-\alpha$	0	0	0	0	0	3.6×10^{-4}	2.0×10^{-4}
35	$+\alpha$	0	0	0	0	0	2.5×10^{-4}	2.3×10^{-4}
36	0	$-\alpha$	0	0	0	0	0.0	-1.3×10^{-4}
37	0	$+\alpha$	0	0	0	0	3.8×10^{-4}	3.5×10^{-4}
38	0	0	$-\alpha$	0	0	0	1.4×10^{-5}	7.8×10^{-5}
39	0	0	$+\alpha$	0	0	0	4.4×10^{-4}	2.6×10^{-4}
40	0	0	0	$-\alpha$	0	0	3.1×10^{-4}	2.5×10^{-4}
41	0	0	0	$+\alpha$	0	0	4.3×10^{-4}	3.3×10^{-4}
42	0	0	0	0	$-\alpha$	0	3.8×10^{-4}	3.0×10^{-4}
43	0	0	0	0	$+\alpha$	0	3.5×10^{-4}	1.7×10^{-4}
44	0	0	0	0	0	$-\alpha$	2.3×10^{-4}	1.4×10^{-4}
45	0	0	0	0	0	$+\alpha$	4.0×10^{-4}	3.2×10^{-4}
46	0	0	0	0	0	0	3.2×10^{-4}	2.7×10^{-4}

Table 3.14 Factors and levels of the central composite surface design for PRK activity, with observed and predicted kinetics based on the generated model.

ANOVA was used to compare the measured kinetic activity of the chosen factors and levels, against the outcome predicted by the regression model to determine the fitness of the predicted model (Table 3.15).

Source	Adjusted Sum of Squares	Degrees of Freedom	Adjusted Mean of Squares	F-Value	P-Value
Model	2.4×10^{-6}	29	8.3×10^{-8}	17.13	0
Linear	1.8×10^{-6}	6	3.0×10^{-7}	60.01	0
Square	1.2×10^{-7}	6	2.0×10^{-8}	3.93	0.001
2-Way Interaction	3.5×10^{-7}	15	2.3×10^{-8}	4.74	0
Error	4.8×10^{-7}	97	4.9×10^{-9}		
Lack-of-Fit	2.4×10^{-7}	15	1.6×10^{-8}	5.67	0
Pure Error	2.4×10^{-7}	82	2.9×10^{-9}		
Total	2.9×10^{-6}	126			

Table 3.15 Results of the analysis of variance between predicted and measured PRK activity. $R^2=83.66\%$

Analysis of variance between the predications of the model, and the measured rates was run and is found in Table 3.15. The regression model was deemed significant, with a p -value $< \alpha$. The determination coefficient of how the data fit the modeled line was 83.66 %. The percentage of points outside the line was shown to be statistically significant, due to the low p value of the lack-of-fit points found through ANOVA modeling.

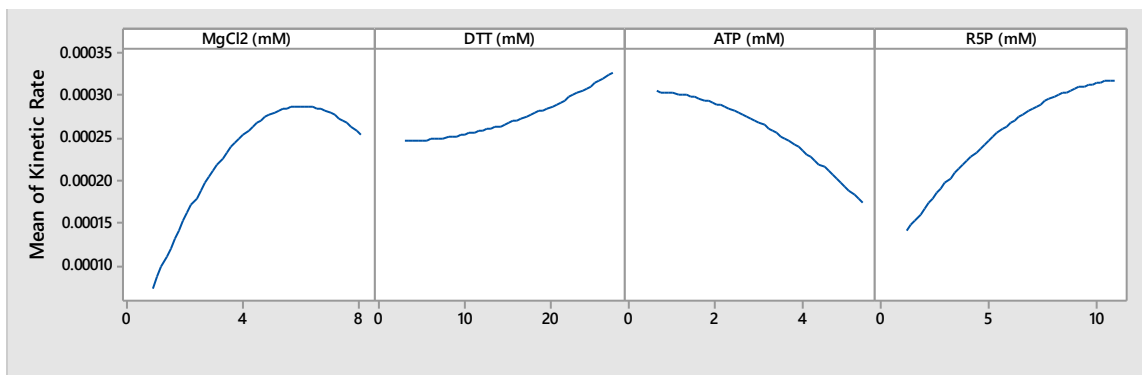


Figure 3.20 The main effects of four factors on the mean activity rate of PRK.

Second model:

A second response surface experimental domain was designed (Table 0.20). The experimental results were entered into a Minitab spreadsheet, and the results were analyzed via surface regression using an α level of 0.05. The calculated model (Table 3.16) was deemed statistically significant based on p -value $< \alpha$.

Term	Coefficient	Standard Error of Coefficient	T-Value	P-Value
Constant	3.3×10^{-4}	2.3×10^{-5}	14.25	0
A	1.0×10^{-5}	6.0×10^{-6}	1.61	0.123
B	-5.4×10^{-5}	6.0×10^{-6}	-8.27	0
B*B	-2.5×10^{-5}	1.3×10^{-5}	-1.93	0.069
A*A	3.0×10^{-5}	1.3×10^{-5}	2.29	0.034
A*B	1.4×10^{-6}	9.0×10^{-6}	0.16	0.875

Table 3.16 Coded results of the second experimental regression analysis of the activity of PRK.

The second order quadratic model found below is composed of the statistically significant factors and interactions, and is given in coded units:

$$\text{Kinetic Activity (y)} = 3.3 \times 10^{-4} - 5.4 \times 10^{-5}B + 3.0 \times 10^{-5}A^2$$

The proposed model was used to predict theoretical rates based on the chosen levels and factors. The experimental design, in addition to both observed and predicted reaction rates, is found in Table 3.17.

Order	pH	Temperature	Measured v_0 ($\Delta\text{abs}_{340\text{nm}}/\text{sec}$)	Predicted v_0 ($\Delta\text{abs}_{340\text{nm}}/\text{sec}$)
1	-1	-1	4.3×10^{-4}	3.8×10^{-4}
2	+1	-1	4.3×10^{-4}	4.0×10^{-4}
3	-1	+1	3.0×10^{-4}	2.7×10^{-4}
4	+1	+1	3.5×10^{-4}	3.0×10^{-4}
5	0	0	3.8×10^{-4}	3.3×10^{-4}
6	$-\alpha$	0	2.4×10^{-4}	2.7×10^{-4}
7	$+\alpha$	0	2.6×10^{-4}	3.0×10^{-4}
8	0	$-\alpha$	4.3×10^{-4}	4.7×10^{-4}
9	0	$+\alpha$	2.7×10^{-4}	3.2×10^{-4}
10	0	0	3.7×10^{-4}	3.3×10^{-4}

Table 3.17 Factors and levels of the second composite surface design for PRK activity, with observed and predicted kinetics.

ANOVA was used to compare the predicted rates with the rates that were observed experimentally, to determine the goodness of fit of the model Table 3.18.

Source	Adjusted Sum of Squares	Degrees of Freedom	Adjusted Mean of Squares	F-Value	P-Value
Model	1.5×10^{-7}	6	2.6×10^{-8}	25.30	0
Linear	7.2×10^{-8}	2	3.6×10^{-8}	35.47	0
Square	3.6×10^{-8}	2	1.8×10^{-8}	17.79	0
2-Way Interaction	0	1	0	0.03	0.875
Error	1.9×10^{-8}	19	9.5×10^{-9}		
Lack-of-Fit	4.6×10^{-9}	2	2.2×10^{-9}	2.65	0.1
Pure Error	1.5×10^{-8}	17	7.5×10^{-9}		
Total	1.72×10^{-7}	25			

Table 3.18 Results of the second analysis of variance of predicted and observed kinetic rates of PRK. $R^2=88.87\%$

Analysis of variance between the predications of the model, and the measured rates was run and is found in Table 3.15. The regression model was deemed significant, with a p -value $< \alpha$. The determination coefficient of how the data fit the modeled line was 88.87%. The percentage of points outside the line was shown to not be statistically significant, due to the high p value of the lack-of-fit points found through ANOVA modeling.

Enzyme	v_0 under original conditions	Original condition levels	v_0 under optimized conditions	Optimized condition levels	Change in v_0 compared to initial conditions
Rpi	31.2 nmols/s	pH 7.5 32° C 55 mM R5P 55 mM Tris-HCl	49.3 nmols/s	pH 7.7 35.3 °C 76mM R5P 10mM Tris-HCl	36.7 %
PRK	43.4 pmols/s	pH 7.5 37° C 4 mM R5P 15 mM DTT 4.5 mM MgCl ₂ 3 mM ATP	54.9 pmols/s	pH 7.9 39.9 °C 10 mM R5P 20 mM DTT 6 mM MgCl ₂ 2 mM ATP	20.9 %

Table 3.19 Comparison of the original factor levels investigated to the optimal levels

Kinetic assays to determine v_0 were run for both Rpi and PRK, following the procedures established in sections 2.9.1 and 2.10.1. The conditions (factors) used in these assays were both the original levels and the optimal levels as found in Table 3.19.

3.5 Polymer results

The molecular weight of the polymer was estimated using GPC analysis. The GPC software calculated molecular weight was approximately 8400 g/mol for the combined block co-polymer.

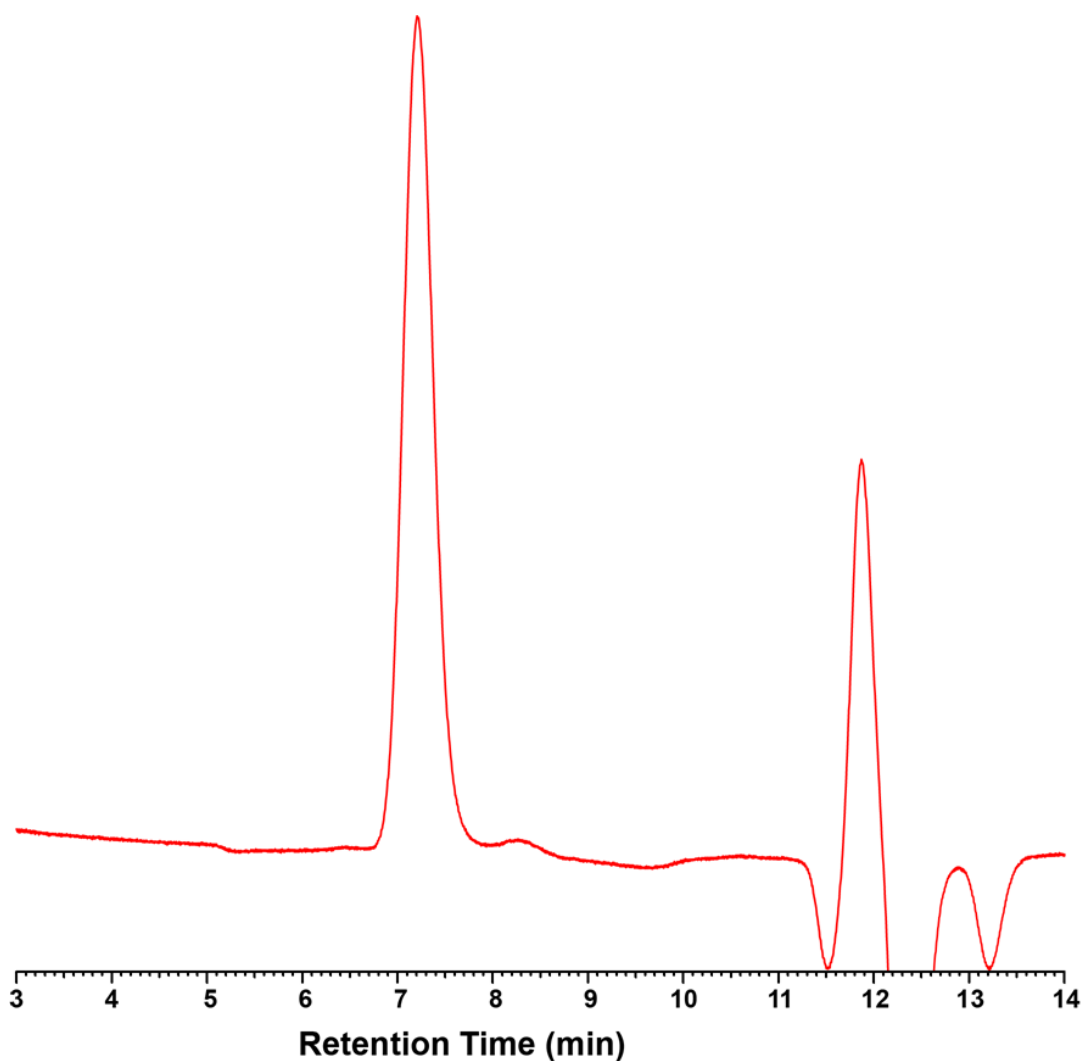


Figure 3.21 Gel permeation chromatogram of the triblock copolymer dissolved in chloroform. The first peak is the eluting polymer, the second is the solvent.

3.6 Polymersome purification and characterization

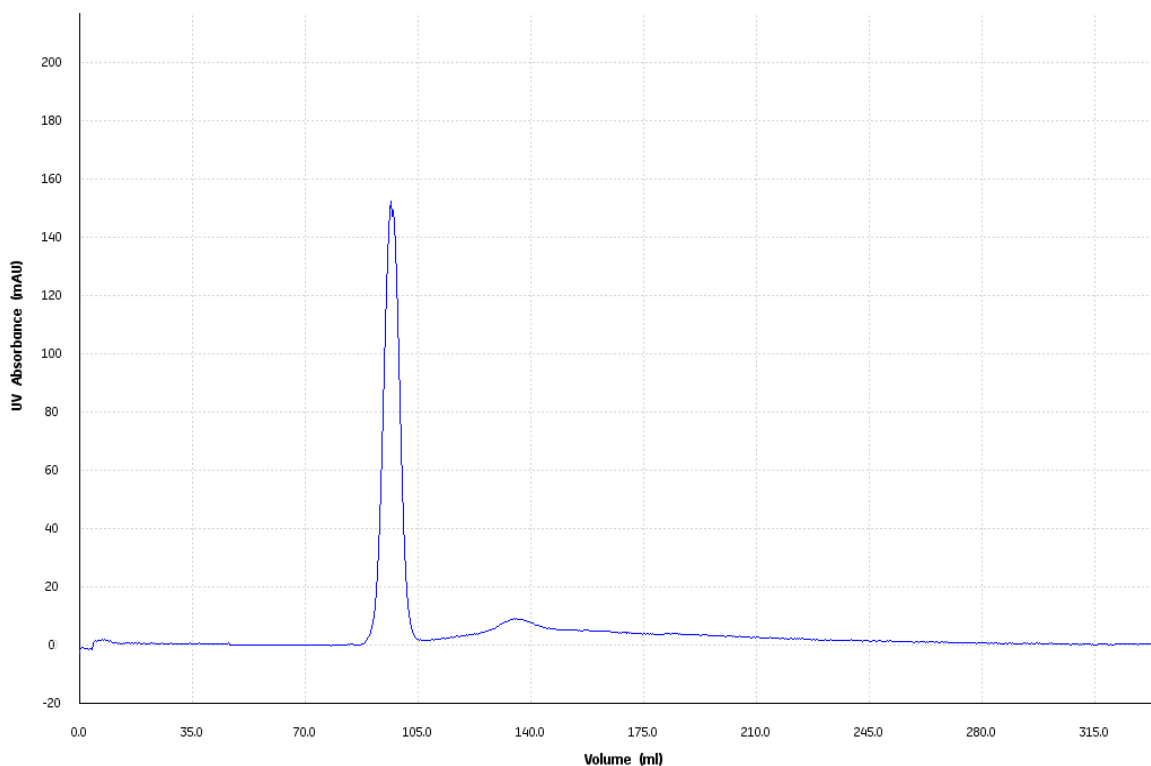


Figure 3.22 Elution profile of polymersomes (first peak) and of unencapsulated enzyme and remaining polymers (second peak and tail). The Y-axis UV absorbance is measured at 280nm, with units being milliabsorbance units.

Polymersomes were separated from free Rpi by a combination of centrifugal filtration and size-exclusion chromatography (Figure 3.22). In the absence of enzyme, polymersomes were purified using only size-exclusion chromatography.

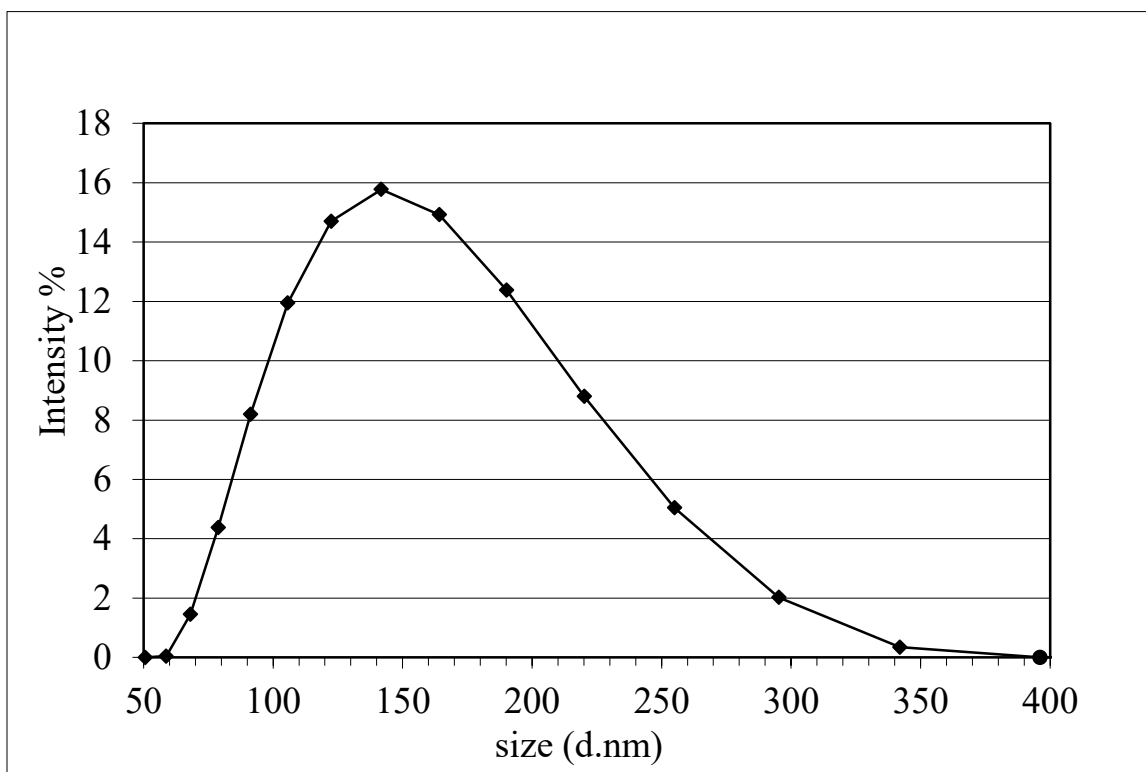


Figure 3.23 Size distribution curve by intensity of polymersomes laden with Rpi. Z-average=152nm. PDI=0.135

The same sample of polymersomes was purified as shown in the chromatogram (Figure 3.22) as was measured by DLS (Figure 3.23). A different batch of polymersomes, formed using the same batch of polymer, were used for SEM and TEM imaging (Figure 3.24 and Figure 3.25 respectively).

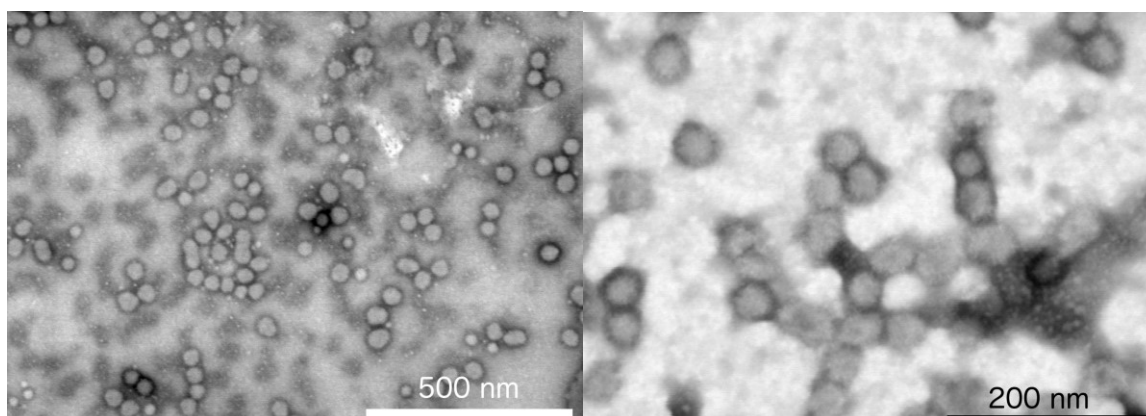


Figure 3.24 SEM images of polymersomes laden with Rpi.

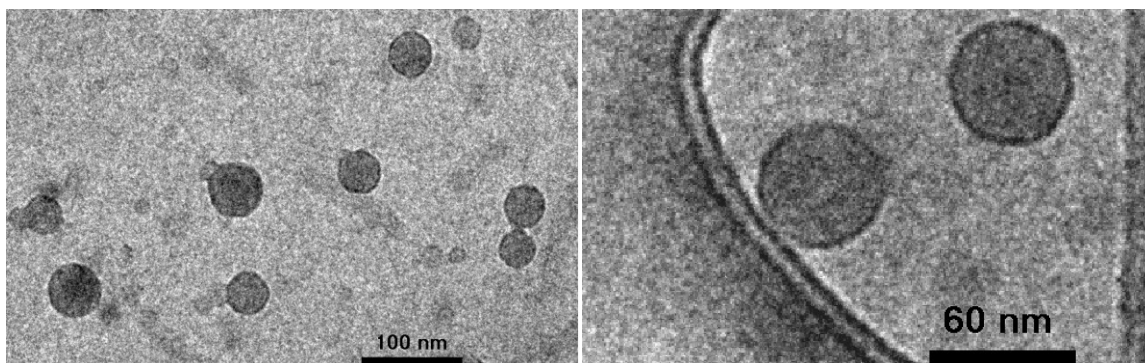


Figure 3.25 Cryo-TEM images of polymersomes.

3.7 Post encapsulation experimental results

3.7.1 Digestion

To demonstrate the effectiveness of encapsulation as a means of protection, a digestive assay was employed. Free Rpi, as well as enzyme-laden polymersomes were incubated in the presence of Proteinase K and Ca^{2+} . Following 9 hours of incubation, the two treated and one control solutions were assayed for activity. The control showed activity, while the two digested samples showed none (Figure 3.26).

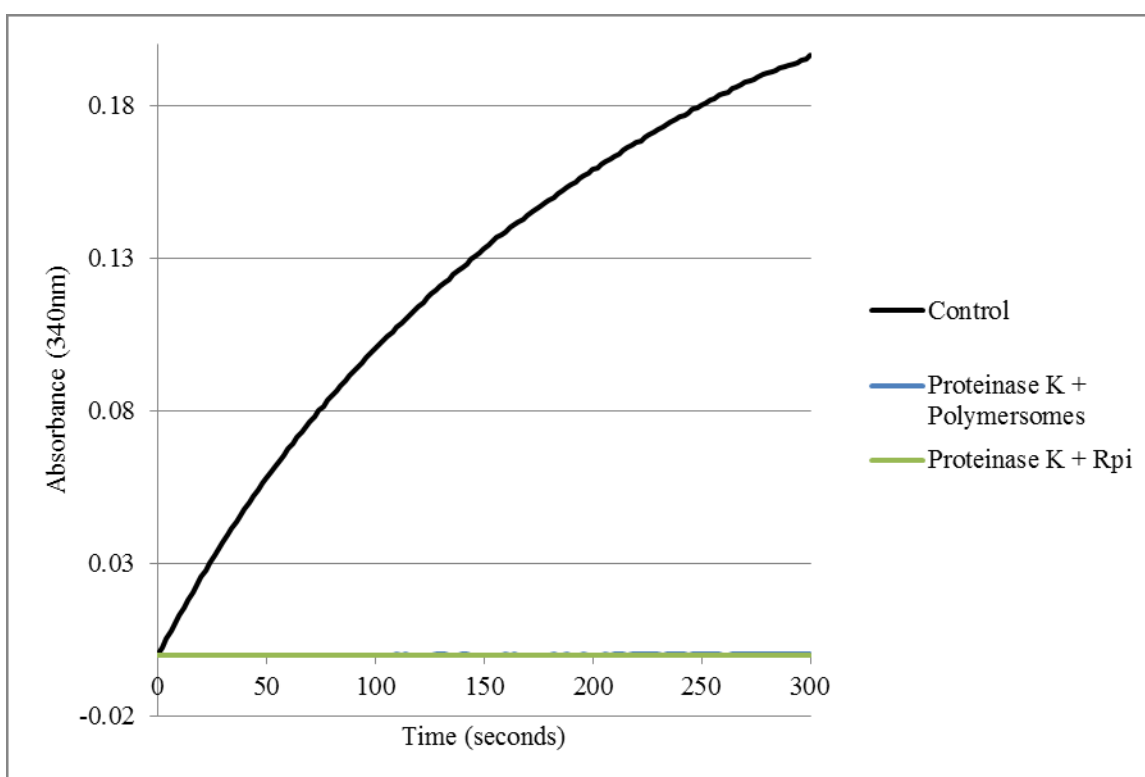


Figure 3.26 Kinetic activity of digested free Rpi and encapsulated Rpi prior to PMSF and lysis treatments. N=3 for each assay.

PMSF was added to the three samples, to the recommended concentration of 5 mM for complete inactivation of Proteinase K¹⁸⁶. Following a further 10 minutes of incubation, the samples were again assayed for activity. ANOVA was run on the kinetic results, and showed that there was no statistical difference between a blank with R5P, the free Rpi and polymersome solutions prior to surfactant treatment (Table 3.20).

ANOVA table	Sum of squares	Degrees of freedom	Mean of squares	F-Value	P-value
Variance between treatments	1.1×10^{-12}	2	5.7×10^{-13}	1.33	0.34

Table 3.20 ANOVA results

Polysorbate-20 was then added to a final concentration of 5 % v/v. This detergent had been found previously to not affect Rpi activity, and would serve to disrupt the polymersome shell, and release the encapsulated enzymes. ANOVA was again run on the kinetic results, and showed that the activity of the polymersomes post-treatment was statistically different from the previous pre-treated measurements (Table 3.21). Activity of the lysed polymersomes approached 3.7 % of the rate of the Rpi control (Figure 3.27)

ANOVA table	Sum of squares	Degrees of freedom	Mean of squares	F-Value	P-value
Variance between pre-treatments and free Rpi	7.9×10^{-12}	3	2.6×10^{-12}	4.3	0.0506
Variance between pre-treatments and lysed polymersomes	6.1×10^{-10}	3	2.0×10^{-10}	206.7	<0.0001

Table 3.21 ANOVA results comparing pre-treatments to free Rpi and lysed polymersomes

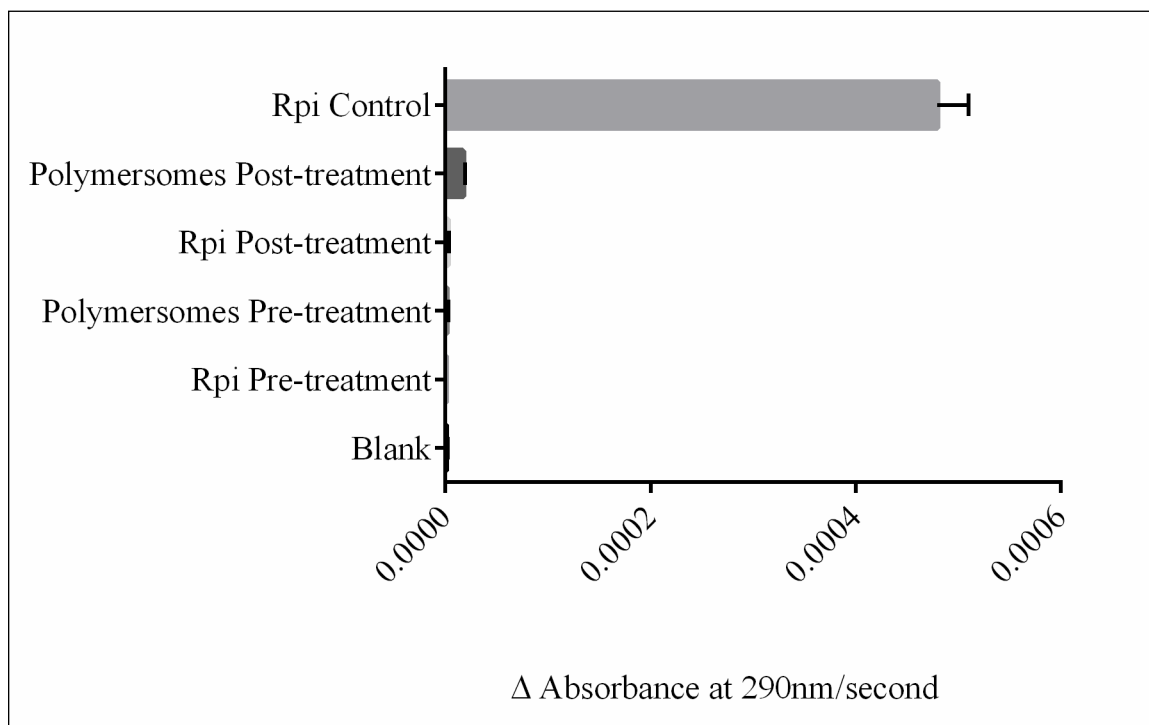


Figure 3.27 Comparison of activities of solutions both before and after the addition of Tween-20.

3.7.2 Fluorescence correlation spectroscopy

To further demonstrate that Rpi had been encapsulated, an experiment using fluorescence correlation spectroscopy was run. This technique measures fluctuations in fluorescence intensity of particles in a solution. The fluorescent molecule fluorescein isothiocyanate was conjugated to Rpi by way of a fluorescent labeling kit. The free fluorescent molecules were removed from Rpi by way of a size-exclusion column (Figure 3.28)

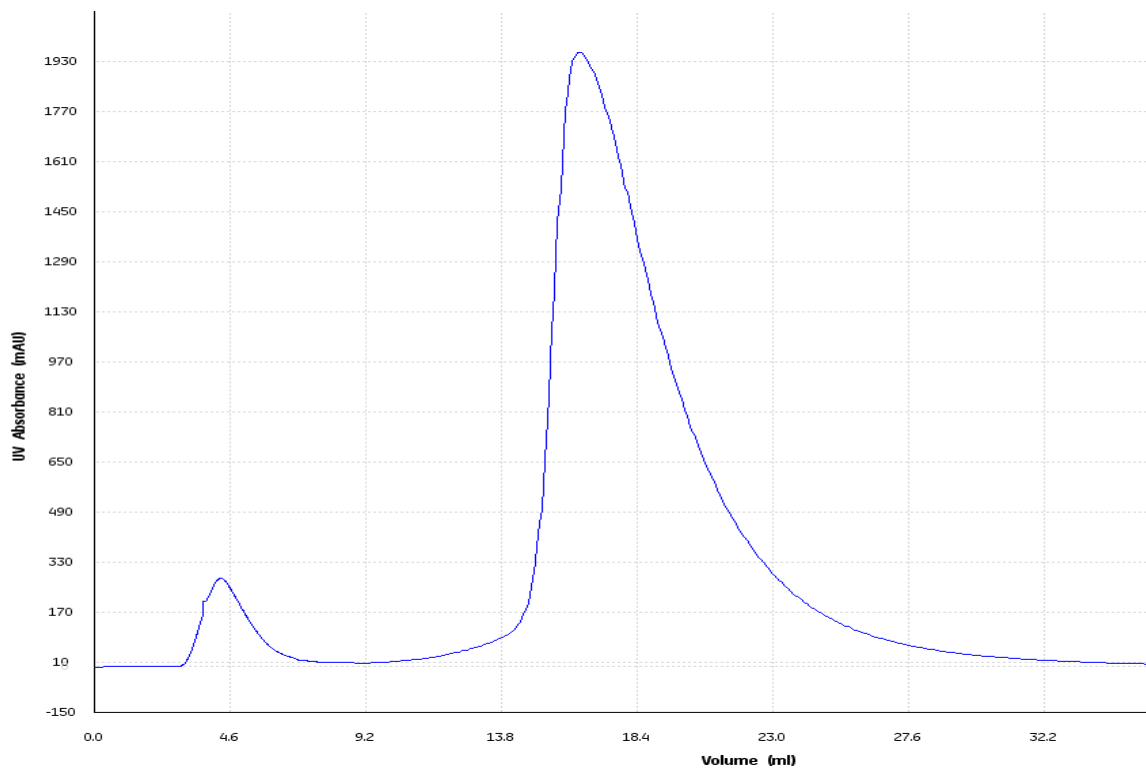


Figure 3.28 Elution profile of Rpi/FitC conjugates (first peak) and free FitC (second peak).

Following elution, the labeling efficiency of the FitC/Rpi conjugates was calculated using Equation 14, revealing that an average of 1.7 molecules of FitC were bound to each molecule of Rpi in solution. Following encapsulation of the FitC/Rpi conjugate within polymersomes, dilute concentrations were left to equilibrate at room temperature. Ten fluorescent intensity measurements were collected and averaged, and the count rate of the three species can be found in Figure 3.29.

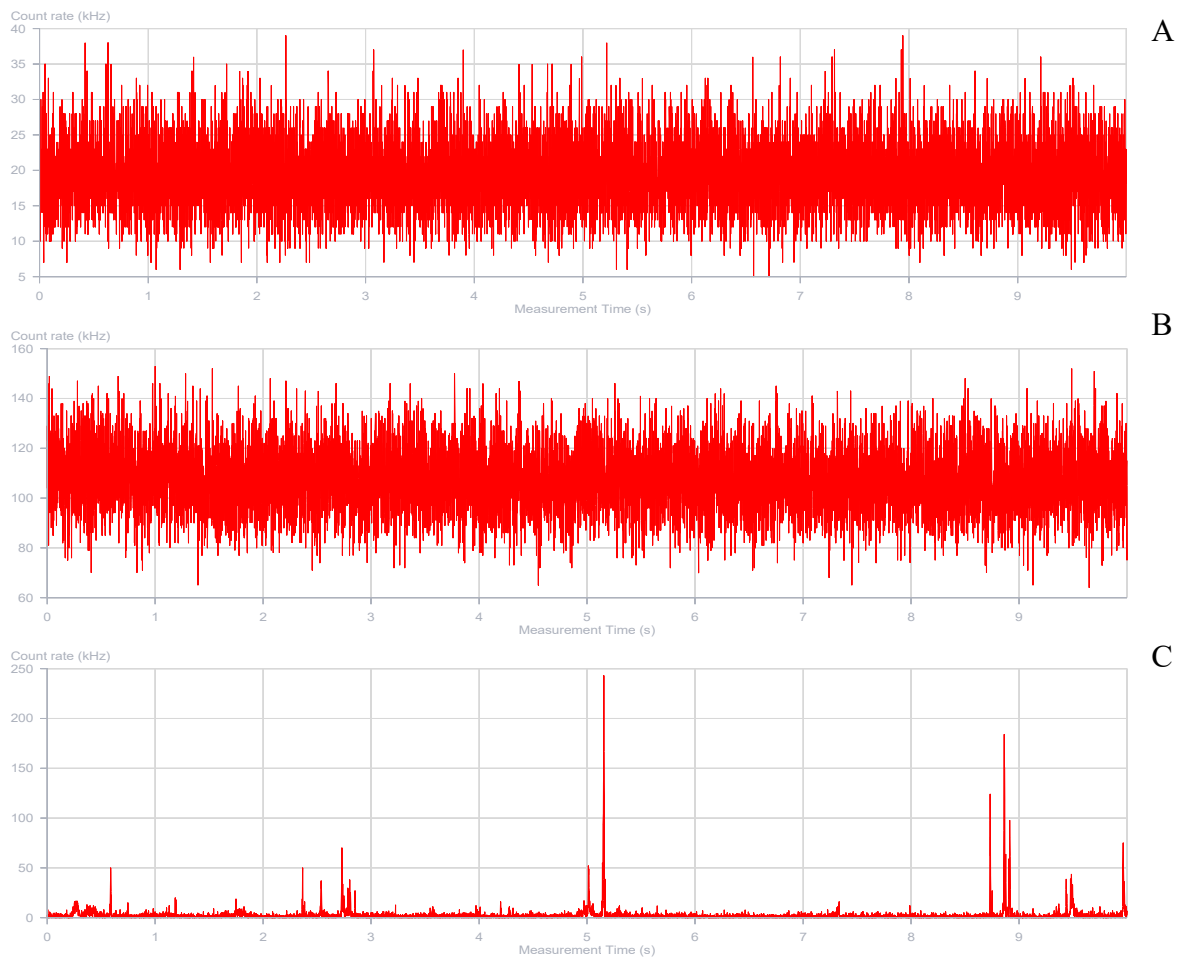


Figure 3.29 Measured count rate averages of fluorescent samples. A) Free fluorescein dye B) Rpi/FitC conjugate C) Rpi/FitC laden polymersomes.

Autocorrelation calculations were performed on each species using the collection software. Line fitting was used on the data, via non-linear least squares method in the collection software. The autocorrelation data was normalized between the ranges of 0-1 using Microsoft Excel, and plotted against the log of lag times (Figure 3.30).

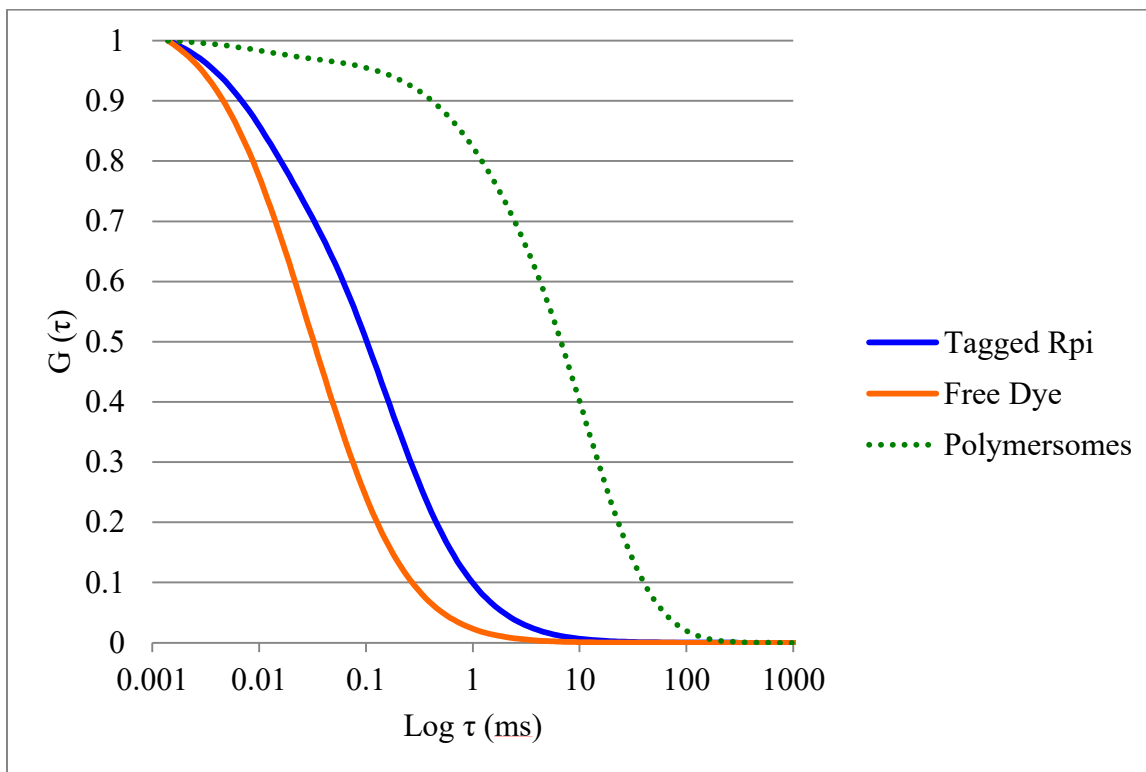


Figure 3.30 Normalized autocorrelation curve of fluorescent conjugate samples.

3.7.3 Absorbance spectroscopy

To calculate the concentration of Rpi encapsulated within polymersomes, absorbance spectroscopy was used. To increase the value of the molar extinction coefficient of the enzyme, the FitC/Rpi conjugate from section 3.7.2 was used. The extinction coefficient of Rpi at 280 nm was calculated to be $9970 \text{ M}^{-1}\cdot\text{cm}^{-1}$ using the online bioinformatics software ProtParam¹⁸⁷. Following conjugation with FitC, the extinction coefficient was calculated experimentally at 494 nm to be $62957 \text{ M}^{-1}\cdot\text{cm}^{-1}$ using a standard curve (Figure 3.31).

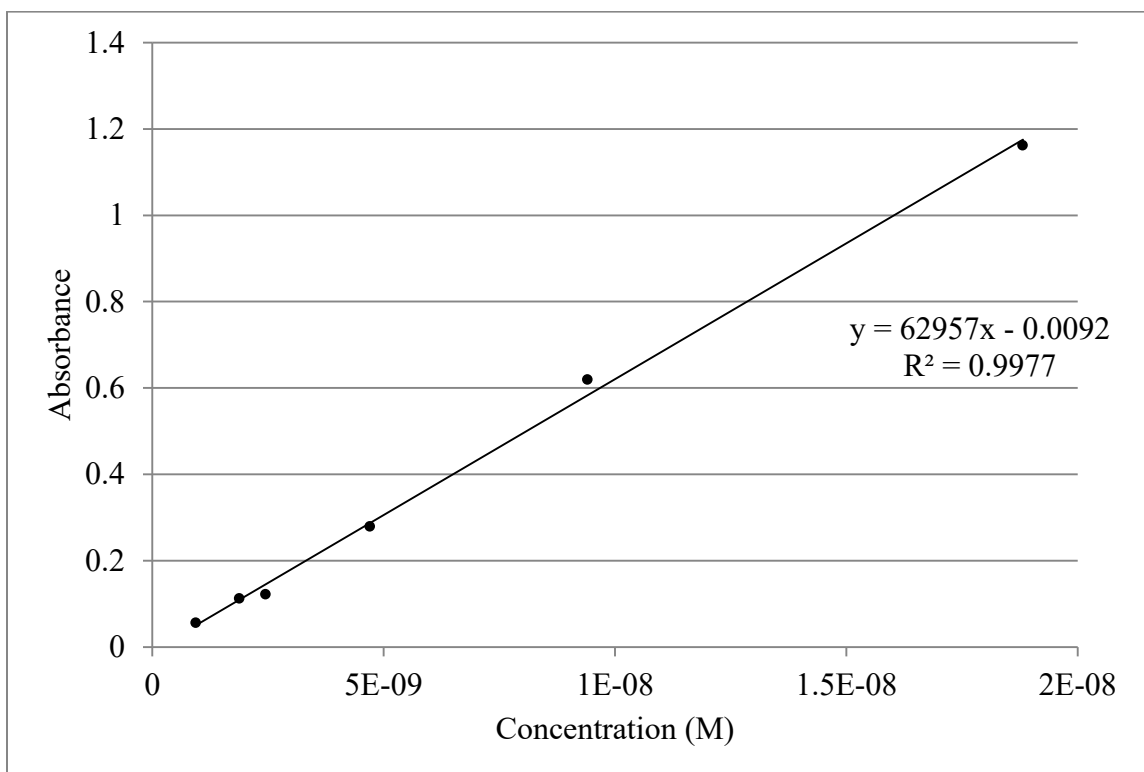


Figure 3.31 Standard curve of Rpi/fluorescein conjugate.

This tagged conjugate was encapsulated and purified. The absorbance of the polymersomes at 494 nm was measured via spectroscopy, using two different blanks. One blank contained a concentration of polymer that was equivalent to the initial concentration used for encapsulation (0.71 μM), while the second blank had no polymer present.

Polymer concentration in blank	Absorbance of polymersome solution (OD_{494})	Approximated encapsulation efficiency
0.71 μM	0.039 ± 0.004	1.5 %
0.00 μM	1.09 ± 0.013	37.0 %

Table 3.22 Effects of the blank polymer concentration on encapsulation efficiency calculations

To accurately measure enzyme loading, the concentration of polymer present must be determined. To do this, a phase emulsion strategy was employed. Following determination of the amount of polymer present in the polymersome solution, an

appropriate blank was prepared. The resulting encapsulation efficiency of Rpi loading was calculated using the equation:

$$\frac{[Enzyme]_{initial}}{[Enzyme]_{final}} \times 100\% \quad (15)$$

Enzyme concentration was calculated from absorbance spectroscopy data using the equation $y=62957x-0.0092$ (equation of the line in figure Figure 3.31). The mean enzyme concentration of three measurements from one batch of polymersomes was $1.2 \times 10^{-6} \pm 8.0 \times 10^{-8}$ M. The initial enzyme concentration was 5.1×10^{-5} M, resulting in an encapsulation efficiency and relative standard error of 23.4 ± 6.7 %. To determine the number of enzymes encapsulated per polymersome (E), Equation 16 was used¹⁸⁸:

$$E = C \times N_A \times \frac{4}{3} (\pi \times R_h^3) \quad (16)$$

where C is the calculated concentration of Rpi encapsulated, N_A is the Avogadro number, R_H is the hydrodynamic radius calculated via light scattering experiments (section 3.6, determined to be 76 ± 27 nm) and π is a constant value of 3.14.

Uncertainty in the number of enzymes encapsulated was calculated assuming independence between the concentration and radius of the polymersomes using the formula:

$$\sigma_E = \sqrt{\left(\left(\frac{\delta E}{\delta C} \right)^2 \times \sigma_C^2 \right) + \left(\left(\frac{\delta E}{\delta R_h} \right)^2 \times \sigma_{R_h}^2 \right)} \quad (17)$$

where σ is the standard deviation, δ is the partial derivative of the respective variable from Equation 16, which treated $N_A \times \frac{4}{3} \times \pi$ as a constant. Using Equations 16 and 17, the calculated average number of enzymes per polymersome was $9.9 \times 10^{-4} \pm 1.4 \times 10^{-3}$.

Chapter 4. Discussion of results and conclusion

4.1 PRK expression and purification

4.1.1 PRK from *S. oleracea*

Phosphoribulokinase is not a commercially available enzyme. It must be purified in order to investigate its properties. Being able to produce the protein from an in-house platform such as *E. coli* is ideal, as it reduces dependence on external sources, and the randomness with variables such as seasonal yield and availability. Phosphoribulokinase from *S. oleracea* (spinach) was the first choice of enzyme, as it had been previously expressed and purified in the bacterial system *E. coli* and has the second highest specific activity rate among PRK variants as reported in literature at 410 $\mu\text{mol}/\text{min}/\text{mg}$ ⁹⁴.

PRK from spinach possesses a single site where disulfide bond formation may occur under reduced conditions¹⁸⁹. This site is responsible for its regulatory mechanism in the chloroplast, as well as being involved in ATP binding. The bond is located very close to the N-terminal end of the protein, only 16 amino acids away. As the N-terminal portion of the protein could be compromised by the addition of a fusion protein or tag, it was decided to purify the native form of the enzyme. This would allow near native activity of the enzyme, removing the possibility of interference within the active site, as well as negative interactions with the regulatory mechanism of the enzyme.

Hudson *et al.* (1992) reported that during the purification of recombinant PRK from *S. oleracea* in *E. coli*, that only 0.7% of the total soluble protein was PRK proper¹⁷². This was largely attributed to plasmid instability, the toxicity of PRK, and later suggested by Brandes *et al.* (1996) to be due to the difference in codon usage between spinach and *E. coli*¹⁹⁰. To improve the expression levels of a recombinant protein from a eukaryote in a prokaryote organism, two of the above problems were directly addressed through: codon optimization to select codons which have a favourable bias in the *E. coli* host, and the use of several different host strains to investigate toxicity/expression levels.

The amino acid sequence that was chosen was selected from the UniProt Knowledgebase, PRIDE entry P09559¹⁹¹. The sequence has a length of 402 amino acids, with a mass of 45,007 Da. This sequence was trimmed of the first 51 peptides, which forms a transit peptide not relevant to the activity of the protein, leaving 351 total amino acids¹⁹². This was undertaken by first reverse translating the amino acid composition of spinach PRK into a DNA sequence using the online software Sequence Manipulation Suite¹⁹³, hosted at www.bioinformatics.org, to provide a genetic sequence of the mature protein. The default *E. coli* codon table was used. To further ensure that the calculated codons would be frequently used within *E. coli*, the sequence was analyzed using the *E. coli* Codon Usage Analyzer 2.1 hosted by the University Of California Riverside Department Of Biology¹⁹⁴. A threshold level was enforced, if less than 10% of the calculated codon is used for chosen amino acid, it was to be discarded in favour of a codon which is more often employed. This sequence was then submitted to an online vendor for synthesis, and was successfully cloned into a plasmid vector.

Testing of expression was needed for the construct, as the plasmid being used had not been used for expression of this protein previously. Three cell types were ultimately chosen. T7 was chosen as they have been engineered to allow proteins with disulfide bonds to form more readily in the cytoplasm. As wild type *E. coli* tend to reduce these stabilizing bonds in the cytoplasm, it was postulated that amelioration of this estate might improve folding and expression of the enzyme. C43 cells were chosen as they improve survivability of cells in the presence of toxic protein expression. Overexpression of proteins which perform non-native functions can lead to a reduction in cell efficiency, lower propagation and premature cell death¹⁹⁵ and are thus deemed toxic to the cell. PRK has been previously shown to convert sugars from the pentose phosphate pathway into a metabolic dead-end when expressed as an individual enzyme in *E. coli*¹⁷².

By using a cell type which better tolerates toxic protein expression, it was hypothesized that PRK would be expressed in greater quantities than non-tolerant cell types. The BL-21 (DE3) cell type was a type of control, as it is regularly used to express recombinant proteins. It does not contain the engineered properties present in T7 and C43

cell types. The conditions were first compared using band width as calculated using the imaging software. Comparison between gels containing samples of the same cell type was not possible due differences in image sizes and positioning. To overcome this, band thickness and the intensity of staining were compared visually, to background proteins, between the largest bands found on different gels. Interestingly, the cells with the highest growth density were the BL-21 cells, which were subsequently chosen for PRK expression. The results of the expression of *S. oleracea* PRK were satisfactory. The amount of PRK in relation to other contaminating bands in lanes 10-13 in Figure 3.5 indicate that PRK was successfully expressed at a high enough concentration for purification.

The initial portion of the purification protocol followed a published procedure by Hudson *et al.* (1992)¹⁷². The first steps involve lysing the cells, followed by ultracentrifugation at high speeds to sediment contaminants. Following this step, ammonium sulfate was used to “salt out” contaminants. Ions in solution interact with protein surface charges, and at ideal concentrations, will lead to an overall balance wherein the protein can remain soluble and stable in solution. If the concentration of ions is lowered, proteins can aggregate due to the lack of shielding ions on their surface, and may also misfold and become unstable. As the concentration of ions increases, as is the case in ammonium sulfate precipitation, the surface of the proteins become very charged, and lead to aggregation. Ammonium sulfate is preferred as it is highly soluble in aqueous solutions, not an expensive product and is available in a pure form¹⁹⁶.

The first salting out step removed protein contaminants that were salted out at 37% w/v. The second step salted out PRK, and removed the contaminants which remained soluble at 60% w/v ammonium sulfate. Polyethylene glycol was then added drop wise to a final concentration of 20% w/v. This polymer attracts water molecules from the solvation layer of the proteins, increasing the probability of protein interactions with each other which leads to an overall reduction in their solubility.

Following dialysis of the protein solution, a deviation was made from Hudson protocol by addition of a purification step. The bioinformatics software Compute pI/mw, hosted on ExPASy, estimated an isoelectric point of 5.3 for PRK¹⁸⁷. Using this information, ion exchange chromatography was chosen to further purify the protein from contaminants. This did result in a more purified sample of PRK, albeit with contaminants still present (Figure 3.5).

A second chromatographic purification step was undertaken to remove these remaining contaminants. The chosen method was substrate-like affinity column, which contained Cibacron Blue F3G-A covalently attached to cross linked agarose. This technique was first used by Siebert *et al.* (1981) for the purification of PRK¹⁹⁷. Cibacron Blue is an adenine mimic, which has been shown to interact with enzymes containing a nucleotide binding site¹⁹⁸. As PRK is a kinase, it contains an adenosine triphosphate binding site, which is presumably the portion of the protein which would have affinity towards the Cibacron Blue dye.

In general, during the process of protein purification, each successive step results in a higher purity of target protein, with an overall loss in total enzyme¹⁹⁹. This was the case with the *S. oleracea* variant, as the purification using the Cibacron blue column resulted in very little purified PRK (Figure 3.6). The low yield may have been due to reasons such as: protein precipitation, degradation over the course of purification and early fractionation with other contaminants. Troubleshooting the loss of protein in the purification protocol could have taken considerable time, and likely would have required another purification step based on a final contaminating band being present in the purified solution. Due to the low protein yield following the second chromatographic step, in addition to the constraints of time, it was decided to halt efforts in purifying the recombinant spinach PRK in favour of another variant of PRK.

4.1.2 PRK from *S. elongatus*

This second variant enzyme originates from *Synechococcus elongatus*, a freshwater-based unicellular cyanobacterium. This construct contains an N-terminal

hexahistidine purification tag (6xHis-tag), which removed many of the additional purification steps required with native enzymes, such as those found in the protocol for the *S. oleracea* construct. It has been reported that PRK from *Synechococcus* is more resistant to oxidative inactivation than higher eukaryote counterparts; however, they have been hinted as being less stable as well^{200,201}.

The second enzyme was successfully purified on the first attempt, which occurred immediately after the final results from the purification of PRK from *S. oleracea* was obtained. The satisfactory yield, ease of the purification and purity made it a much more ideal candidate for study over the spinach variant. As such, the 6His-tagged PRK was chosen as the variant for investigation.

4.2 Kinetic characterization

The kinetics of the two enzymes was successfully characterized by way of the Michaelis-Menten model. The immediate goal of the experiments was to verify the Michaelis constant, K_m , which is the concentration at which the reaction occurs at half-maximal speed. The Michaelis constants of Rpi and PRK were measured following the procedures outlined in section 2.9.1 and 2.10.1 respectively, using the optimized condition levels found in section 3.4. Optimization of the conditions affecting v_0 was one of the last experiments conducted in this thesis. As such, the local optimal conditions were not investigated in regards to their effects on stability at room temperature or UV light exposure work.

4.2.1 Rpi

There have been several methods of investigating the activity of Rpi published in past literature. When the enzyme was first purified by Jang *et al.* in 1954, a discontinuous assay was employed⁸⁶. This assay was an adaptation of the cystein-carbazole method, in which an aliquot is removed and assayed over a period of a half hour²⁰². This assay, in addition to the phloroglucinol method, relies on colourmetric changes, which have been reported to give variations in the depth of colour given a standard amount of substrate²⁰³.

In lieu of these cumbersome methods, a direct and continuous real time assay was chosen as the method for determining the activity of Rpi, that of Wood¹⁷⁴.

RpiA from *E. coli* has a larger K_m than has been previously reported on, with an average that was nearly 50% higher than the highest reported level (section 3.2.1). This could be due to the differing assay conditions as mentioned with PRK, in addition to the fact that RpiA had been freshly thawed from a previously stored frozen stock, prior to being assayed. Oda *et al.* (1978) reported on the change in K_m value of phenol oxidase which had been thawed from a frozen stock over time²⁰⁴. The group found that assaying the enzyme immediately following thawing, the K_m measured 0.02 M. Six hours following thawing, the enzyme was again assayed, yielding a K_m that measured 0.0047 M. Oda *et al.*, as well as others, suggest that certain enzymes may be hysteretic, and undergo slow, minor conformational changes between activation states following a transition from one temperature to another²⁰⁵. In a final note, the K_m value of 3.1 mM reported in literature was obtained using a Hanes-Woolf plot, which is a method of double-reciprocal linearization of kinetic data⁷³. The higher K_m value of 5.9 mM was calculated using non-linear regression modeling, and is not too far removed from the value of 9.4 mM reported for the recombinantly produced Rpi⁸¹.

4.2.2 PRK

The results of the regression fitting in section 3.2.2 indicated that PRK from *S. elongatus* had a slightly lower K_m for ATP than has been reported. This can be attributed to the differing assay conditions between the published and experimental results. As the experimental temperature was much higher, at 40 °C, compared to the 25 °C in literature, the K_m would likely be different²⁰⁶. This is in addition to the differing amounts of DTT and MgCl₂. The experimental value does remain in good agreement with previous literature. The calculated K_m for ribulose 5-phosphate was much lower by comparison, by a factor of over 2. Again, the assay conditions were much different from the previous solitary work on this enzyme variant, which would likely contribute to the difference¹⁰³. The authors of the previously mentioned paper chose to calculate the K_m values of both

ATP and Ru5P through linear double-reciprocal methods, the drawbacks of this method are highlighted in section 2.1.3.

The substrate NADH used by the coupling enzymes in the PRK assay has been claimed to be unstable in past reports, and will slowly oxidize over time²⁰⁷. It has been shown that at a pH of 7.8, and at a temperature of 25 °C, 4% of the NADH in solution will be oxidized after 40 minutes²⁰⁸. As the NADH was kept on ice until use, and the kinetic assay for PRK had a duration of only 5 minutes, the oxidation of NADH was not considered as a significant source of error in the assay.

4.2.3 Stability

The stability experiments were carried out prior to optimization of kinetic assay conditions. As such, most of the original assay conditions found in literature were used (procedures in sections 2.9.1 and 2.10.1), with the exception of temperature. The chosen temperature (ambient) was due to trial reactions of the custom bioprocess unit. At the time, experiments with Rpi were being performed, necessitating some knowledge of its stability. PRK stability experiments subsequently took place at ambient temperature, to facilitate comparison between the two.

Rpi had been previously shown to be thermostable in a past report⁸¹. The results in section 3.3.1 further confirmed that Rpi is able to retain kinetic activity under a variety of *in vitro* conditions, demonstrating a half-life of 89 hours. The concentration was low (176 nM) and no stabilizing molecules were present in this solution. Rpi appeared relatively much more stable when compared to PRK, which had a half-life of 177 minutes (section 3.3.2). There are no comparable published results for the half-life of PRK from *S. elongatus*. The data produced yielded important insight into the stability of this enzyme.

The effects of UV light exposure on the activity of the enzymes were reported in section 3.3.3. The v_0 of each enzyme was measured following exposure. Graphs of Rpi and PRK activities were prepared (Figure 3.17 and 4.18 respectively). The wavelength of light used (254 nm) corresponds to UV-C light. This wavelength is not typically

appreciable in nature, as it is almost entirely absorbed by the ozone layer. It is most often used as a germicidal tool, and there is only occasional research into its effect on enzymatic activity^{209,210}. Su and Bogorad (1991) found that a single substitution for phenylalanine at serine-222 created a light sensitive PRK mutant in the cyanobacterium *Synechocystis* 6803²¹¹. They report that the single mutation made the enzyme highly susceptible to degradation, and reduced its catalytic activity by a factor of 10 when exposed to bright light. A single mutation is possible, but unlikely given that the PRK carrying plasmid was sequenced prior to submission, and the results of the kinetic assays of PRK indicated a fully active form⁹¹. The data which was produced in section 3.3.3 followed an attempt to permeabilize the polymersome membrane by using a photoreactant¹⁶⁷, and was included to further demonstrate the inherent instability that can be found in some enzymes.

As it assumed that the atmospheric oxygen was removed and replaced with argon, the sole process of inactivation which will be considered is absorption of UV light by the protein structure itself, and not indirect oxidation via reactions with singlet oxygen molecules. The greatest contributors to absorbance of UV light in this spectrum are three amino acids: tyrosine (Tyr), tryptophan (Trp) and phenylalanine (Phe). When excited, the triplet states of these residues are much longer lived than singlet, and a host of intra and inter-protein reactions are possible, and are reviewed in depth by Davies and Truscott (2001)²¹². Many of these reactions lead to local denaturation of the protein. PRK contains 28 of these residues, which compose 8.4% of the protein. Rpi has 9, which form 3.3% of the total residues. One reason as to PRK's susceptibility to UV light is could be due to the higher ratio and number of absorbing residues, presenting more opportunities for undesirable reactions which result in inactivation of the enzyme.

The cystine site and its regulation of PRK activity is mentioned in depth in section 4.3.2. Cystine does undergo photo-dissociation, as it also absorbs UV-C light. The radicals formed undergo dimerization in the absence of oxygen, restoring the disulphide bond²¹². This would lead to inactivation of the enzyme, if not for the presence of the reducing agent DTT. Reduced DTT, which is the form of interest in reducing the

disulfide bond, shows nearly no absorbance at 254 nm²¹³. It is unlikely that the agent was altered or destroyed, as only one reference has been found in literature to support the sensitivity of DTT to light, which itself was a reference to a paper which made no mention of DTT²¹⁴. The high concentration of DTT present in solution, in addition to lack of support of DTT sensitivity in literature, further endorses the theory that the inactivation of PRK following UV light exposure was due to the intrinsic sensitivity of the enzyme's amino acid composition.

4.3 Optimization results

4.3.1 Optimization of Rpi

Optimization of the enzymatic activity was carried out using response surface methodology, via central composite designed experiments (Table 0.17). This method reduced the number of runs from a multilevel factorial design of 1875, to just 84. As the assay for Rpi has only a few components, each factor was subsequently investigated for its relevancy in effecting the reaction rate.

The effect of pH on the activity of Rpi has been previously investigated by and Jang *et al.* (1954) who were the first to purify the enzyme from *Medicago sativa*⁸⁶. They found that the enzyme operated best at pH 7. When Rpi was first purified from *E. coli*, it was assayed at pH 7.5, with no mention to the choice of level⁸¹. Rpi from animal tissues was later found to have greater activity at more basic conditions such as pH 8, than enzyme from plants²¹⁵. As the range of pH levels reported Rpi variants is broad, and with no data existing on the optimal pH for *E. coli* Rpi, the range chosen contained broad axial points from pH 6.5 to 8.5.

The lower factor level for ribose 5-phosphate concentration was selected based on the reported K_m of Rpi from *E. coli* at 4.4 mM⁸¹. As this constant is representative of the half-maximal activity of the enzyme, maximal activity should occur in theory, at a concentration of 8.8 mM. By having a lower limit substrate concentration of 10 mM, the enzyme should be saturated. This ensured that the enzymes activity would not be compromised due to lack of substrate. The higher level was chosen due to the cost

associated with the substrate, as well as the solubility issues that could occur using chilled buffer to dissolve the substrate at high concentrations.

Assay temperature conditions involving Rpi sourced from *E. coli* have been performed from 20 °C⁸⁴ to 37 °C^{73,81}. No references as to the method of determining the temperatures used were found in the literature, so points were designed to investigate a range. The lower axial point chosen was set at 22 °C, as this was the ambient room temperature. The higher axial point was set at 44 °C, as this is near the maximum limit that the plate reader can reach.

The final factor investigated was the buffering capacity of the Tris-HCl buffer, which was controlled via the concentration of Tris-HCl present. Past reported buffers have ranged in concentration from 50 to 250 mM^{73,81}. There is no indication in literature as to why these concentrations were chosen. To this end, factorial points were chosen which were near past reported levels at 32.5, 55 and 77.5 mM.

The first predicted model of Rpi activity generated in section 3.4.1 was tested through analysis of variance, comparing the predicted rate to the experimentally determined one. Due to the *p*-value of the lack-of-fit points being less than the established level of α , the model was determined to not satisfactorily fit the data. An unfit model would not be ideal to predict the levels needed to produce maximized kinetic results.

A new model, which achieved the degree of predicted accuracy required, would need to be produced. A new model could be generated through several methods: increasing the number of replicates in the experiment, changing the range of levels based on discovered trends, simplification of the model through the reduction of terms²¹⁶. By adding replicates to the experiment, the generated model could be less susceptible to skewed data, as enzymatic assays are not guaranteed to be robust even in triplicate. Based on the extensive experience with the assay, this was deemed an unlikely candidate. A

second experiment would need to be run, and could very likely produce a very similar, unfit model.

Changing the levels of the factors investigated could reduce the number of interactive terms, and reduce the overall complexity of the model. If the new levels spanned too wide of a range, the results could be heavily skewed towards one level. If they were too short, the entire factor could be deemed insignificant. This choice would require a second full experiment, and may not help in modeling if the newly chosen levels were not appropriate.

In reducing the number of factors, the complexity of the model would also be reduced. By reducing the complexity, it is typical for the precision to increase. This reduction further diminishes the potential investigation into interactions among the chosen factors, in the fact that some may be entirely removed. This also could lead to an increase in bias in the model. As such, the global optimization would no longer be pursued, in favour of a less complex, local optimization. This method was the quickest, and was combined with the previously optimized factor levels.

The second, simplified experiment with fewer factors was designed using the knowledge gained from the results of the first experiment. Locally optimal levels of R5P and buffering strength were selected. Although the first proposed model was not statistically fit, a general idea of the direction of influence the independent factor levels had on activity had been gained. It was shown that of the levels investigated, 76 mM R5P was where the activity peaked (Figure 3.19). From the buffering concentration effects plot, it was shown that, on average, higher activity was associated with a more dilute concentration of buffer. As such, 10 mM was chosen as the optimal concentration of buffer. These levels were chosen to be locally optimal, as the interaction between these factors and others were minimal based on the trend in the model. The main effects plots of both pH and temperature were quite linear in the first experiment, with positive slopes, indicating that higher factorial and axial points could be investigated in viewing these factors as independent. These factors showed no significant interaction in the first model.

Following the generation of the second, simplified model of Rpi activity, ANOVA was used to compare experimental results against predicted results. The second regression model was deemed significant, with a p -value $< \alpha$. The coefficient of determination was 95.7 %, implying that only 4.3 % of the residual points do not fit within the model. The small percentage of points outside of the model was deemed to be not statistically significant due to the high p value of the lack-of-fit points. This suggests that the second quadratic model would accurately predict the activity of RpiA.

Using the proposed second model, response optimization was run in Minitab. This provided the calculated factor levels that would result in the maximized reaction rate within the statistical constraints of the model. Using a pH of 7.7, temperature of 35.3° C and the previously determined optimal levels for R5P and buffer, the activity of the enzyme was measured. Concurrent with this, the activity was measured using the central point factor levels in the first experiment, using the same concentration from the same batch of enzyme. The v_0 of the locally optimized reaction at the initial state was 36.7 % faster than the measured v_0 using the central points (Table 3.19).

4.3.2 Optimization of PRK

There are several assays that have been used in the past for quantifying the activity of PRK. The earliest involved cleavage of the two phosphate groups from ribulose 1,5-biphosphate, the product of the reaction of PRK and Ru5P. The concentration of the inorganic phosphate group was then determined²¹⁷. This assay was not widely used following the adoption of a linked enzyme method²¹⁸. This linked method measures the ADP generated by PRK, when the phosphate group is added to the ribulose sugar. As ADP is used at a 1:1 molar ratio with Ru5P, and the assay can be measured spectroscopically, it makes for an ideal enzymatic assay.

The assay makes use of 8 components, of which only 5 are directly related to PRK activity. In addition to these 5, temperature and pH are also important factors in determining enzymatic activity. As mentioned in section 2.1.6, PEP has been found to be

an allosteric inhibitor in some PRK enzymes. This substrate must be in excess in order to keep the coupled enzyme reaction from becoming the rate limiting step. Inhibitory effects were not investigated for this PRK construct, and have not been reported in literature. In the interest of reducing the total number of runs needed, buffering strength as a factor was not investigated. This decision was partly based on previous work, in which the buffers used for PRK from *Synechococcus* were typically at a concentration of 100 mM of either Tris-HCl or HEPES-KOH^{103,200}.

The effect of pH on PRK activity has not been previously investigated on PRK from *Synechococcus*. From the references found in section 2.1.6, it was decided to set the central pH point at a slightly more basic level 7.5, as points of the design would reach into the very basic level of 8.7, as well as give some insight into the effects of acidity on the purified PRK¹⁹⁷.

PRK makes use of two substrates, ATP and Ru5P, in forming ribulose 1,5-bisphosphate. An optimal concentration of ATP for PRK from *Synechococcus* has not been previously reported on. Hurwitz *et al.* found that PRK activity reached a maximum rate when ATP concentration was 0.7 mM¹⁰⁵. At higher concentrations, the increased ATP did not lead to increased activity rates. MacElroy *et al.* (1968) reported that PRK from *T. ferrooxidans* reached its maximal velocity at 4 mM ATP, and experienced a reduction in rate following deviation from this amount²¹⁹. Siebert *et al.* similarly reported a sigmoidal ATP saturation curve for PRK from *Alcaligenes eutrophus*¹⁹⁷. Using the ranges employed in these past reports, ATP levels were varied from a low axial point of 0.6, to a high of 5.4. Considering the highest reported K_{mATP} for a PRK variant is 1.42 mM, the chosen levels of ATP concentration cover an appropriate range in respect to published amounts²²⁰.

The concentration of the substrate Ru5P was manipulated by controlling the amount of substrate for the prerequisite step involving Rpi forming Ru5P from R5P. The turnover rate of Rpi is faster, at 2100 molecules/second, compared to 630 molecules/second for PRK based on the highest reported specific activity in literature^{73,95}.

This method of producing Ru5P for the PRK assay has been readily used in the past, as Ru5P in solution is both readily hydrolysable, with a half-life of 50 minutes, and the equilibrium reaction between the two sugars strongly favours conversion to R5P^{86,174,221}. By using R5P and Rpi, the substrate can be made readily available by employing an excess of Rpi, and at a reduction in cost compared to Ru5P. The effects of the coupled use of R5P concentration, as well using the direct substrate Ru5P, have not been previously reported on *Synechococcus* PRK activity. Surek *et al.* reported a saturation curve for R5P on PRK from *T. spelta*, which gave a maximum activity at approximately 1.5 mM levels¹⁰⁷. Ru5P saturation curves have been readily published for Ru5P for a variety of PRK variants. Brandes *et al.* reported that recombinant PRK from *Rhodobacter sphaeroides* reached its maximal reaction rate at approximately 11 mM Ru5P¹⁹⁰. Hariharan *et al.* reported that PRK from *Heterosigma carterae* reached maximal activity at 0.6 mM Ru5P¹⁷⁷. From this large range of concentrations, it was decided to vary the concentration of R5P from a low of 1.3 mM, to a high of 10.7 mM. The central point level was set at 6 mM R5P, which was slightly higher than the original assay R5P level described by Kagawa²²².

Wadano *et al.* (1998) ran several experiments investigating the relationship between Ru5P and Mg²⁺ concentration, and found that the optimal reaction rate occurred within a narrow range between 1 and 10 mM Mg²⁺¹⁰³. These experiments found this local maximum through a method of steepest ascent, as was revealed in the parabolic curve on a graph showing kinetic activity vs. Mg²⁺. Further investigation into this specific range would be performed, as greater resolution could be obtained through surface response methodology, including the possible revelation of relevant interaction effects.

The reducing agent DTT was included in the surface response design, as it is typically present in kinetic assays, and there have been no previous works published which investigate the levels of reducing agent and their effects on PRK. The levels chosen were based on published assays, which vary from a low of 5 mM of reducing agent, up to 25 mM.

In a recent study, the cyanobacteria *Synechoccus* was shown to have optimal growth at 33 °C²²³. In literature, PRK is typically assayed at 25 °C¹⁰³. It was decided to have a lower axial point between these two temperatures, near 30 °C, with the higher point at the maximum temperature of the plate reader. The factorial and upper axial points were spread evenly, to give a good distribution in finding the local maximum level for temperature.

With results similar to the first model calculated for Rpi, the chosen factors were deemed too complex when investigated in tandem. It was decided to use the trends found for the factors, independent of interaction, in preparing a second regression model. These trends are found in Figure 3.20. The factor MgCl₂ produced a parabolic curve, which indicated the maximal rate was achieved at 6 mM. This concentration was chosen as the local optimal level. DTT and R5P both produced faster reaction rates as the concentration increased. The positive alpha values of these factors were chosen as the local optimal values. ATP produced faster rates when it was present in dilute concentrations. A lower level of 2 mM was chosen as the new local optimum.

These new optimal levels were used in coordination with a narrowed range of temperature, and a higher range of pH, in a second surface response experiment. The second regression model was produced, and deemed significant, with a p -value $< \alpha$. The determination coefficient was 88.87 implying that 11.13 % of the residual points did not fit within the model. The small percentage of points outside of the model was deemed to be not statistically significant due to the high p value of the lack-of-fit points. This suggests that the quadratic model from the second round of optimization accurately predicts the activity of PRK.

Using the proposed second model, response optimization was run in Minitab. This provided the calculated factor levels, which would result in the maximized reaction rate within the statistical constraints of the model. Using the predicted pH of 7.9, and a temperature of 39.9 °C, the activity of the enzyme was measured, as was the activity of the enzyme using the central point factor levels from the first experiment. The v_0 of the

locally optimized reaction at the initial state was 20.9 % faster than the measured v_0 using the central points (Table 3.19).

4.4 Characterization of polymersomes

4.4.1 Morphological characterization

The narrow range revealed in GPC analysis (Figure 3.21) corresponded with an average molecular weight of 8400 g/mol for the triblock copolymer as calculated by the GPC software. The functionality of the polymer in forming polymersomes was the standard to which the polymer was subjected. To determine this functionality, dynamic light scattering was used. This has been used to investigate polymersomes composed of PMOXA-PDMS-PMOXA from their inception¹⁵⁶. Dynamic light scattering resulted in a distribution of polymersome sizes based on measured intensities. The polydispersity index (PDI) reports the distribution through a method proposed by Koppel in 1972²²⁴. This method simplifies the correlation function of measurement through a method of cumulants, which results in an overall mean size (Z-average) based on intensity, and an overall polydispersity width. The PDI from DLS analysis is typically reported as the square of the mean divided by the width. A smaller number indicates a less disperse sample. The reported average hydrodynamic diameter of 152 nm was in good agreement with previous work and gave one indication of the morphological size of the polymersomes^{167,225}, while the PDI of 0.135 indicated an acceptably narrow range of distribution.

Cryogenic transmission electron microscopy is typically used to image PMOXA-PDMS-PMOXA polymersomes^{231,169}. This high-resolution technique allows measurement of flash-frozen samples. This has the added benefit of keeping the aqueous surroundings of the polymersomes in a glass-like state, which is lost during SEM, as the sample must be dried prior to imaging. A higher electron dose can also be used at these low temperatures, which at room temperature with SEM would lead to radiation damage of the polymersomes²²⁶. Both imaging techniques were used, SEM to first verify the

presence of polymersomes and general morphology, followed with cryo-TEM for greater detail. The average size of imaged polymersomes appeared to be smaller on average than what was expected, showing an apparent diameter of 60 nm, which is three times smaller than the z-average reported by DLS measurements.

The apparent size difference reported by the two techniques is common enough to have warranted investigation in published literature. Gaumet *et al.* (2008) reviewed many publications in which the size characterization of nanoparticles are reported on²²⁷. They found that in some extreme cases, DLS sizes were reported that were up to nine times larger than sizes measured through electron microscopy. The reasons, which were relevant to this work, that were given for these differences include: the fact that DLS is extremely sensitive to aggregates which may skewer the mean size; temperature, pH and buffer composition were different in the two methods; batch differences may result in size variation, and the hydration sphere surrounding the particles contributes to a larger apparent size.

Axthelm *et al.* (2008)²²⁸ encapsulated superoxide dismutase within PMOXA-PDMS-PMOXA polymersomes. The groups reported DLS measured diameter was 300 nm, while their cryo-TEM images revealed an average size slightly lower than 200 nm. Other groups that made use of the same polymer also report larger DLS measurements when compared to cryo-TEM imaging^{231,225}.

4.4.2 Enzyme-laden polymersomes

The triblock polymer used to encapsulate was chosen in part due to the expertise of research group members with this polymer, as well as its mechanical strength in comparison to liposomes, flexibility and the ease of preparation of polymersomes¹⁶⁹. It has seen widespread use in the encapsulation of a variety of enzymes, of differing molecular weights and activities, in literature²²⁹. These polymers are able to confer robustness to the system, as the inherent properties of the polymersome result in long lasting, protective coatings for holding the enzymes²³⁰. Their nanoscale nature is ideal for

the downstream operations system, as once they are permeabilized, they may reduce problems associated with mass transfer in other types of diffusive systems²³¹.

The method of encapsulation used was thin-film rehydration. This method has seen the most use in literature, is simple to perform and is performed using aqueous solvents²³², making it ideal for the encapsulation of enzymes. Three methods were used to demonstrate that enzyme had been encapsulated: a digestion assay, fluorescence correlation spectroscopy and absorbance spectroscopy.

Digestion assay

Rpi was the only model enzyme used in the digestion assay, due to the short half-life of PRK and the long digestion times. Proteinase K is a non-specific serine-protease, which cleaves peptide bonds next to carboxylic group of aliphatic and aromatic amino acids²³³. This enzyme was predicted to cut at 115 cleavage sites within Rpi based on the software PeptideCutter (hosted at ExPASy)¹⁸⁷. Proteinase K is active over a wide range of temperatures and pH's, and is most active in the presence of Ca^{2+} . The enzyme solution was assayed over a period of time, with ANOVA being run between the blank ribose 5-phosphate and the digested samples. No statistical variance was detected at the 9 hour mark. This timespan would have resulted in a large reduction in PRK activity due to its short half-life, and when compounded with the coupled assay conditions and variables presented by those many reagents, resulted in only Rpi being investigated in this assay. The effects of both PMSF and Tween-20 had both been investigated prior to the assay, and no extreme inhibitory effects were discovered on the enzymatic rate of activity.

The activity of digested Rpi and digested polymersomes were compared to their activities prior to the addition of detergent and PMSF through ANOVA. These solutions were not normalized to account for the difference in composition, leading to a very low p value in Table 3.21 for the free Rpi. The assay revealed that 3.7% of the Rpi activity was recovered in relation to the control. This could be interpreted as a dynamic type of encapsulation efficiency. Typically polymersomes composed of PMOXA-PDMS-PMOXA triblock polymers are described as being highly stable; however, as the polymersomes were subjected to shear forces in the incubator, as well as elevated

temperatures over an extended period of time, this may have lysed some of the polymersomes, resulting in a non-static encapsulation efficiency¹⁶⁹. Pata *et al.* (2006) published results showing that polymersome membrane thickness corresponds to a linear relationship with resistance to solubilization via detergents²³⁴. The thicker a membrane is, the slower it is to solubilize, and an increased concentration of detergent is needed to completely dissolve it. The most relatable polymer employed in this published study was a diblock polymer composed of ethylene oxide and butadiene, with a number averaged molecular weight of 3600 g/mol, which is nearly half the size of the triblock polymer used in Rpi encapsulation. Near complete solubilization of polymersomes formed of this polymer was achieved using a Triton X-100 concentration of approximately 160 mM, and a shaking time of 10 minutes. The digestion assay used in this work had a final detergent concentration of 42 mM Tween, and was shaken for one minute.

With the previously reported encapsulation efficiency of 23%, the low percentage of recovered activity in lysed polymersomes can be attributed to incomplete dissolution of the polymersome membranes due to the low detergent concentration, short shaking times, and the possibility of polymersomes being lysed during the incubation and digestion process. Variability in encapsulation efficiency was not investigated, and may also be part of the problem with the difference in reported activity. Enzyme concentration from lysed polymersomes may be quantified through a Bradford assay in future work, to reduce possible errors due to variance in encapsulation efficiency. These results show that encapsulation of the enzyme occurred, and that protection was afforded from the enzymatic cleavage that befell the free Rpi.

Fluorescence correlation spectroscopy

A second experiment to demonstrate that Rpi had been encapsulated within polymersomes was employed using fluorescence correlation spectroscopy (FCS). This technique allows for high resolution of both the spatial and temporal properties of biomolecules at dilute concentrations²³⁵. Using this technique, the intensity fluctuations of the molecule of interest are measured. Depending on the timescale of interest, FCS can measure, in order of fastest to slowest processes: the emission of the photon itself,

rotational fluctuation, excited triplet states and diffusion of the molecule. The difference in timescale is large enough between these processes for diffusion to be investigated separately. Following collection of experimental data, the correlation analysis compares the signal over a period of time to itself, indicating its self-similarity. Over a period of time, this self-similarity decreases from a normalized value of 1 (exactly similar), eventually approaching 0. For a molecule that exhibits slower Brownian diffusion through the focal volume, its fluorescent signals' self-similarity over time will likewise decrease slowly. This slower diffusivity is representative of a larger molecular weight.

Direct comparison of autocorrelation results is difficult between studies due to variances in machinery, buffers, molecules used and temperature. Rigler and Meier (2006) encapsulated an avadin-Alexa fluor 488 complex (67 kDa) within a PMOXA-PDMS-PMOXA polymersome system²³⁶. This was the first publication demonstrating encapsulation of enzyme within polymersomes via FCS, and several more have followed, with each reporting similar qualitative results through autocorrelation curves^{188,237}. The variation in lag times between the free FitC dye, free FitC/Rpi conjugate and encapsulated conjugate in Figure 3.30 appeared consistent with these past studies encapsulating dye-conjugates within polymersomes.

FCS can provide results other than the aforementioned empirical information. Concentration and aggregation can be measured, as may mobility, molecular interactions and conformational changes²³⁵. Concentration of Rpi was not calculated due to the photophysical damage associated with the excitation of fluorescein²³⁸. Lomorra *et al.* (2015)¹⁸⁸ reported that the concentration of encapsulated pyranine within polymersomes using FCS was, on average, halved when compared to concentration measured through UV-spectroscopy. This was attributed solely to the photosensitivity of the pyranine dye, which along with fluorescein, has been reported to have an extremely high photochemical decay rate; however, it should be noted that the author's use of UV-spectroscopy makes no mention of the method of determining the blank polymer concentration level, which may further contribute to the difference in calculated EE²³⁹.

Encapsulation efficiency

The efficiency of encapsulation (EE) is an important metric mentioned in literature, indicating the final amount of material encapsulated when compared to the original concentration. It can vary significantly depending on the nature of the encapsulated molecule, method of encapsulation, carrier and ambient conditions. Lee *et al.* (2001) estimated an EE of human albumin (66.5 kDa) in a PEO-PBD polymer system at 5 %²⁴⁰. The method of encapsulation was film rehydration, and the EE was determined using spectrofluorometry. Martin *et al.* (2015) reported an EE of 72 %, when loading CM-Dextran tagged with fluorescein (4 kDa) into PEG-decyl methacrylate polymersomes²⁴¹. Film rehydration was used, and efficiency was calculated using a spectral intensity scan between 510 and 700 nm compared to a standard curve. The wide variety of the materials and conditions can make direct comparison difficult.

Using the polymer PMOXA-PDMS-PMOXA and the film rehydration method for encapsulation of enzymes has been employed successfully many times previously^{166,188}. The method of determining EE has suffered from a lack of forethought, or oversight in these publications. Initial concentrations of enzyme solutions are typically measured using their natural extinction coefficient, and final concentrations are likewise measured following encapsulation^{167,242,243}. These measurements do not take into account the potential of the polymersomes to either absorb or refract light, or do not make mention of proper controls and the process of taking these phenomena into account. The effect of polymersome concentration on absorbance measurements was shown in Table 3.22.

Rpi exhibits natural absorbance at 280 nm due to its amino acid composition²⁴⁴. To increase the absorbance coefficient of Rpi, and allow the detection of more dilute concentrations, the fluorescent dye fluorescein was conjugated to Rpi. Following conjugation, the efficiency of labeling required knowledge of the protein concentration. Fluorescein has very little emission at 595 nm, which is the wavelength used for quantification of protein in the Bradford assay²⁴⁵. This allowed for a rough estimate of final protein concentration, as Coomassie Blue G-250 and FitC compete for binding to Arginine, which makes up 4.3 % of the amino acid content in Rpi. This tag increased the

molecular weight of the enzyme by approximately 300 daltons per FitC molecule, and its effect on protein stability, solubility and other properties related to encapsulation were discounted based on the low degree of labelling at 1.7 FitC molecules per molecule of Rpi^{246,247}.

In section 3.7.3 the results of a method for determining the encapsulation efficiency is shown. This direct spectroscopic method addresses the issue of the polymersome interference in absorbance measurements. If the polymersome concentration were to not be addressed, the reported encapsulation efficiency of Rpi would have been inflated from 23 % to 37 %.

4.5 Conclusion and future work

The immediate goals of this thesis were to: discover a source of PRK, characterize the kinetic activities of the enzymes Rpi and PRK, optimize the conditions affecting kinetic activity of these two enzymes and to investigate the viability of encapsulation as a method of immobilization.

A reliable source of PRK was established, by expressing a recombinant gene within *E. coli*. This enzyme was successfully harvested with a yield approaching 33 mg/L of culture. The kinetic activities of the enzymes PRK and Rpi were investigated through Michaelis-Menten modeling and stability studies at room temperature over time. The K_m of RpiA from *E. coli* is reported at 9.4 mM for ribose 5-phosphate isomerase, while the K_m of PRK from ATP and Ru5P is 0.069 and 0.12 mM respectively. The stability of the enzymes was characterized by the enzymatic activity half-life, where v_0 was reduced to half its initial rate at a certain point. The calculated half-lives of PRK and Rpi were 177 minutes and 89 hours respectively.

The *in vitro* assays used to measure enzymatic activity involve several components. The levels of several of these components were locally optimized using surface response modeling software. The v_0 of the enzymes was measured using the

initial component levels and the optimized ones. The calculated v_0 of PRK and Rpi had an apparent increase of 20.9 and 36.7 % respectively.

The enzyme Rpi was encapsulated within polymersomes. This was demonstrated qualitatively through both a digestion assay and FCS measurements. The enzyme was quantified using absorbance spectroscopy, with 23.4 % of the original enzyme concentration being present within polymersomes. This represents a final enzyme concentration of 2.6 μM having been encapsulated.

4.5.1 Future work

With the statistical method used for optimization, a narrowing of levels and factors to further increase activity via global maximization would likely produce diminishing returns if more experiments were designed and pursued²⁴⁸. That being said, the coupled enzymatic reaction for PRK involves the substrate PEP, which has been found to be an inhibitor of some PRK constructs. Effects of this substrate on the kinetic activity of PRK were not investigated in this work, as such, the effects and levels of PEP on the v_0 should be investigated in the future to determine optimal levels and investigate inhibitory actions.

The stability of the enzymes was quantified through half-life measurements at room temperature. With optimized levels for assay conditions now known, a new experiment investigating the half-lives under these optimized conditions should be performed in the future. This would allow insight into enzyme stability, allowing a model to be investigated to find the optimal compromise between stability and activity, to maximize the output of a bioprocess unit including these enzymes.

Encapsulation of enzyme within polymersomes was only partially investigated as part of the research goals. The impermeability of the membrane prevented further work on this system in regards to the effects on encapsulation on the stability, v_0 and K_m of the enzyme. The present polymer may be retained through use of a membrane protein channel, which once incorporated, could readily allow passive diffusion of molecules

across the polymer membrane up to 600 Da in size²⁴⁹. This would allow further investigation into the characteristics of the enzymes following encapsulation, and future studies on recyclability and diffusion limitations of the system.

References

- ¹ Sands, P. The United Nations Framework Convention on Climate Change. (1992). *Review of European Community International Environmental Law*, 1, 270–277.
- ² Fischer, C., & Newell, R. G. (2008). Environmental and technology policies for climate mitigation. *Journal of Environmental Economics and Management*, 55(2), 142–162.
- ³ Hasanbeigi, A., Price, L., & Lin, E. (2012). Emerging energy-efficiency and CO₂ emission-reduction technologies for cement and concrete production: A technical review. *Renewable and Sustainable Energy Reviews*, 16(8), 6220–6238.
- ⁴ Romeo, L. M., Catalina, D., Lisbona, P., Lara, Y., & Martínez, A. (2011). Reduction of greenhouse gas emissions by integration of cement plants, power plants, and CO₂ capture systems. *Greenhouse Gases: Science and Technology*, 1(1), 72–82.
- ⁵ Canada, Environment Canada. *Canada's Emission Trends 2014*. Cat. No.: En81-18/2014E-PDF. Pg iv, accessed Feb. 2, 2016, https://ec.gc.ca/ges-ghg/E0533893-A985-4640-B3A2-008D8083D17D/ETR_E%202014.pdf.
- ⁶ U.S. EPA, Inventory of U.S. greenhouse gas emissions and sinks: 1990-2013. Pg. ES-5, accessed Feb. 8, 2016, <http://www3.epa.gov/climatechange/Downloads/ghgemissions/US-GHG-Inventory-2015-Main-Text.pdf>.
- ⁷ Mondal, M. K., Balsora, H. K., & Varshney, P. (2012). Progress and trends in CO₂ capture/separation technologies: A review. *Energy*, 46(1), 431–441.
- ⁸ J.D. Figueroa, T. Fout, S. Plasynski, H. McIlvried, R.D. Srivastava. (2008). Review advances in CO₂ capture technology – the U.S. department of energy's carbon sequestration program. *International Journal of Greenhouse Gas Control*, 2 pp. 9–20.
- ⁹ Songolzadeh, M., Soleimani, M., Takht Ravanchi, M., & Songolzadeh, R. (2014). Carbon dioxide separation from flue gases: a technological review emphasizing reduction in greenhouse gas emissions. *The Scientific World Journal*, 2014, 828131.
- ¹⁰ Finkenrath, M. (2012). Carbon Dioxide Capture from Power Generation – Status of Cost and Performance. *Chemical Engineering & Technology*, 35(3), 482–488.
- ¹¹ Hossain, M. M., & de Lasa, H. I. (2008). Chemical-looping combustion (CLC) for inherent separations—a review. *Chemical Engineering Science*, 63(18), 4433–4451.
- ¹² Buhre, B. J. P., Elliott, L. K., Sheng, C. D., Gupta, R. P., & Wall, T. F. (2005). Oxy-fuel combustion technology for coal-fired power generation. *Progress in Energy and Combustion Science*, 31(4), 283–307.
- ¹³ Brunetti, A., Scura, F., Barbieri, G., & Drioli, E. (2010). Membrane technologies for CO₂ separation. *Journal of Membrane Science*, 359(1-2), 115–125.
- ¹⁴ Figueroa, J. D., Fout, T., Plasynski, S., McIlvried, H., & Srivastava, R. D. (2008). Advances in CO₂ capture technology-The U.S. Department of Energy's Carbon Sequestration Program. *International Journal of Greenhouse Gas Control*, 2(1), 9–20.
- ¹⁵ Choi, W.-J., Seo, J.-B., Jang, S.-Y., Jung, J.-H., & Oh, K.-J. (2009). Removal characteristics of CO₂ using aqueous MEA/AMP solutions in the absorption and regeneration process. *Journal of Environmental Sciences*, 21(7), 907–913.
- ¹⁶ Yu, C. H., Huang, C. H., & Tan, C. S. (2012). A review of CO₂ capture by absorption and adsorption. *Aerosol and Air Quality Research*, 12(5), 745–769.
- ¹⁷ Davis, J., & Rochelle, G. (2009). Thermal degradation of monoethanolamine at stripper conditions. *Energy Procedia*, 1(1), 327–333.

-
- ¹⁸ Pellegrini, G., Strube, R., & Manfrida, G. (2010). Comparative study of chemical absorbents in postcombustion CO₂ capture. *Energy*, 35(2), 851–857.
- ¹⁹ Builes, S., López-Aranguren, P., Fraile, J., Vega, L. F., & Domingo, C. (2015). Analysis of CO₂ Adsorption in Amine-Functionalized Porous Silicas by Molecular Simulations. *Energy & Fuels*, 29(6), 3855–3862.
- ²⁰ Olajire, A. A. (2010). CO₂ capture and separation technologies for end-of-pipe applications – A review. *Energy*, 35(6), 2610–2628.
- ²¹ Pierre, A. C. (2012). Enzymatic Carbon Dioxide Capture. *ISRN Chemical Engineering*, 2012, 1–22.
- ²² Lacroix, O., & Larachi, F. (2008). Scrubber Designs for Enzyme-Mediated Capture of CO₂. *Recent Patents on Chemical Engineering*, 1(2), 93–105.
- ²³ Dzedzic, D., Gross, K. B., Gorski, R. A., & Johnson, J. T. (2006). Feasibility study of using brine for carbon dioxide capture and storage from fixed sources. *Journal of the Air & Waste Management Association (1995)*, 56(12), 1631–1641.
- ²⁴ Berg JM, Tymoczko JL, Stryer L. (2002) Biochemistry, Section 9.2, Making a Fast Reaction Faster: Carbonic Anhydrases. 5th edition. New York:
- ²⁵ Alvizo, O., Nguyen, L. J., Savile, C. K., Bresson, J. A., Lakhapatri, S. L., Solis, E. O. P., Lalonde, J. J. (2014). Directed evolution of an ultrastable carbonic anhydrase for highly efficient carbon capture from flue gas. *Proceedings of the National Academy of Sciences*, 111 (46), 16436–16441.
- ²⁶ IPCC (2005) Special report on carbon dioxide capture and storage. In: Metz B, Davidson O, de Coninck HC, Loos M, Meyer LJ (eds) Prepared by Working Group III of the Intergovernmental Panel on Climate Change. Cambridge University Press, Cambridge, United Kingdom/New York, NY, USA. Pg. 260.
- ²⁷ Seibel, B. A., & Walsh, P. J. (2001). Potential Impacts of CO₂ Injection on Deep-Sea Biota. *Science*, 294(5541), 319–320.
- ²⁸ Aresta, M., & Dibenedetto, A. (2007). Utilisation of CO₂ as a chemical feedstock: opportunities and challenges. *Dalton Transactions*, (28), 2975–2992.
- ²⁹ Leung, D. Y. C., Caramanna, G., & Maroto-Valer, M. M. (2014). An overview of current status of carbon dioxide capture and storage technologies. *Renewable and Sustainable Energy Reviews*, 39, 426–443.
- ³⁰ Porosoff, M. D., Yan, B., & Chen, J. G. (2014). Catalytic reduction of CO₂ by H₂ for synthesis of CO, methanol and hydrocarbons: Challenges and opportunities. *Journal of Materials Chemistry*, 2(2), 303.
- ³¹ Chakrabarti, S., Bhattacharya, S., & Bhattacharya, S. K. (2003). Immobilization of D-ribulose-1,5-bisphosphate carboxylase/oxygenase: a step toward carbon dioxide fixation bioprocess. *Biotechnology and Bioengineering*, 81(6), 705–711.
- ³² Choi, H.-J., & Montemagno, D. C. (2013). Recent Progress in Advanced Nanobiological Materials for Energy and Environmental Applications. *Materials*.
- ³³ Foyer, C. H., Bloom, A. J., Queval, G., & Noctor, G. (2009). Photorespiratory metabolism: genes, mutants, energetics, and redox signaling. *Annual Review of Plant Biology*, 60, 455–484.
- ³⁴ Tcherkez, G. G. B., Farquhar, G. D., & Andrews, T. J. (2006). Despite slow catalysis and confused substrate specificity, all ribulose bisphosphate carboxylases may be nearly

perfectly optimized. *Proceedings of the National Academy of Sciences of the United States of America*, 103(19), 7246–7251.

³⁵ Whitney, S. M., Houtz, R. L., & Alonso, H. (2011). Advancing our understanding and capacity to engineer nature's CO₂-sequestering enzyme, Rubisco. *Plant Physiology*, 155(1), 27–35.

³⁶ Andersson, I., & Backlund, A. (2008). Structure and function of Rubisco. *Plant Physiology and Biochemistry : PPB / Societe Francaise de Physiologie Vegetale*, 46(3), 275–291.

³⁷ Marcus, Y., Altman-Gueta, H., Wolff, Y., & Gurevitz, M. (2011). Rubisco mutagenesis provides new insight into limitations on photosynthesis and growth in *Synechocystis* PCC6803. *Journal of Experimental Botany*.

³⁸ Lin, M. T., Occhialini, A., Andralojc, P. J., Parry, M. A. J., & Hanson, M. R. (2014). A faster Rubisco with potential to increase photosynthesis in crops. *Nature*, 513(7519), 547–550.

³⁹ Whitney, S. M., Birch, R., Kelso, C., Beck, J. L., & Kapralov, M. V. (2015). Improving recombinant Rubisco biogenesis, plant photosynthesis and growth by coexpressing its ancillary RAF1 chaperone. *Proceedings of the National Academy of Sciences*, 112(11), 3564–3569.

⁴⁰ Monson, R. K., & Baldocchi, D. D. (2014). *Terrestrial biosphere-atmosphere fluxes*. Cambridge ; New York : Cambridge University Press, 2014. Pg. 73.

⁴¹ Parry, M. A. J., Keys, A. J., Madgwick, P. J., Carmo-Silva, A. E., & Andralojc, P. J. (2008). Rubisco regulation: a role for inhibitors. *Journal of Experimental Botany*, 59(7), 1569–1580.

⁴² Wendell, D., Todd, J., & Montemagno, C. (2010). Artificial photosynthesis in ranaspumin-2 based foam. *Nano Letters*, 10(9), 3231–6.

⁴³ Boyd, J., Jalal, K., Rogers, P., (2008) *Sustainable Fashion and Textiles: Design Journeys*. London U.K: Earthscan. Pg. 138.

⁴⁴ Knecht, M. R., & Wright, D. W. (2004). Dendrimer-Mediated Formation of Multicomponent Nanospheres. *Chemistry of Materials*, 16(24), 4890–4895.

⁴⁵ Shimizu, K., Cha, J., Stucky, G. D., & Morse, D. E. (1998). Silicatein α : Cathepsin L-like protein in sponge biosilica. *Proceedings of the National Academy of Sciences*, 95(11), 6234–6238.

⁴⁶ Cha, J. N., Stucky, G. D., Morse, D. E., & Deming, T. J. (2000). Biomimetic synthesis of ordered silica structures mediated by block copolypeptides. *Nature*, 403(6767), 289–292.

⁴⁷ Mukai, C., Gao, L., Bergkvist, M., Nelson, J. L., Hinchman, M. M., & Travis, A. J. (2013). Biomimicry Enhances Sequential Reactions of Tethered Glycolytic Enzymes, TPI and GAPDHS. *PLoS ONE*, 8(4), e61434.

⁴⁸ Miki, K., Qu, W., Goulding, E. H., Willis, W. D., Bunch, D. O., Strader, L. F., ... O'Brien, D. A. (2004). Glyceraldehyde 3-phosphate dehydrogenase-S, a sperm-specific glycolytic enzyme, is required for sperm motility and male fertility. *Proceedings of the National Academy of Sciences of the United States of America*, 101(47), 16501–16506.

⁴⁹ Karan, R., Capes, M. D., & DasSarma, S. (2012). Function and biotechnology of extremophilic enzymes in low water activity. *Aquatic Biosystems*, 8, 4.

-
- ⁵⁰ Bhattacharya, S., Schiavone, M., Gomes, J., & Bhattacharya, S. K. (2004). Cascade of bioreactors in series for conversion of 3-phospho-d-glycerate into d-ribulose-1,5-bisphosphate: kinetic parameters of enzymes and operation variables. *Journal of Biotechnology*, *111*(2), 203–217.
- ⁵¹ Tian, W., & Skolnick, J. (2003). How Well is Enzyme Function Conserved as a Function of Pairwise Sequence Identity? *Journal of Molecular Biology*, *333*(4), 863–882.
- ⁵² Zaushitsyna, O., Berillo, D., Kirsebom, H., & Mattiasson, B. (2013). Cryostructured and Crosslinked Viable Cells Forming Monoliths Suitable for Bioreactor Applications. *Topics in Catalysis*, *57*(5), 339–348.
- ⁵³ Carlson, E. D., Gan, R., Hodgman, C. E., & Jewett, M. C. (2012). Cell-free protein synthesis: Applications come of age. *Biotechnology Advances*, *30*(5), 1185–1194.
- ⁵⁴ Sezonov, Guennadi, Danièle Joseleau-Petit, and Richard D’Ari. “*Escherichia Coli* Physiology in Luria-Bertani Broth .” *Journal of Bacteriology* *189*.23 (2007): 8746–8749.
- ⁵⁵ Rosano, Germán L., and Eduardo A. Ceccarelli. “Recombinant Protein Expression in *Escherichia Coli*: Advances and Challenges.” *Frontiers in Microbiology* *5* (2014): 172. PMC. Web. 20 Jan. 2016.
- ⁵⁶ Johnson, K. A., & Goody, R. S. (2011). The Original Michaelis Constant: Translation of the 1913 Michaelis–Menten Paper. *Biochemistry*, *50*(39), 8264–8269.
- ⁵⁷ Park, S., & Agmon, N. (2008). Theory and Simulation of Diffusion-Controlled Michaelis–Menten Kinetics for a Static Enzyme in Solution†. *The Journal of Physical Chemistry B*, *112*(19), 5977–5987.
- ⁵⁸ Copeland, Robert Allen *Enzymes : a practical introduction to structure, mechanism, and data analysis*. VCH Publishers, New York, 1996.
- ⁵⁹ Benner, S. A. (1989). Enzyme kinetics and molecular evolution. *Chemical Reviews*, *89*(4), 789–806.
- ⁶⁰ Abu-Reesh, M. I. (n.d.). Predicting the performance of immobilized enzyme reactors using reversible Michaelis–Menten kinetics. *Bioprocess Engineering*, *17*(3), 131–137.
- ⁶¹ McClure, W. R. (1969). Kinetic analysis of coupled enzyme assays. *Biochemistry*, *8*(7), 2782–2786.
- ⁶² Easterby, J. S. (1973). Coupled enzyme assays: A general expression for the transient. *Biochimica et Biophysica Acta (BBA) - Enzymology*, *293*(2), 552–558.
- ⁶³ Cleland, W. W. (1979). Optimizing coupled enzyme assays. *Analytical Biochemistry*, *99*(1), 142–145.
- ⁶⁴ Lineweaver, H., & Burk, D. (1934). The Determination of Enzyme Dissociation Constants. *Journal of the American Chemical Society*, *56*(3), 658–666.
- ⁶⁵ Ritchie, R. J., & Prvan, T. (1996). Current statistical methods for estimating the K_m and V_{max} of Michaelis–Menten kinetics. *Biochemical Education*, *24*(4), 196–206.
- ⁶⁶ Ranaldi, F., Vanni, P., & Giachetti, E. (1999). What students must know about the determination of enzyme kinetic parameters. *Biochemical Education*, *27*(2), 87–91.
- ⁶⁷ Yamane, T., Sirote, P., & Shimizu, S. (1987). Evaluation of half-life of immobilized enzyme during continuous reaction in bioreactors: A theoretical study. *Biotechnology and Bioengineering*, *30*(8), 963–969.
- ⁶⁸ Sadana, A. (1988). Enzyme deactivation. *Biotechnology Advances*, *6*(3), 349–446.

-
- ⁶⁹ Peterson, M. E., Eisenthal, R., Danson, M. J., Spence, A., & Daniel, R. M. (2004). A new intrinsic thermal parameter for enzymes reveals true temperature optima. *The Journal of Biological Chemistry*, *279*(20), 20717–20722
- ⁷⁰ Palla, C. A., Pacheco, C., & Carrín, M. E. (2011). Preparation and modification of chitosan particles for *Rhizomucor miehei* lipase immobilization. *Biochemical Engineering Journal*, *55*(3), 199–207.
- ⁷¹ Wang, Z., Van Oers, M. C. M., Rutjes, F. P. J. T., & Van Hest, J. C. M. (2012). Polymersome colloidosomes for enzyme catalysis in a biphasic system. *Angewandte Chemie - International Edition*, *51*(43), 10746–10750.
- ⁷² Skinner, A. J., & Cooper, R. A. (1974). Genetic studies on ribose 5-phosphate isomerase mutants of *Escherichia coli* K-12. *Journal of Bacteriology*, *118*(3), 1183–1185.
- ⁷³ Zhang, R. G., Andersson, C. E., Savchenko, A., Skarina, T., Evdokimova, E., Beasley, S., Mowbray, S. L. (2003). Structure of *Escherichia coli* ribose-5-phosphate isomerase: a ubiquitous enzyme of the pentose phosphate pathway and the Calvin cycle. *Structure*, *11*(1), 31–42.
- ⁷⁴ Rangarajan, E. S., Sivaraman, J., Matte, A., & Cygler, M. (2002). Crystal structure of D-ribose-5-phosphate isomerase (RpiA) from *Escherichia coli*. *Proteins: Structure, Function, and Genetics*, *48*(4), 737–740.
- ⁷⁵ Stern, A. L., Burgos, E., Salmon, L., & Cazzulo, J. J. (2007). Ribose 5-phosphate isomerase type B from *Trypanosoma cruzi*: kinetic properties and site-directed mutagenesis reveal information about the reaction mechanism. *The Biochemical Journal*, *401*(1), 279–285.
- ⁷⁶ Ishikawa, K., Matsui, I., Payan, F., Cambillau, C., Ishida, H., Kawarabayasi, Y., Roussel, A. (2002). A hyperthermostable D-ribose-5-phosphate isomerase from *Pyrococcus horikoshii* characterization and three-dimensional structure. *Structure*, *10*(6), 877–886.
- ⁷⁷ Jung, C. H., Hartman, F. C., Lu, T. Y., & Larimer, F. W. (2000). D-ribose-5-phosphate isomerase from spinach: heterologous overexpression, purification, characterization, and site-directed mutagenesis of the recombinant enzyme. *Archives of Biochemistry and Biophysics*, *373*(2), 409–417.
- ⁷⁸ Yoon, R.-Y., Yeom, S.-J., Kim, H.-J., & Oh, D.-K. (2009). Novel substrates of a ribose-5-phosphate isomerase from *Clostridium thermocellum*. *Journal of Biotechnology*, *139*(1), 26–32.
- ⁷⁹ Roos, A. K., Mariano, S., Kowalinski, E., Salmon, L., & Mowbray, S. L. (2008). D-ribose-5-phosphate isomerase B from *Escherichia coli* is also a functional D-allose-6-phosphate isomerase, while the *Mycobacterium tuberculosis* enzyme is not. *Journal of Molecular Biology*, *382*(3), 667–679.
- ⁸⁰ David, J., Wiesmeyer, H., (1970). Regulation of ribose metabolism in *Escherichia coli*: II. Evidence for two ribose-5-phosphate isomerase activities. *Biochimica et Biophysica Acta (BBA) - General Subjects*, *208*(1), 56–67.
- ⁸¹ Essenberg, M. K., & Cooper, R. a. (1975). Two ribose-5-phosphate isomerases from *Escherichia coli* K12: partial characterisation of the enzymes and consideration of their possible physiological roles. *European Journal of Biochemistry*, *55*(2), 323–32.
- ⁸² Ward, O. P., & Moo-Young, M. (1988). Thermostable enzymes. *Biotechnology Advances*, *6*(1), 39–69.

-
- ⁸³ Feierberg, I., & Åqvist, J. (2002). Computational modeling of enzymatic keto-enol isomerization reactions. *Theoretical Chemistry Accounts*, 108(2), 71–84.
- ⁸⁴ David, J., & Wiesmeyer, H. (1970). Regulation of ribose metabolism in *Escherichia coli*. *Biochimica et Biophysica Acta (BBA) - General Subjects*, 208(1), 45–55.
- ⁸⁵ Hove-Jensen, B., & Maigaard, M. (1993). *Escherichia coli* rpiA gene encoding ribose phosphate isomerase A. *Journal of Bacteriology*, 175(17), 5628–35.
- ⁸⁶ Axelrod, B. & Jang, R. (1954) Purification and properties of Phosphoriboisomerase from Alfalfa. *Journal of Biological Chemistry*, 209, 847–855
- ⁸⁷ Chen, Y. R., Hartman, F. C., Lu, T. Y., & Larimer, F. W. (1998). D-Ribulose-5-phosphate 3-epimerase: cloning and heterologous expression of the spinach gene, and purification and characterization of the recombinant enzyme. *Plant Physiology*, 118(1), 199–207.
- ⁸⁸ Kawashima, N., & Tanabe, Y. (1976). Stabilization of ribose-5-phosphate isomerase from tobacco. *Plant and Cell Physiology*, 17(4), 765–769.
- ⁸⁹ Mizioroko, H. M. (2000). Phosphoribulokinase: current perspectives on the structure/function basis for regulation and catalysis. *Advances in Enzymology and Related Areas of Molecular Biology*, 74, 95–127.
- ⁹⁰ Harrison, D. H. T., Runquist, J. A., Holub, A., & Mizioroko, H. M. (1998). The Crystal Structure of Phosphoribulokinase from *Rhodobacter sphaeroides* Reveals a Fold Similar to That of Adenylate Kinase. *Biochemistry*, 37(15), 5074–5085.
- ⁹¹ Hallenbeck, P. L., & Kaplan, S. (1987). Cloning of the Gene for Phosphoribulokinase Activity from *Rhodobacter sphaeroides* and Its Expression in *Escherichia coli*, 169(8).
- ⁹² Milanez, S., Mural, R. J., & Hartman, F. C. (1991). Roles of cysteinyl residues of phosphoribulokinase as examined by site-directed mutagenesis. *The Journal of Biological Chemistry*, 266(16), 10694–10699.
- ⁹³ Parikh, M. R., Greene, D. N., Woods, K. K., & Matsumura, I. (2006). Directed evolution of RuBisCO hypermorphs through genetic selection in engineered *E. coli*. *Protein Engineering, Design & Selection: PEDS*, 19(3), 113–9.
- ⁹⁴ Porter, A., Milanez, S., Hartman, F. C., & Stringer, D. (1986). Purification and Characterization of Ribulose-5-phosphate Kinase from Spinach. *Archives of Biochemistry and Biophysics*, 245(1), 14–23.
- ⁹⁵ Kobayashi, D., Tamoi, M., Iwaki, T., Shigeoka, S., & Wadano, A. (2003). Molecular Characterization and Redox Regulation of Phosphoribulokinase from the Cyanobacterium *Synechococcus* sp. PCC 7942. *Plant Cell Physiology*, 44(3), 269–276.
- ⁹⁶ Thieulin-Pardo, G., Remy, T., Lignon, S., Lebrun, R., & Gontero, B. (2015). Phosphoribulokinase from *Chlamydomonas reinhardtii*: a Benson-Calvin cycle enzyme enslaved to its cysteine residues. *Molecular bioSystems*, 11(4), 1134–1145.
- ⁹⁷ Michels, A. K., Wedel, N., & Kroth, P. G. (2005). Diatom plastids possess a phosphoribulokinase with an altered regulation and no oxidative pentose phosphate pathway. *Plant Physiology*, 137(3), 911–920.
- ⁹⁸ Hariharan, T., Johnson, P. J., & Cattolico, R. A. (1998). Purification and Characterization of Phosphoribulokinase from the Marine Chromophytic Alga *Heterosigma carterae*. *Plant Physiology*, 1, 321–329.

-
- ⁹⁹ Mikkelsen, S. R., & Cortón, E. (2004). Immobilized Enzymes. In *Bioanalytical Chemistry* (pp. 61–85). John Wiley & Sons, Inc. Pg. 63
- ¹⁰⁰ Phosphoribulokinase, chloroplastic. UniProtKB-P09559. Retrieved from <http://www.uniprot.org/uniprot/P09559>.
- ¹⁰¹ Miziorko, H. M., & Eckstein, F. (1984). The stereochemical course of the ribulose-5-phosphate kinase-catalyzed reaction. *Journal of Biological Chemistry*, *259* (21), 13037–13040.
- ¹⁰² Racker, E. (1957). The reductive pentose phosphate cycle. I. Phosphoribulokinase and ribulose diphosphate carboxylase. *Archives of Biochemistry and Biophysics*, *69*, 300–310.
- ¹⁰³ Wadano, A., Nishikawa, K., Hirahashi, T., Satoh, R., & Iwaki, T. (1998). Reaction mechanism of phosphoribulokinase from a cyanobacterium, *Synechococcus* PCC7942. *Photosynthesis Research*, *56*(1), 27–33.
- ¹⁰⁴ Avilan, L., Gontero, B., Lebreton, S., & Ricard, J. (1997). Information Transfer in Multienzyme Complexes. *European Journal of Biochemistry*, *250*(2), 296–302.
- ¹⁰⁵ Hurwitz, J., Weissbach, A., Horecker, B. L., Smyrniotis, P. Z., (1956) Spinach Phosphoribulokinase. *Journal of Biological Chemistry*, *218*. 769-783.
- ¹⁰⁶ MacElroy, R. D., Mack, H. M., & Johnson, E. J. (1972). Properties of Phosphoribulokinase from *Thiobacillus neapolitanus*. *Journal of Bacteriology*, *112* (1), 532–538.
- ¹⁰⁷ Surek, B., Heilbronn, A., Austen, A., & Latzko, E. (1985). Purification and characterization of phosphoribulokinase from wheat leaves. *Planta*, *165*(4). 507-512.
- ¹⁰⁸ Murakami, A., Takeda, T., & Shigeoka, S. (1998). Lack of light-dark regulation of enzymes involved in the photosynthetic carbon reduction cycle in cyanobacteria, *Synechococcus* PCC 7942 and *Synechocystis* PCC 6803. *Bioscience, Biotechnology, and Biochemistry*, *62*(2). 374-376.
- ¹⁰⁹ Hurwitz, J., Weissbach, A., Smyrniotis, P. Z., Horecker, B. L., & Smyrniotis, P. Z. (1956). SPINACH PHOSPHORIBULOKINASE. *Journal of Biological Chemistry*, *218* (2), 769–783.
- ¹¹⁰ Storer, A. C., & Cornish-Bowden, A. (1976). Concentration of MgATP²⁻ and other ions in solution. Calculation of the true concentrations of species present in mixtures of associating ions. *The Biochemical Journal*, *159*(1), 1–5.
- ¹¹¹ Runquist, J. A., Harrison, D. H. T., & Miziorko, H. M. (1999). Rhodospira rubra Phosphoribulokinase: Identification of Lysine-165 as a Catalytic Residue and Evaluation of the Contributions of Invariant Basic Amino Acids to Ribulose 5-Phosphate Binding. *Biochemistry*, *38*(42), 13999–14005.
- ¹¹² Abdelal, A. T., & Schlegel, H. G. (1974). Purification and regulatory properties of phosphoribulokinase from *Hydrogenomonas eutropha* H 16. *The Biochemical Journal*, *139*(3), 481–489.
- ¹¹³ Woodrow, I. E., & Mott, K. A. (n.d.). Modelling C3 photosynthesis: A sensitivity analysis of the photosynthetic carbon-reduction cycle. *Planta*, *191*(4), 421–432.
- ¹¹⁴ Rippel, S., Bowien, B. (1984). Phosphoribulokinase from *Rhodospseudomonas acidophila*. *Archives of Microbiology*, *139*, 207-212.

-
- ¹¹⁵ Finn, Michael W., and F. Robert Tabita. "Modified Pathway To Synthesize Ribulose 1,5-Bisphosphate in Methanogenic Archaea." *Journal of Bacteriology* 186.19 (2004): 6360–6366.
- ¹¹⁶ Finn, Michael W., and F. Robert Tabita. "Modified Pathway To Synthesize Ribulose 1,5-Bisphosphate in Methanogenic Archaea." *Journal of Bacteriology* 186.19 (2004): 6360–6366.
- ¹¹⁷ Sato, T., Atomi, H., & Imanaka, T. (2007). Archaeal Type III RuBisCOs Function in a Pathway for AMP Metabolism. *Science*, 315(5814), 1003–1006.
- ¹¹⁸ Aono, R., Sato, T., Yano, A., Yoshida, S., Nishitani, Y., Miki, K., Atomi, H. (2012). Enzymatic Characterization of AMP Phosphorylase and Ribose-1,5-Bisphosphate Isomerase Functioning in an Archaeal AMP Metabolic Pathway. *Journal of Bacteriology*, 194 (24), 6847–6855.
- ¹¹⁹ Kamber, L., & Feller, U. (1998). Influence of the activation status and of ATP on phosphoribulokinase degradation. *Cell*, 49(319), 139–144.
- ¹²⁰ Iyer, P. V., & Ananthanarayan, L. (2008). Enzyme stability and stabilization—Aqueous and non-aqueous environment. *Process Biochemistry*, 43(10), 1019–1032.
- ¹²¹ Marri, L., Trost, P., Pupillo, P., & Sparla, F. (2005). Reconstitution and Properties of the Recombinant Phosphoribulokinase Supramolecular Complex, *I39*(November), 1433–1443.
- ¹²² Cauchy, A.-L. (1847). Méthode générale pour la résolution des systèmes d'équations simultanées [Translated: (2010)]. *Compte Rendu Des S'éances de L'Acad'emie Des Sciences*, 25(2), 536–538.
- ¹²³ Chen, H., Zhang, J., Dang, Y., & Shu, G. (2014). Optimization for immobilization of β -galactosidase using plackett-burman design and steepest ascent method, 6(4), 612–616.
- ¹²⁴ Talat, M., Singh, A. K., & Srivastava, O. N. (2011). Optimization of process variables by central composite design for the immobilization of urease enzyme on functionalized gold nanoparticles for various applications. *Bioprocess and Biosystems Engineering*, 34(6), 647–657.
- ¹²⁵ Liu, J., Zhang, Y., Xia, Y., & Su, F. (2010). Optimization of Immobilization Conditions of *Candida antarctica* Lipase Based on Response Surface Methodology, 24(2), 203–209.
- ¹²⁶ Hamsaveni, D. R., Prapulla, S. G., & Divakar, S. (2001). Response surface methodological approach for the synthesis of isobutyl isobutyrate. *Process Biochemistry*, 36(11), 1103–1109.
- ¹²⁷ Pessarakli, M. (2005). *Handbook of photosynthesis*. Boca Raton, FL : Taylor & Francis, 2005. Pg. 260
- ¹²⁸ Patterson, D. P., Prevelige, P. E., & Douglas, T. (2012). Nanoreactors by Programmed Enzyme Encapsulation Inside the Capsid of the Bacteriophage P22. *ACS Nano*, 6(6), 5000–5009. <http://doi.org/10.1021/nn300545z>
- ¹²⁹ Chen, A. H., & Silver, P. A. (2012). Designing biological compartmentalization. *Trends in Cell Biology*, 22(12), 662–670.
- ¹³⁰ Xu, P., Ranganathan, S., Fowler, Z. L., Maranas, C. D., & Koffas, M. A. G. (2011). Genome-scale metabolic network modeling results in minimal interventions that cooperatively force carbon flux towards malonyl-CoA. *Metabolic Engineering*,

13(5), 578–587.

¹³¹ Ellis, R. J. (2016). Macromolecular crowding: obvious but underappreciated. *Trends in Biochemical Sciences*, 26(10), 597–604.

¹³² Pritchard, M. L., Pegg, A. E., & Jefferson, L. S. (1982). Ornithine decarboxylase from hepatoma cells and a variant cell line in which the enzyme is more stable. *Journal of Biological Chemistry*, 257 (10), 5892–5899.

¹³³ Rhee, J.-K., Ahn, D.-G., Kim, Y.-G., & Oh, J.-W. (2005). New Thermophilic and Thermostable Esterase with Sequence Similarity to the Hormone-Sensitive Lipase Family, Cloned from a Metagenomic Library. *Applied and Environmental Microbiology*, 71 (2), 817–825.

¹³⁴ Giver, L., Gershenson, A., Freskgard, P.-O., & Arnold, F. H. (1998). Directed evolution of a thermostable esterase. *Proceedings of the National Academy of Sciences*, 95 (22), 12809–12813.

¹³⁵ Kondo, A., & Teshima, T. (1995). Preparation of immobilized enzyme with high activity using affinity tag based on proteins A and G. *Biotechnology and Bioengineering*, 46(5), 421–428.

¹³⁶ Suma, Y., Kang, C. S., & Kim, H. S. (2015). Noncovalent and covalent immobilization of oxygenase on single-walled carbon nanotube for enzymatic decomposition of aromatic hydrocarbon intermediates. *Environmental Science and Pollution Research International*.

¹³⁷ Cao, L., van Rantwijk, F., & Sheldon, R. A. (2000). Cross-linked enzyme aggregates: a simple and effective method for the immobilization of penicillin acylase. *Organic Letters*, 2(10), 1361–1364.

¹³⁸ Reetz, M. T., Zonta, A., & Simpelkamp, J. (1996). Efficient immobilization of lipases by entrapment in hydrophobic sol-gel materials. *Biotechnology and Bioengineering*, 49(5), 527–534.

¹³⁹ Nallani, M., Benito, S., Onaca, O., Graff, A., Lindemann, M., Winterhalter, M., Schwaneberg, U. (2006). A nanocompartment system (Synthosome) designed for biotechnological applications. *Journal of Biotechnology*, 123(1), 50–59.

¹⁴⁰ Brena, B., Batista-Viera F., (2006) *Immobilization of Enzymes and Cells*. New York City, NY: Humana Press. Pg. 15

¹⁴¹ Ching-Ching Yu, Yu-Ying Kuo, Chien-Fu Liang, Wei-Ting Chien, Huan-Ting Wu, Tsung-Che Chang, Fan-Dan Jan, and Chun-Cheng Lin. (2012). Site-Specific Immobilization of Enzymes on Magnetic Nanoparticles and Their Use in Organic Synthesis. *Bioconjugate Chemistry*, 23, 714–724.

¹⁴² Sachin Talekar, Asavari Joshi, Gandhali Joshi, Priyanka Kamat, Rutumbara Haripurkar, Shashikant Kambale. (2013). Parameters in preparation and characterization of cross linked enzyme aggregates (CLEAs). *RSC Advances*, 3, 12485–12511.

¹⁴³ Dong-Hao, Z., Li-Xia, Y., & Li-Juan, P. (2013). Parameters Affecting the Performance of Immobilized Enzyme. *Journal Of Chemistry*, Article ID 946248.

¹⁴⁴ Zelisko, P. M. (2014). *Bio-inspired silicon-based materials*. Dordrecht : Springer, 2014.

¹⁴⁵ Mahajan, R., Gupta, V. K., & Sharma, J. (2010). Comparison and suitability of gel matrix for entrapping higher content of enzymes for commercial applications.

Indian Journal of Pharmaceutical Sciences, 72(2), 223–228.

¹⁴⁶ Polshettiwar, V., & Asefa, T. (2013). *Nanocatalysis: synthesis and applications*. Hoboken, New Jersey: Wiley.

¹⁴⁷ Zhang, F., Wang, M., Liang, C., Jiang, H., Shen, J., & Li, H. (2014). Thin-Layer Polymer Wrapped Enzymes Encapsulated in Hierarchically Mesoporous Silica with High Activity and Enhanced Stability. *Scientific Reports*, 4, 4421.

¹⁴⁸ Gustafsson, H., Johansson, E. M., Barrabino, A., Oden, M., & Holmberg, K. (2012). Immobilization of lipase from *Mucor miehei* and *Rhizopus oryzae* into mesoporous silica--the effect of varied particle size and morphology. *Colloids and Surfaces B: Biointerfaces*, 100, 22–30.

¹⁴⁹ Yoshimoto, M. (2011). Stabilization of enzymes through encapsulation in liposomes. *Methods in Molecular Biology*, 679, 9–18.

¹⁵⁰ Nasseau, M., Boublik, Y., Meier, W., Winterhalter, M., & Fournier, D. (2001). Substrate-permeable encapsulation of enzymes maintains effective activity, stabilizes against denaturation, and protects against proteolytic degradation. *Biotechnology and Bioengineering*, 75(5), 615–618.

¹⁵¹ Vamvakaki, V., & Chaniotakis, N/A (2007). Pesticide detection with a liposome-based nano-biosensor. *Biosensors and Bioelectronics*, 22(12), 2848–2853.

¹⁵² Gregoriadis, G., & Ryman, B. E. (1971). Liposomes as carriers of enzymes or drugs: a new approach to the treatment of storage diseases. *Biochemical Journal*, 124(5), 58P.

¹⁵³ Allen, T. M., & Cullis, P. R. (2013). Liposomal drug delivery systems: From concept to clinical applications. *Advanced Drug Delivery Reviews*, 65(1), 36–48.

¹⁵⁴ Colletier, J.-P., Chaize, B., Winterhalter, M., & Fournier, D. (2002). Protein encapsulation in liposomes: efficiency depends on interactions between protein and phospholipid bilayer. *BMC Biotechnology*, 2, 9.

¹⁵⁵ Doherty, G. J., & McMahon, H. T. (2009). Mechanisms of Endocytosis. *Annual Review of Biochemistry*, 78(1), 857–902.

¹⁵⁶ Nardin, C., Thoeni, S., Widmer, J., Winterhalter, M., & Meier, W. (2000). Nanoreactors based on (polymerized) ABA-triblock copolymer vesicles. *Chemical Communications*, (15), 1433–1434.

¹⁵⁷ Brinkhuis, R. P., Rutjes, F. P. J. T., & van Hest, J. C. M. (2011). Polymeric vesicles in biomedical applications. *Polymer Chemistry*, 2(7), 1449–1462.

¹⁵⁸ Christian, D. A., Cai, S., Bowen, D. M., Kim, Y., Pajerowski, J. D., & Discher, D. E. (2009). Polymersome Carriers: from Self-Assembly to siRNA and Protein Therapeutics. *European Journal of Pharmaceutics and Biopharmaceutics : Official Journal of Arbeitsgemeinschaft Fur Pharmazeutische Verfahrenstechnik e.V.*, 71(3), 463–474.

¹⁵⁹ Egli, S., Schlaad, H., Bruns, N., & Meier, W. (2011). Functionalization of Block Copolymer Vesicle Surfaces. *Polymers*, 3(1), 252–280.

¹⁶⁰ Mecke, A., Dittrich, C., & Meier, W. (2006). Biomimetic membranes designed from amphiphilic block copolymers. *Soft Matter*, 2(9), 751–759.

¹⁶¹ Discher, B. M. (1999). Polymersomes: Tough Vesicles Made from Diblock Copolymers. *Science*, 284(5417), 1143–1146.

¹⁶² Rother, C., Nidetzky, B., & Flickinger, M. C. (2009). Enzyme Immobilization by

Microencapsulation: Methods, Materials, and Technological Applications. *Encyclopedia of Industrial Biotechnology*. John Wiley & Sons, Inc. Pg. 5

¹⁶³ Vriezema, D. M., Hoogboom, J., Velonia, K., Takazawa, K., Christianen, P. C. M., Maan, J. C., Nolte, R. J. M. (2003). Vesicles and polymerized vesicles from thiophene-containing rod-coil block copolymers. *Angewandte Chemie – International Edition*, 42(7), 772–776.

¹⁶⁴ Kuiper, S. M., Nallani, M., Vriezema, D. M., Cornelissen, J. J. L. M., van Hest, J. C. M., Nolte, R. J. M., & Rowan, A. E. (2008). Enzymes containing porous polymersomes as nano reaction vessels for cascade reactions. *Organic & Biomolecular Chemistry*, 6(23), 4315–4318.

¹⁶⁵ Wang, X., Liu, G., Hu, J., Zhang, G., & Liu, S. (2014). Concurrent Block Copolymer Polymersome Stabilization and Bilayer Permeabilization by Stimuli-Regulated “Traceless” Crosslinking. *Angewandte Chemie International Edition*, 53(12), 3138–3142.

¹⁶⁶ Ihle, S., Onaca, O., Rigler, P., Hauer, B., Rodriguez-Ropero, F., Fioroni, M., & Schwaneberg, U. (2011). Nanocompartments with a pH release system based on an engineered OmpF channel protein. *Soft Matter*, 7(2), 532.

¹⁶⁷ Spulber, M., Najer, A., Winkelbach, K., Glaied, O., Waser, M., Piele, U., ... Bruns, N. (2013). Photoreaction of a hydroxyalkylphenone with the membrane of polymersomes: a versatile method to generate semipermeable nanoreactors. *Journal of the American Chemical Society*, 135(24), 9204–12.

¹⁶⁸ Choi, H.-J., & Montemagno, C. D. (2005). Artificial organelle: ATP synthesis from cellular mimetic polymersomes. *Nano Letters*, 5(12), 2538–2542.

¹⁶⁹ Jaskiewicz, K., Makowski, M., Kappl, M., Landfester, K., & Kroeger, A. (2012). Mechanical Properties of Poly(dimethylsiloxane)-block-poly(2-methylloxazoline) Polymersomes Probed by Atomic Force Microscopy. *Langmuir*, 28(34), 12629–12636.

¹⁷⁰ Bradford, M. M. (1976). A rapid and sensitive method for the quantitation of microgram quantities of protein utilizing the principle of protein-dye binding. *Analytical Biochemistry*, 72, 248–254.

¹⁷¹ Sambrook, J., Fritsch, E. F., & Maniatis, T. (1989). *Molecular cloning : a laboratory manual*. Cold Spring Harbor, N.Y. : Cold Spring Harbor Laboratory, 1987.

¹⁷² Hudson, G. Morell, M., Arvidsson, Y., Andrews, T. (1992). Synthesis of Spinach Phosphoribulokinase and Ribulose 1, 5-bisphosphate in Escherichia coli. *Australian Journal of Plant Physiology*, 19. 213-221

¹⁷³ Duong-Ly, K. C., & Gabelli, S. B. (2014). Chapter Seven - Salting out of Proteins Using Ammonium Sulfate Precipitation. In J. L. B. T.-M. in *Enzymology (Ed.), Laboratory Methods in Enzymology: Protein Part C* (Vol. Volume 541, pp. 85–94).

¹⁷⁴ Wood, T. (1970). Spectrophotometric assay for d-ribose-5-phosphate ketol-isomerase and for d-ribulose-5-phosphate 3-epimerase. *Analytical Biochemistry*, 33(2), 297–306.

¹⁷⁵ http://www.biozentrum.unibas.ch/fileadmin/redaktion/Forschung/Research_Groups/BF/instruments/Fluo_platereader_manual.pdf. Accessed Feb. 15, 2016.

¹⁷⁶ <https://support.office.com/en-us/article/LINEST-function-84d7d0d9-6e50-4101-977a-fa7abf772b6d>. Accessed Feb. 16, 2016.

¹⁷⁷ Hariharan, T., Johnson, P. J., & Cattolico, R. A. (1998). Purification and Characterization of Phosphoribulokinase from the Marine Chromophytic Alga *Heterosigma carterae*. *Plant Physiology*, 1, 321–329.

-
- ¹⁷⁹ Minitab 17 Statistical Software (2010). [Computer software]. State College, PA: Minitab, Inc. (www.minitab.com).
- ¹⁸⁰ <http://149.171.168.221/partcat/wp-content/uploads/Malvern-Zetasizer-LS.pdf>. Accessed Feb. 17, 2016. Pg. 48
- ¹⁸¹ <http://imagej.nih.gov/ij/>
- ¹⁸² Sievers, F., Wilm, A., Dineen, D., Gibson, T. J., Karplus, K., Li, W. Higgins, D. G. (2011). Fast, scalable generation of high-quality protein multiple sequence alignments using Clustal Omega. *Molecular Systems Biology*, 7(1).
- ¹⁸³ http://www.bioinformatics.org/sms/rev_comp.html. Accessed Feb. 19, 2016
- ¹⁸⁴ Krieger, T. J., & Miziorko, H. M. (1986). Affinity Labeling and Purification of Spinach Leaf Ribulose-5-phosphate Kinase. *Biochemistry*, 25(12), 3496–3501.
- ¹⁸⁵ Hochuli, E., Bannwarth, W., Dobeli, H., Gentz, R., & Stuber, D. (1988). Genetic Approach to Facilitate Purification of Recombinant Proteins with a Novel Metal Chelate Adsorbent. *Nature Biotechnology*, 6(11), 1321–1325.
- ¹⁸⁶ Wood, E. J. (1993). Enzymes of molecular biology volume 16 Edited by M M Burrell. The Humana Press, Totowa, NJ, USA. ISBN 0-89603-234-5. *Biochemical Education*, 21(4), 307.
- ¹⁸⁷ Gasteiger, E., Hoogland, C., Gattiker, A., Duvaud, S., Wilkins, M., Appel, R., & Bairoch, A. (2005). Protein Identification and Analysis Tools on the ExPASy Server. In J. Walker (Ed.), *The Proteomics Protocols Handbook SE - 52* (pp. 571–607).
- ¹⁸⁸ Lomora, M., Garni, M., Itef, F., Tanner, P., Spulber, M., & Palivan, C. G. (2015). Polymersomes with engineered ion selective permeability as stimuli-responsive nanocompartments with preserved architecture. *Biomaterials*, 53, 406–414.
- ¹⁸⁹ Hirasawa, M., Brandes, H. K., Hartman, F. C., & Knaff, D. B. (1998). Oxidation-reduction properties of the regulatory site of spinach phosphoribulokinase. *Archives of Biochemistry and Biophysics*, 350(1), 127–131.
- ¹⁹⁰ Brandes, K., Hartman, F. C., Lu, T., Larimer, F. (1996). Efficient Expression of the Gene for Spinach Phosphoribulokinase in *Pichia pastoris* and Utilization of the Recombinant Enzyme to Explore the Role of Regulatory Cysteinyll Residues by Site-directed Mutagenesis. *Journal of Biological Chemistry*, 271(11), 6490–6496.
- ¹⁹¹ UniProt Consortium (2015). UniProt: a hub for protein information. *Nucleic Acids Research*, 43 (D1).
- ¹⁹² Porter, M. A., & Hartman, F. C. (1986). Commonality of catalytic and regulatory sites of spinach phosphoribulokinase: characterization of a tryptic peptide that contains an essential cysteinyl residue. *Biochemistry*, 25(23), 7314–7318.
- ¹⁹³ Stothard, P. (2000). The sequence manipulation suite: JavaScript programs for analyzing and formatting protein and DNA sequences. *BioTechniques*, 28(6), 1102-1104.
- ¹⁹⁴ E. coli codon usage analyzer. (n.d.). Retrieved November 13, 2015, from <http://www.faculty.ucr.edu/~mmaduro/codonusage/usage.htm>
- ¹⁹⁵ Rosano, G. L., & Ceccarelli, E. A. (2014). Recombinant protein expression in *Escherichia coli*: advances and challenges. *Frontiers in Microbiology*, 5(172).
- ¹⁹⁶ Duong-Ly, K. C., & Gabelli, S. B. (2014). Salting out of proteins using ammonium sulfate precipitation. *Methods in Enzymology*, 541, 85–94.

-
- ¹⁹⁷ Siebert, K., Schobert, P., & Bowien, B. (1981). Purification, some catalytic and molecular properties of phosphoribulokinase from *Alcaligenes eutrophus*. *Biochimica et Biophysica Acta*, 658(1), 35–44.
- ¹⁹⁸ Beissner, R. S., & Rudolph, F. B. (1978). Interaction of Cibacron Blue 3G-A and related dyes with nucleotide-requiring enzymes. *Archives of Biochemistry and Biophysics*, 189(1), 76–80.
- ¹⁹⁹ Etienne Dako, Anne-Marie Bernier, Adjéhi Thomas Dadie and Christopher K. Jankowski (2012). The Problems Associated with Enzyme Purification, Chemical Biology, edited by Prof. Deniz Ekinci.
- ²⁰⁰ Wadano, A., Nishikawa, K., Hirahashi, T., Satoh, R., & Iwaki, T. (1998). Reaction mechanism of phosphoribulokinase from a cyanobacterium, *Synechococcus* PCC7942. *Photosynthesis Research*, 56(1), 27–33.
- ²⁰¹ Wadano, A., Kamata, Y., Iwaki, T., Nishikawa, K., & Hirahashi, T. (1995). Purification and Characterization of Phosphoribulokinase from the Cyanobacterium *Synechococcus* PCC7942, *Plant Cell Physiology*, 36(7), 1381–1385.
- ²⁰² Dische, Z., & Borenfreund, E. (1951). A new spectroscopic method for the detection and determination of keto sugars and trioses.. *Journal of Biological Chemistry*, 192 (2), 583–587.
- ²⁰³ Dische, Z., & Borenfreund, E. (1957). A new color reaction for the determination of aldopentose in presence of other saccharides. *Biochimica et Biophysica Acta*, 23, 639–642.
- ²⁰⁴ Oda, Y., Oh-E, S., Saito, G., & Matsuoka, H. (1978). Effects of phenolic compounds on the mitochondrial phenol oxidase of spinach leaves. *Agricultural and Biological Chemistry*, 42(2). 253-258.
- ²⁰⁵ Kleczkowski, L. A., Villand, P., Olsen, O. (1993). Hysteresis and Reversible Cold-Inactivation of ADP-Glucose Pyrophosphorylase From Barley Seeds. *Zeitschrift für Naturforschung C*, 48(5). 457-460.
- ²⁰⁶ Londesborough, J., & Lukkari, T. M. (1980). The pH and temperature dependence of the activity of the high Km cyclic nucleotide phosphodiesterase of bakers' yeast. *Journal of Biological Chemistry* , 255 (19), 9262–9267.
- ²⁰⁷ Fawcett, C. P., Ciotti, M. M., & Kaplan, N. O. (1961). Inhibition of dehydrogenase reactions by a substance formed from reduced diphosphopyridine nucleotide. *Biochimica et Biophysica Acta*, 54(1), 210–212.
- ²⁰⁸ Rover Junior, L., Fernandes, J. C., de Oliveira Neto, G., Kubota, L. T., Katekawa, E., & Serrano, S. H. (1998). Study of NADH stability using ultraviolet-visible spectrophotometric analysis and factorial design. *Analytical Biochemistry*, 260(1), 50–55.
- ²⁰⁹ Burgener, J. (2006). Position Paper on the Use of Ultraviolet Lights in Biological Safety Cabinets. *Applied Biosafety*, 11(4), 228–230.
- ²¹⁰ Lante, A., Tinello, F., & Lomolino, G. (2013). Effect of UV light on microbial proteases: From enzyme inactivation to antioxidant mitigation. *Innovative Food Science & Emerging Technologies*, 17. 130–134.
- ²¹¹ Su, X., & Bogorad, L. (1991). A residue substitution in phosphoribulokinase of *Synechocystis* PCC 6803 renders the mutant light-sensitive. *Journal of Biological Chemistry* , 266 (35), 23698–23705.

-
- ²¹² Davies, M. J., & Truscott, R. J. W. (2001). Photo-oxidation of proteins and its role in cataractogenesis. *Journal of Photochemistry and Photobiology B: Biology*, 63(1-3), 114–125.
- ²¹³ Cleland, W. W. (1964). Dithiothreitol, a New Protective Reagent for SH Groups. *Biochemistry*, 3(4), 480–482.
- ²¹⁴ Charrier, J. G., & Anastasio, C. (2012). On dithiothreitol (DTT) as a measure of oxidative potential for ambient particles: evidence for the importance of soluble transition metals. *Atmospheric Chemistry and Physics*, 12(5), 11317–11350.
- ²¹⁵ Dickens, F., & Williamson, D. H. (1956). Pentose phosphate isomerase and epimerase from animal tissues. *Biochemical Journal*, 64(3), 567–578.
- ²¹⁶ Sauerbrei, W. (1999). The Use of Resampling Methods to Simplify Regression Models in Medical Statistics. *Journal of the Royal Statistical Society*, 48(3), 313–329.
- ²¹⁸ Kornberg, A., & Pricer, W. E. (1951). Enzymatic phosphorylation of adenosine and 2,6-diaminopurine riboside. *Journal of Biological Chemistry*, 193 (2), 481–496.
- ²¹⁹ MacElroy, R. D., Johnson, E. J., & Johnson, M. K. (1968). Allosteric regulation of phosphoribulokinase activity. *Biochemical and Biophysical Research Communications*, 30(6), 678–682.
- ²²⁰ Serra, J. L., Llama, M. J., Rowell, P., & Stewart, W. D. P. (1989). Purification and characterization of phosphoribulokinase from the N₂-fixing cyanobacterium *Anabaena cylindrica*. *Plant Science*, 59(1), 1–9.
- ²²¹ Wood, T. (1985). *The pentose phosphate pathway*. Orlando : Academic Press, 1985.
- ²²² Hariharan, T., Johnson, P. J., & Cattolico, R. A. (1998). Purification and Characterization of Phosphoribulokinase from the Marine Chromophytic Alga *Heterosigma carterae* 1, 321–329.
- ²²³ Kuan, D., Duff, S., Posarac, D., & Bi, X. (2015). Growth optimization of *Synechococcus elongatus* PCC7942 in lab flasks and a 2-D photobioreactor. *The Canadian Journal of Chemical Engineering*, 93(4), 640–647.
- ²²⁴ Koppel, D. E. (1972). Analysis of Macromolecular Polydispersity in Intensity Correlation Spectroscopy: The Method of Cumulants. *The Journal of Chemical Physics*, 57(11).
- ²²⁵ Kumar, M., Grzelakowski, M., Zilles, J., Clark, M., & Meier, W. (2007). Highly permeable polymeric membranes based on the incorporation of the functional water channel protein Aquaporin Z. *Proceedings of the National Academy of Sciences*, 104 (52), 20719–20724.
- ²²⁶ Milne, J. L. S., Borgnia, M. J., Bartesaghi, A., Tran, E. E. H., Earl, L. A., Schauder, D. M., Subramaniam, S. (2013). Cryo-electron microscopy--a primer for the non-microscopist. *The FEBS Journal*, 280(1), 28–45.
- ²²⁷ Gaumet, M., Vargas, A., Gurny, R., & Delie, F. (2008). Nanoparticles for drug delivery: The need for precision in reporting particle size parameters. *European Journal of Pharmaceutics and Biopharmaceutics*, 69(1), 1–9.
- ²²⁸ Axthelm, F., Casse, O., Koppenol, W. H., Nauser, T., Meier, W., & Palivan, C. G. (2008). Antioxidant nanoreactor based on superoxide dismutase encapsulated in superoxide-permeable vesicles. *The Journal of Physical Chemistry. B*, 112(28), 8211–7.

- ²²⁹ Tanner, P., Onaca, O., Balasubramanian, V., Meier, W., & Palivan, C. G. (2011). Enzymatic cascade reactions inside polymeric nanocontainers: a means to combat oxidative stress. *Chemistry*, *17*(16), 4552–60.
- ²³⁰ Lim, S., de Hoog, H.-P., Parikh, A., Nallani, M., & Liedberg, B. (2013). Hybrid, Nanoscale Phospholipid/Block Copolymer Vesicles. *Polymers*, *5*(3), 1102–1114.
- ²³¹ Siti, W., de Hoog, H.-P. M., Fischer, O., Shan, W. Y., Tomczak, N., Nallani, M., & Liedberg, B. (2014). An intercompartmental enzymatic cascade reaction in channel-equipped polymersome-in-polymersome architectures. *Journal of Materials Chemistry B*, *2*(18), 2733
- ²³² Parnell, A. J., Tzokova, N., Topham, P. D., Adams, D. J., Adams, S., Fernyhough, C. M., Jones, R. A. L. (2009). The efficiency of encapsulation within surface rehydrated polymersomes. *Faraday Discussions*, *143*(0), 29–46.
- ²³³ Ebeling, W., Hennrich, N., Klockow, M., Metz, H., Orth, H. D., & Lang, H. (1974). Proteinase K from *Tritirachium album* Limber. *European Journal of Biochemistry*, *47*(1), 91–97.
- ²³⁴ Pata, V., Fariyal, A., Dis, D. E., Dan, N., Ahmed, F., Discher, D. E., & Dan, N. (2004). Membrane Solubilization by Detergent: Resistance Conferred by Thickness. *Langmuir*, *20*(10), 3888–3893.
- ²³⁵ Schwille, P. (2001). Fluorescence correlation spectroscopy and its potential for intracellular applications. *Cell Biochemistry and Biophysics*, *34*(3), 383–408.
- ²³⁶ Rigler, P., & Meier, W. (2006). Encapsulation of fluorescent molecules by functionalized polymeric nanocontainers: Investigation by confocal fluorescence imaging and fluorescence correlation spectroscopy. *Journal of the American Chemical Society*, *128*(1), 367–373.
- ²³⁷ Tanner, P., Balasubramanian, V., & Palivan, C. G. (2013). Aiding nature's organelles: Artificial peroxisomes play their role. *Nano Letters*, *13*(6), 2875–2883.
- ²³⁸ Song, L., Hennink, E. J., Young, I. T., & Tanke, H. J. (1995). Photobleaching kinetics of fluorescein in quantitative fluorescence microscopy. *Biophysical Journal*, *68*(6), 2588–2600.
- ²³⁹ Smart, P. L., & Laidlaw, I. M. S. (1977). An evaluation of some fluorescent dyes for water tracing. *Water Resources Research*, *13*(1), 15–33.
- ²⁴⁰ Lee, J. C., Bermudez, H., Discher, B. M., Sheehan, M. A., Won, Y. Y., Bates, F. S., & Discher, D. E. (2001). Preparation, stability, and in vitro performance of vesicles made with diblock copolymers. *Biotechnology and Bioengineering*, *73*(2), 135–145.
- ²⁴¹ Martin, C., Dolmazon, E., Moylan, K., Fowley, C., Mchale, A. P., Callan, J. F., & Callan, B. (2015). A charge neutral , size tuneable polymersome capable of high biological encapsulation efficiency and cell permeation. *International Journal of Pharmaceutics*, *481*(1-2), 1–8.
- ²⁴² Pace CN, Vajdos F, Fee L, Grimsley G, Gray T. (1995) How to measure and predict the molar absorption coefficient of a protein. *Protein Science : A Publication of the Protein Society*, *4*(11), 2411-2423.
- ²⁴³ Dinu, M. V., Spulber, M., Renggli, K., Wu, D., Monnier, C. A., Petri-fink, A., & Bruns, N. Filling Polymersomes with Polymers by Peroxidase-Catalyzed Atom Transfer Radical Polymerization. *Macromolecular Rapid Communications*, *36*, 507–514.

-
- ²⁴⁴ Gill, S. C., & von Hippel, P. H. (1989). Calculation of protein extinction coefficients from amino acid sequence data. *Analytical Biochemistry*, 182(2), 319–326.
- ²⁴⁵ Sjöback, R., Nygren, J., & Kubista, M. (1995). Absorption and fluorescence properties of fluorescein. *Spectrochimica Acta Part A: Molecular and Biomolecular Spectroscopy*, 51(6), L7–L21.
- ²⁴⁶ Hawe A, Sutter M, Jiskoot W. (2008) Extrinsic Fluorescent Dyes as Tools for Protein Characterization. *Pharmaceutical Research*, 25(7), 1487-1499.
- ²⁴⁷ Vira, S., Mekhedov, E., Humphrey, G., & Blank, P. S. (2010). Fluorescent-labeled antibodies: Balancing functionality and degree of labeling. *Analytical Biochemistry*, 402(2), 146–150.
- ²⁴⁸ Shengjie, G., Stroupe, W., Papparozzi, E., Conley, E. (2006) A comparison of models and designs for experiments with nonlinear does response relationships. *Annual Conference on applied statistics in agriculture*. Paper 13.
- ²⁴⁹ Nardin, C., Thoeni, S., Widmer, J., Winterhalter, M., & Meier, W. (2000). Nanoreactors based on (polymerized) ABA-triblock copolymer vesicles. *Chemical Communications*, (15), 1433–1434.

Appendix

Order	Estimated band width (% of lane)
1	2.01
2	0.89
3	1.33
4	1.28
5	1.15
6	0.53
7	1.04
8	1.01
9	0.30
10	1.91
11	2.01
12	2.13
13	2.02
14	2.29
15	2.30
16	2.21
17	2.20
18	2.18
19	2.18
20	2.23
21	2.25
22	2.15
23	2.22
24	1.33
25	1.27
26	1.15
27	1.44
28	0.53
29	0.90
30	1.05
31	0.97
32	0.97
33	1.08
34	0.60
35	0.61
36	0.99

37	0.69
38	0.68
39	0.77
40	0.81
41	0.90
42	1.52
43	1.17
44	0.88
45	1.51
46	1.88
47	1.17
48	1.67
49	1.54
50	1.55
51	1.89
52	1.55
53	2.03
54	2.17
55	1.95
56	2.48
57	2.81
58	1.76
59	1.88
60	1.85
61	0.78
62	0.75
63	0.71
64	1.90
65	1.30
66	1.31
67	1.32
68	1.30
69	1.35
70	1.30
71	1.28
72	1.25
73	1.26
74	1.21
75	1.40
76	1.20

77	1.32
78	1.22
79	1.42
80	1.41
81	1.48

Table A1. Band width of PRK on SDS-Gels as a percentage of total lane width. Sample order is the same as in Table 3.8.